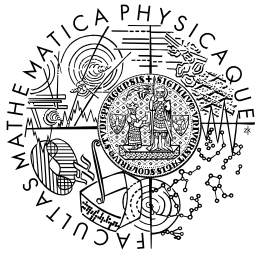


FACULTY
OF MATHEMATICS
AND PHYSICS
Charles University

**MASTER THESIS**

Róbert Králik

# Sterile neutrino physics at NOvA experiment

Institute of Particle and Nuclear Physics

| | |
|---|---|
| Supervisor of the master thesis: | RNDr. Karel Soustružník, Ph.D. |
| Study programme: | Physics |
| Study branch: | Nuclear and Subnuclear Physics |

Prague 2020

I declare that I carried out this master thesis independently, and only with the cited sources, literature and other professional sources.

I understand that my work relates to the rights and obligations under the Act No. 121/2000 Sb., the Copyright Act, as amended, in particular the fact that the Charles University has the right to conclude a license agreement on the use of this work as a school work pursuant to Section 60 subsection 1 of the Copyright Act.

In ..... date .....  signature of the author

I want to dedicate this thesis to all the people that supported me through entire past year. They gave me strength and courage to finish this piece of work and to not give up entirely.

This includes my dear dear friend from my home in Poprad, my friend from Prague, especially Raju, Efka, Beka and Tomas, who gave me so much needed comfort when I needed it.

I want to thank all of the people at the LDT, where I write these last words and who has been most helpful during these hard past days. Thanks you that you are!

I also dedicate this thesis to my family, who supports me as much as they can.

Also to my colleagues at the NOvA experiment, who helped me and guided me in my academic path to become a scientist and none of this would have ever happened without a large portion of them, mainly to the conveners of the sterile neutrino group, Gavin Davies, Brian Rebel and Adam Aurisano, and also to Jeremy Hewes and Pavel Snopok. All of which have been a great help for me.

Last but not least I want to dedicate this thesis to my supervisor who introduced me to this wonderful world of neutrinos, where I found many of my passions.

Title: Sterile neutrino physics at NOvA experiment

Author: Róbert Králik

Institute: Institute of Particle and Nuclear Physics

Supervisor: RNDr. Karel Soustružník, Ph.D., Institute of Particle and Nuclear Physics

Abstract: NOvA sterile neutrinos search via neutral current (NC) disappearance analysis is moving to a two-detector fit method to be able to fit to a wider range of sterile neutrino oscillations parameters. This introduces among other things a bigger contribution of the neutrino flux systematic uncertainty, which currently makes up the largest overall uncertainty for the ongoing NC disappearance analysis. This thesis focuses on reducing this uncertainty and looks for different ways of making a more precise prediction of the neutrino flux. We point out Horn-Off analysis as the base for doing so and describe the production of a new Horn-Off simulation and the analysis of the Horn-Off results. We were not able to draw any conclusions that would reduce the NC disappearance systematic uncertainty, but the results showed herein can be helpful in the future attempts at a better neutrino flux prediction and a lower neutrino flux systematic uncertainty.

Keywords: sterile neutrino neutrino flux NOvA

# Contents

# 1. Neutrino physics

## 1.1 From prediction to precision measurements

### Early beginnings

We can trace the beginning of neutrino physics to the famous letter by Wolfgang Pauli in 1930, in which he proposes the existence of a new very-penetrating electrically-neutral half-spin particle, as a "desperate remedy" to salvaging conservation of energy and angular momentum in beta decays [1]. This particle was shortly after named *neutrino*, or "small neutral thing" by Eduardo Amaldi in his correspondence with Enrico Fermi[2], who adopted it and used it in his theory of Beta decay (1934). Fermi adapted the theory of photon emission to the beta rays in what is the first successful theory of the creation and annihilation of material particles [3] laying base for the theory of weak interactions [4]. Fermi derived expressions for the lifetime of beta decay and for the shape of the beta-ray emission spectrum, from which he deduced that the rest mass of neutrino must be either zero or at least very small in comparison to electron. F. Perrin comes to the same conclusion in 1933 [3]. Neutrino can be regarded as one of the first (if not the first) of new particles that made the new physics of the 1930's [1].

Soon after Fermi's description of neutrino interaction, in 1934, Bethe and Peierls realized the possibility of reverting the process of beta decay as a mean of direct detection of the neutrino [5]. For example an interaction in which incident neutrino interacts with proton, transforming it into neutron and creating a positron:

$$\nu + p \rightarrow n + e^{+}. \tag{1.1}$$

From the lifetime of then-known beta decays they estimated the interaction cross-section to be $< 10^{-44}\,\mathrm{cm}^2$ for a neutrino with a few MeV energy, or about $10^{-20}$ times the more familiar nuclear values at the time and concluded that "there is no practically possible way of observing the neutrino" [5]. Just month later they added to this statement, devising means of confirming the existence of neutrino without its direct detection. Namely by looking at recoils of light (artificial) nuclei and searching for a lack of observable energy [6]. This method, now known as a missing-mass experiment, was utilized by several experiments, namely by Crane and Halpern in 1938 [7] who concluded that the momentum is not conserved in the system consisting of electron and nucleus alone [8].

The advent of fission reactors brought increase of neutrino rate of about $10^7$, as well as higher neutrino energies, making the neutrino detection worth reinvestigating [4]. In 1953 C. L. Cowan and F. Reines placed a liquid scintillation detector near the Hanford reactor reporting uncertain results [9]. They later moved the detector to the Savannah River Plant and in 1956 confirmed [10] the detection of the antineutrino, verifying the neutrino hypothesis [4]. Frederick Reines was awarded the Nobel Prize in Physics in 1995 "for the detection of the neutrino" [11].

The fact that Cowan and Reines discovered antineutrino ($\overline{\nu}$), not neutrino ($\nu$), and that these are two distinct particles, came from negative results of another experiment at the Savannah River Plant in 1956. R. Davis looked for $^{37}Ar$ in

$CCl_4$ (result of a neutrino interaction $\nu + n \rightarrow p + e^-$) and was only able to place an upper limit on the cross section of one-third the predicted value [4].

This led B. Pontecorvo, inspired by already known $K^0 \leftrightarrow \overline{K^0}$ oscillations, to consider $\nu \leftrightarrow \overline{\nu}$ transitions (oscillations), in case the conservation of neutrino charge does not apply[12]. Pontecorvo later built upon this statement in 1958 considering that oscillations between $\nu$ and $\overline{\nu}$ are due to them being combinations of particles $\nu_1$ and $\nu_2$ and that the transformation lifetime is related to the mass difference between $\nu_1$ and $\nu_2$ [13], laying foundation for neutrino oscillations as we know them today.

### More neutrinos - more mixing

In 1960 Mel Schwartz designed the first neutrino beam made by accelerated protons striking a target, producing pions (mostly), which would decay into neutrinos [14][15]. Leon Lederman, Jack Steinberger and others joined Schwartz and using a spark chamber detector in 1962 observed[16] a different kind of neutrino, which we now call the muon neutrino ($\nu_\mu$), produced in pion decay ($\pi^\pm \rightarrow \mu^\pm + \nu$), while the previously known neutrino, produced in beta decays, was dubbed the electron neutrino ($\nu_e$). The Nobel Prize "for the neutrino beam method and the demonstration of the doublet structure of the leptons through the discovery of the muon neutrino" was awarded jointly to Lederman, Schwartz and Steinberg in 1988 (even before the Prize for Reines) [11].

In 1962 Z. Maki, M. Nakagawa and S. Sakata applied Pontecorvo's idea of neutrino oscillations to *weak neutrino* eigenstates $\nu_\alpha$ ($\nu_e$, $\nu_\mu$) produced in weak interactions. They assumed that oscillation $\nu_\alpha \leftrightarrow \nu_\beta$ are driven by a non-zero mass difference (therefore if true implying at least one neutrino has a non-zero mass) between *true neutrinos* (= mass neutrino eigenstates $\nu_i$ ($\nu_1$, $\nu_2$)), which are related to weak eigenstates via a linear combination. This relation in general case looks like [17]

$$|\nu_\alpha\rangle = \sum_{i=1}^{n} U^*_{\alpha i} |\nu_i\rangle , \tag{1.2}$$

where $U$ is a unitary matrix now know as Pontecorvo-Maki-Nakagawa-Sakata (PMNS) matrix and $n$ is the (general) number of light neutrino species [18].

In the contemporary description of neutrino interactions it is common to treat neutrino as a plane wave in a relativistic approximation, which after a distance $L$ evolves as [18]

$$|\nu_\alpha (L)\rangle = \sum_{\alpha'} \sum_i U^*_{\alpha i} U_{\alpha' i} e^{-i m_i^2 L/2E} |\nu_{\alpha'}\rangle . \tag{1.3}$$

Neutrino $\nu_\alpha$ can oscillate and therefore be detected as a different neutrino flavour $\nu_\beta$ with a probability

$$P_{\nu_\alpha \rightarrow \nu_\beta} (L) = |\langle \nu_\beta | \nu_\alpha (L)\rangle|^2 = \sum_{i,j} U_{\beta i} U^*_{\alpha i} U^*_{\beta j} U_{\alpha j} e^{-i\left(m_i^2 - m_j^2\right) L/2E}, \tag{1.4}$$

where the difference of the masses squared is usually denoted as

$$\Delta m^2_{ij} = m_i^2 - m_j^2. \tag{1.5}$$

Oscillation probability can be also expressed as

$$P_{\nu_\alpha \to \nu_\beta}(L) = \delta_{\alpha\beta} - 4\sum_{i>j} \mathrm{Re}\left(U_{\beta i} U^*_{\alpha i} U^*_{\beta j} U_{\alpha j}\right) \sin^2 \Delta_{ij} + 2\sum_{i>j} \mathrm{Im}\left(U_{\beta i} U^*_{\alpha i} U^*_{\beta j} U_{\alpha j}\right) \sin 2\Delta_{ij}, \quad (1.6)$$

where[18]

$$\Delta_{ij} \equiv \Delta m^2_{ij} \frac{L}{4E} = 1.267 \frac{\Delta m^2_{ij}}{\mathrm{eV}^2} \frac{L/E}{\mathrm{m/MeV}}.$$

Since real neutrino beams are not monochromatic, what is measured in experiments is an **average** oscillation probability with $\langle \sin^2 \Delta_{ij} \rangle$ and $\langle \sin 2\Delta_{ij} \rangle$ in eq.1.6. We can notice that if $E/L \gg \Delta m^2_{ij}$ the oscillation does not show any effect yet and if $E/L \ll \Delta m^2_{ij}$ the oscillating phase goes through many cycles and is averaged to $\langle \sin^2 \Delta_{ij} \rangle = 1/2$. Therefore different experimental settings can measure different oscillation parameters [19].

### Detecting neutrino oscillations

Several experimental indications for neutrino oscillations were found shortly after its theoretical predictions. Davis continued looking for $^{37}Ar$ in a detector with $^{37}Cl$, but now moving to Homestake Gold Mine with Harmer and Hoffman focusing on detecting the first electron neutrinos from the Sun [20]. Already in 1968 their Homestake Solar Neutrino Observatory saw a solar neutrino flux less than 3 Solar Neutrino Units (SNU = one interaction per $10^{36}$ target atoms $\mathrm{s}^{-1}$), well below the solar model prediction of the time [21]. This discrepancy became the *"solar neutrino problem"*, which is in line with neutrino oscillations, but no direct implications could have been drawn since it might have been caused by a lack of understanding of nuclear physics, astrophysics of the Sun, or particle physics of the neutrino[14].

In 2002, Raymond Davis was together with Masatoshi Koshiba awarded the Nobel prize "for pioneering contributions to astrophysics, in particular for the detection of cosmic neutrinos" [11]. Koshiba was part of the Kamiokande experiment, which confirmed the results from Homestake [22].

Possible explanation of the Solar neutrino problem was proposed in 1978 by L. Wolfenstein, who considered the effect of matter on neutrino oscillations [23]. His modification of neutrino oscillations when passing through matter arises from the coherent forward scattering of electron neutrinos, as a result of their charged current (CC) interaction with electrons, which are abundant in matter, as opposed to other lepton flavours, muons and tauons, resulting in an imbalance between $\nu_e$ and $\nu_\mu/\nu_\tau$. This manifests as an effective potential, which depends on the density and composition of the matter [23]. This idea was later further developed for neutrinos passing through the Sun by Mikheyev and Smirnov in 1985 [24][18] and we now call this effect the Mikheyev-Smirnov-Wolfenstein (MSW) effect.

To showcase this effect we consider only two neutrino flavours, $\nu_e$ and $\nu_X$, where $X$ denotes a combination of all other non-electron flavours. Vacuum oscillations are in this two-neutrino approximation driven by a single mass splitting $\Delta m^2$ and the corresponding PMNS matrix is a rotational matrix parametrized

by one angle $\theta$:

$$U = \begin{pmatrix} \cos\theta & \sin\theta \\ -\sin\theta & \cos\theta \end{pmatrix}. \tag{1.7}$$

The MSW effect can be described as the presence of an Effective Potential [25]

$$V = \pm\sqrt{2}G_F N_e = \pm 3.8 \times 10^{-14} \left(\frac{\rho}{\text{g cm}^{-3}}\right) \left(\frac{Y_e}{0.5}\right) \text{eV}, \tag{1.8}$$

where $G_F$ is the Fermi coupling constant, $N_e$ is the electron density, $Y_e$ is the electron number per nucleon and plus or minus sign is for neutrinos or antineutrinos respectively.

This potential can be seen as having the effect of modifying the $\Delta m^2$ and $\theta$ of the neutrino oscillations: [25]

$$\sin^2 2\theta_m = \frac{\sin^2 2\theta}{\sin^2 2\theta + (\cos 2\theta \mp \xi)^2} \tag{1.9}$$

$$\left(\Delta m^2\right)_{\mathit{eff}} = \Delta m^2 \times \sqrt{\sin^2 2\Theta + (\cos 2\theta \mp \xi)^2}, \tag{1.10}$$

where

$$\xi = \frac{2\sqrt{2}G_F N_e}{\Delta m^2}. \tag{1.11}$$

Measuring atmospheric neutrinos brought about another neutrino conundrum, the *Atmospheric neutrino anomaly*. It came from the disagreement between experiments such as NUSEX[26] and Fréjus[27], which used iron calorimeters detectors, and experiments IMP[28] and Kamiokande[29], which used water Cherenkov detectors. All of these experiments were looking for a deficit of $\nu_\mu$, or an excess of $\nu_e$, compared to prediction. While the first two experiments saw a good agreement between experimental results and predictions, the latter two did not and suggested the possibility of neutrino oscillations, which could explain their disagreement.

Solution to the Atmospheric neutrino anomaly came in 1998, when the Super-Kamiokande (SK) experiment showed for the first time the experimental evidence for neutrino oscillations [30]. SK has however also disfavoured the two neutrino hypothesis, with regards to the existence of an additional neutrino flavour.

The Solar neutrino anomaly was also resolved, when the Sudbury Neutrino Observatory (SNO) provided $> 5\sigma$ evidence for solar $\nu_e$ oscillations in 2002, independent on the solar model [31]. While other solar neutrino experiments measured solar $\nu_e$ only via the charged current (CC) interactions

$$\nu_e + n \to p + e^- \qquad (CC), \tag{1.12}$$

SNO had an ability to also detect neutrinos via the neutral current (NC) interaction

$$\nu + X \to \nu + X' \qquad (NC), \tag{1.13}$$

which are equally sensitive to all active neutrino flavours and their rate is therefore unaffected by standard neutrino oscillations. SNO could compare CC and NC event rates and conclude that $\nu_e$ from the Sun oscillate into other neutrino flavours along the way [31].

Takaaki Kajita from SK and Arthur B. McDonald from SNO were jointly awarded the Nobel Prize in 2015 "for the discovery of neutrino oscillations, which shows that neutrinos have mass" [11].

### 3 neutrino flavours

In 1990 the L3 Collaboration studied properties of the $Z^0$ boson and fitted to its peak cross-section and decay width to determine the total number of active (interacting with $Z^0$) light ($m_\nu < m_Z/2$) neutrino flavours ($N_\nu$). They found the best fit integer value to be 3 and ruled out the possibility of four or more active light neutrino flavours at $4\sigma$ [32]. Latest most precise results put the fitted value to $N_\nu = 2.9840 \pm 0.0082$ [33]. After this result it was only a matter of time, before the third neutrino, the tau neutrino ($\nu_\tau$) was discovered. Evidence for that were shown in 2000 from the DONUT Collaboration at Fermilab [34].

The PMNS matrix describing neutrino oscillations in the so called $3\nu$ paradigm depends on six independent parameters: 3 mixing angles ($\theta_{12}$, $\theta_{13}, \theta_{23}$) and 3 phases. One of the phases is $\delta_{CP}$, which, if different from 0 or $\pi$, implies CP violation, and the other two are $\alpha$ and $\beta$, so called Majorana phases, which are non zero only if neutrinos are Majorana (neutrinos and antineutrinos are described by just one field, i.e. neutrinos are the same particle as antineutrinos). Majorana phases play no role in neutrino oscillations, so they are usually left out in the description [19]. The PMNS matrix in this case can be parametrized as

$$U = \begin{pmatrix} U_{e1} & U_{e2} & U_{e3} \\ U_{\mu 1} & U_{\mu 2} & U_{\mu 3} \\ U_{\tau 1} & U_{\tau 2} & U_{\tau 3} \end{pmatrix} =$$

$$= \begin{pmatrix} 1 & 0 & 0 \\ 0 & c_{23} & s_{23} \\ 0 & -s_{23} & c_{23} \end{pmatrix} \begin{pmatrix} c_{13} & 0 & s_{13}e^{-i\delta} \\ 0 & 1 & 0 \\ -s_{13}e^{i\delta} & 0 & c_{13} \end{pmatrix} \begin{pmatrix} c_{12} & s_{12} & 0 \\ -s_{12} & c_{12} & 0 \\ 0 & 0 & 1 \end{pmatrix} \begin{pmatrix} 1 & 0 & 0 \\ 0 & e^{i\alpha} & 0 \\ 0 & 0 & e^{i\beta} \end{pmatrix}, \tag{1.14}$$

where $c_{ij} \equiv \cos\theta_{ij}$ and $s_{ij} \equiv \sin\theta_{ij}$.

Other than the PMNS matrix, neutrino oscillations depend on the mass squared differences (eq.1.5). In case of 3 neutrinos, those are $\Delta m^2_{21}$ and $\Delta m^2_{31}$. $\Delta m^2_{21}$ mainly drives oscillations of solar neutrinos and is therefore often denoted as $\Delta m^2_\odot$ or $\Delta m^2_{sol}$, while $\Delta m^2_{31}$ drives oscillations on the scale for atmospheric neutrinos and is often written as $\Delta m^2_{atm}$ [18]. There can only be two independent mass squared differences for oscillation of three neutrinos, since

$$\Delta m^2_{21} + \Delta m^2_{32} + \Delta m^2_{13} = 0. \tag{1.15}$$

From experiments we know that [18]

$$\Delta m^2_{sol} \ll \Delta m^2_{atm}. \tag{1.16}$$

There are two possible ordering for neutrino masses, nicknamed Normal Ordering (NO) and Inverted Ordering (IO)[19]

$$m_1 < m_2 < m_3 \Rightarrow \Delta m^2_{32} \simeq \Delta m^2_{31} > 0 \qquad (\mathsf{NO}), \tag{1.17}$$

$$m_3 < m_1 < m_2 \Rightarrow \Delta m^2_{32} \simeq \Delta m^2_{31} < 0 \qquad (\mathsf{IO}). \tag{1.18}$$

This is shown on fig.1.1, together with the currently known flavour composition of the mass eigenstates.

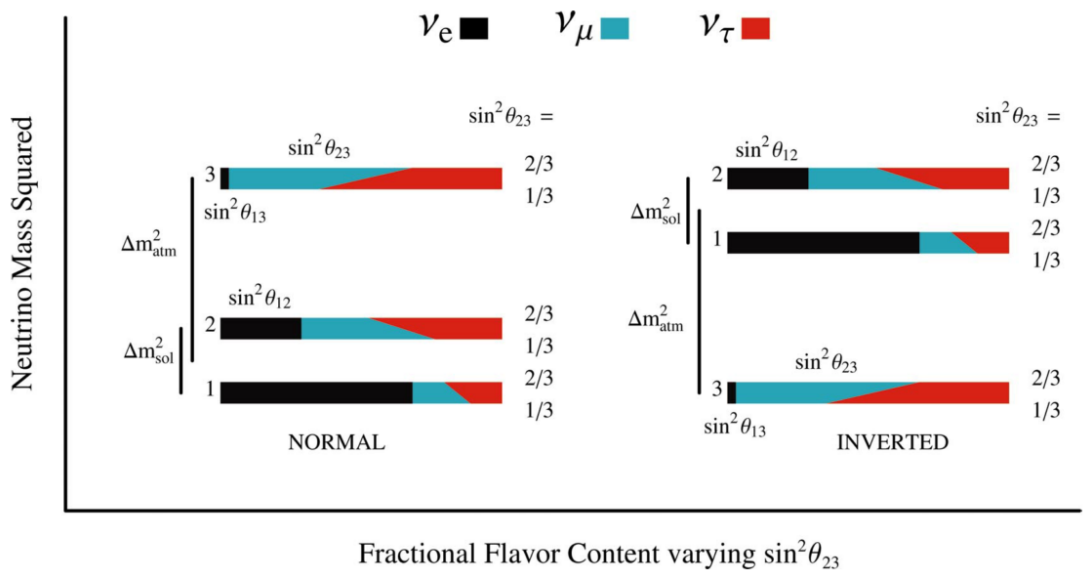


Figure 1.1: An illustration of different hierarchies of the mass splittings and a composition of flavor states in individual mass states corresponding to a 3 flavour model [35].

The oscillations of three neutrinos flavours is a well established phenomenon, with many different neutrino experiments finding consistent results, in particular on the better-known parameters $\theta_{12}, \theta_{13}, \Delta m^2_{21}$ and $|\Delta m^2_{32}|$, which favour the $3\nu$ paradigm. There are still some unknowns, which require further clarification, specifically the value of $\theta_{23}$ (i.e. whether $\nu_3$ has more $\nu_\mu$ or $\nu_\tau$), the mass ordering (=mass hierarchy) and the leptonic CP phase $\delta_{CP}$ [19]. Current best-fit points for $3\nu$ oscillations from global analyses are shown in table 1.1.

| Parameter | best-fit | |
|---|---|---|
| $\Delta m^2_{21}$ | $(7.53 \pm 0.18) \times 10^{-5}\,\mathrm{eV}^2$ | |
| $\Delta m^2_{32}$ | $(2.444 \pm 0.034) \times 10^{-3}\,\mathrm{eV}^2$ | (normal mass hierarchy) |
| $\Delta m^2_{32}$ | $(-2.55 \pm 0.04) \times 10^{-3}\,\mathrm{eV}^2$ | (inverted mass hierarchy) |
| $\sin^2\theta_{12}$ | $0.307 \pm 0.013$ | |
| $\sin^2\theta_{23}$ | $0.512^{+0.019}_{-0.022}$ | (normal mass hierarchy, octant I) |
| $\sin^2\theta_{23}$ | $0.542^{+0.019}_{-0.022}$ | (normal mass hierarchy, octant II) |
| $\sin^2\theta_{23}$ | $0.536^{+0.023}_{-0.028}$ | (inverted mass hierarchy) |
| $\sin^2\theta_{13}$ | $(2.18 \pm 0.07) \times 10^{-2}$ | |
| $\delta/\pi$ | $1.37^{+0.18}_{-0.16}\,\pi\mathrm{rad}$ | |

Table 1.1: Up-to-date best-fit values of neutrino properties for the 3 neutrino flavour model[19].

## 1.2 Sterile neutrinos

However successfully the three-flavour oscillation model explains most of the obtained experimental data, there are some anomalous experimental results which cannot be explained in the standard $3\nu$ framework, pointing towards existence of an additional neutrino flavour with a new mass squared difference ($\Delta m^2$) in the eV scale [19]. As was mentioned in the previous section, we know from the decay width of the $Z^0$ boson that there can only be tree light active neutrinos, which means that any new light neutrino must be "sterile" (i.e. non-interacting with $Z^0$).

The simplest extension would be to include one additional neutrino mass state $\nu_4$ and a sterile neutrino flavour $\nu_s$. This would mean adding 3 new mixing angles $\theta_{14}, \theta_{24}$ and $\theta_{34}$ and two new CP violating phases $\delta_{14}$ and $\delta_{34}$ [36]. We can express the mixing matrix in the $4\nu$ model as:

$$\begin{pmatrix} \nu_e \\ \nu_\mu \\ \nu_\tau \\ \nu_s \end{pmatrix} = \begin{pmatrix} U_{e1} & U_{e2} & U_{e3} & U_{e4} \\ U_{\mu 1} & U_{\mu 2} & U_{\mu 3} & U_{\mu 4} \\ U_{\tau 1} & U_{\tau 2} & U_{\tau 3} & U_{\tau 4} \\ U_{s1} & U_{s2} & U_{s3} & U_{s4} \end{pmatrix} \begin{pmatrix} \nu_1 \\ \nu_2 \\ \nu_3 \\ \nu_4 \end{pmatrix}. \tag{1.19}$$

There are several different ways to parametrize this matrix. We will be using parametrization from [36], in which

$$\begin{aligned} U_{e4} &= \sin_{14} e^{-i\delta_{14}}, \\ U_{\mu 4} &= \cos_{14} \sin_{24}, \\ U_{s4} &= \cos_{14} \cos_{24} \cos_{34}. \end{aligned} \tag{1.20}$$

Existing experimental data indicate that this non-standard massive neutrino $\nu_4$ is mostly sterile [36]. This means that

$$|U_{e4}|^2, |U_{\mu 4}|^2, |U_{\tau 4}|^2 \ll 1. \tag{1.21}$$

Four neutrino mass states could be organized in 6 different orderings, as shown on fig.1.2. However the (2+2) scheme, where there are two pairs of neutrino masses separated by $\sim$ eV gap, has been significantly disfavoured by experimental results [19]. Also the (1+3) mass scheme would mean there is one small mass and three neutrino masses at the eV scale, which is disfavoured by the cosmological upper bound on the neutrino masses [37]. We will therefore only consider the (3+1) mass scheme, where $m_4 \gg m_3, m_2, m_1$ and $\Delta m^2_{41} > 0$.

To better elucidate significance of sterile parameters for different experimental setting we consider the following. Since

$$\Delta m^2_{41} \gg \left|\Delta m^2_{31}\right| \gg \left|\Delta m^2_{21}\right| \tag{1.22}$$

there is a region for low $L/E$ (distance/energy), where the standard $3\nu$ oscillations haven't taken effect yet (as discusses in the previous section) and oscillations are dominated by

$$\Delta m^2_s \equiv \Delta m^2_{41} \approx \Delta m^2_{42} \approx \Delta m^2_{43}. \tag{1.23}$$

This is called the short baseline (SBL) limit [39].

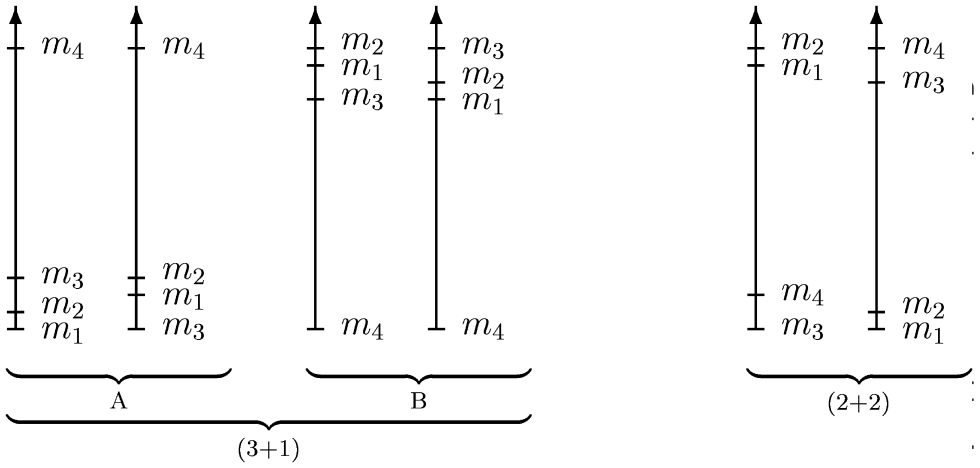


Figure 1.2: Depiction of possible hierarchies of neutrino masses in a four neutrino model [38].

The oscillation probability in this case looks like

$$P^{SBL}_{\nu_\alpha \to \nu_\beta} = \left| \delta_{\alpha\beta} - \sin^2\left(2\theta_{\alpha\beta}\right) \sin^2\left(\Delta m^2_s \frac{L}{4E}\right) \right|, \tag{1.24}$$

where

$$\sin^2\left(2\theta_{\alpha\beta}\right) = 4\left|U_{\alpha 4}\right|^2 \left| \delta_{\alpha\beta} - \left|U_{\beta 4}\right|^2 \right|. \tag{1.25}$$

For the appearance of $\nu_e/\overline{\nu}_e$ in a beam of $\nu_\mu/\overline{\nu}_\mu$ this takes form

$$\sin^2\left(2\theta_{e\mu}\right) = \sin^2\left(2\theta_{\mu e}\right) = 4\left|U_{e4}\right|^2 \left|U_{\mu 4}\right|^2 = \sin^2\left(2\theta_{14}\right) \sin^2\left(\theta_{24}\right). \tag{1.26}$$

For the disappearance of $\nu_e/\overline{\nu}_e$

$$\sin^2\left(2\theta_{ee}\right) = 4|U_{e4}|^2 \left(1 - \left|U_{e4}\right|^2\right) = \sin^2\left(2\theta_{14}\right) \tag{1.27}$$

and for the disappearance of $\nu_\mu/\overline{\nu}_\mu$

$$\begin{aligned} \sin^2\left(2\theta_{\mu\mu}\right) &= 4\left|U_{\mu 4}\right|^2 \left(1 - \left|U_{\mu 4}\right|^2\right) \\ &= \sin^2\left(2\theta_{24}\right) \cos^2\left(\theta_{14}\right) + \sin^2\left(2\theta_{14}\right) \sin^4\left(\theta_{24}\right) \\ &\simeq \sin^2\left(2\theta_{24}\right), \end{aligned} \tag{1.28}$$

where we considered small mixing angles $\cos^2\left(\theta_{14}\right) \simeq 1$ and $\sin^4\left(\theta_{24}\right) \simeq 0$ from eq.1.21.

We can see that electron (anti)neutrino appearance searches link the electron and muon disappearance searches and any sterile signature must be compatible between these channels [36].

We could go beyond a simple model of only one sterile neutrino and try adding another sterile states, increasing degrees of freedom for neutrino oscillations. However, because appearance and disappearance channels remain related for all scenarios with more than one sterile neutrino [39], it has been shown[40] this cannot relax the tension that is currently present in experimental results. We introduce and describe this tension in the following section.

## 1.3 Experimental indications of sterile neutrino

### 1.3.1 $\nu_\mu \to \nu_e$ and $\overline{\nu}_\mu \to \overline{\nu}_e$ appearance at short baseline searches

The appearance of electron (anti)neutrinos in a beam of muon (anti)neutrinos at short baselines was the first channel with anomalous experimental result related to sterile neutrinos [41], since in a case of no sterile neutrinos, no $\nu_e$ are expected in a beam of $\nu_\mu$ at small $L/E$ [36].

The first experiment to measure this channel with antineutrinos was Liquid Scintillator Neutrino Detector (LSND) [41] with baselines of $L/E \approx 1\,\mathrm{m/MeV}$ corresponding to $\Delta m^2_{41} \approx 1\,\mathrm{eV}^2$, which is too small for standard $3\nu$ oscillations to develop. LSND was taking data in 1993-1998 and reported a total of approximately five times more $\overline{\nu}_e$ than was calculated, corresponding to an excess of $87.9 \pm 22.4 \pm 6.0$ or $3.8\sigma$ [41].

To test LSND results, the Mini Booster Neutrino Experiment (MiniBooNE) was build with the same average value of $L/E$, but wider range, different neutrino energies, neutrino fluxes, reconstruction, backgrounds and systematic uncertainties [42], but not detection method, which remained the same. MiniBooNE took data in 2002-2019 with both electron neutrinos and antineutrinos and found a total $\nu_e + \overline{\nu}_e$ excess of $638.0 \pm 132.8$ events with respect to expectation or a $4.8\sigma$ excess [43]. Combining this result with LSND yields an excess of $6.1\sigma$, which is shown on fig.1.3 with comparison to an oscillation probability assuming existence of one sterile neutrino [43]. Preferred sterile neutrino oscillation parameter region is shown on fig.1.4 together with other experiment, which have not been able to confirm MiniBooNE's and LSND findings, but does not rule them out either [39].

One possible explanation of the MiniBooNE excess might be that it is due to photons, not electrons, produced by the decay of $\pi^0$ from $\nu_\mu$ CC interaction [36], since $\pi^0$ is the largest source of systematic uncertainties at low energies, where the excess was observed, and since these photons cannot be distinguished from electrons in the liquid scintillator detector used by MiniBooNE (but also LSND) [36]. This has been already tested by MiniBooNE, which disfavours this explanation [43], and will be further studied by the Fermilab Short Baseline Neutrino (SBN) program and the JSNS$^2$ experiment at J-PARC.

### 1.3.2 $\nu_e$ and $\overline{\nu}_e$ disappearance searches

Solar neutrino experiments GALLEX[44] and SAGE[45] saw a *deficit* of $\nu_e$ rate compared to prediction, when looking at neutrino spectra from radioactive sources $^{51}\mathsf{Cr}$ and $^{37}\mathsf{Ar}$ intended for calibration. This has been called the "gallium anomaly" and one of the possible explanations is an error in the prediction of the production rate of the sources [45]. There is also a possible explanation via sterile neutrinos and recent[46] data/prediction comparison results are in favour of the existence of active-sterile neutrino mixing with a significance about $2.3\sigma$. Preferred region is shown on fig.1.5.

In 2011 the electron antineutrino flux from nuclear reactors was re-evaluated [47] to rely less on nuclear models and exploit all data obtained so far. This led to higher overall flux prediction and a *deficit* in a total $\overline{\nu}_e$ rate in reactor

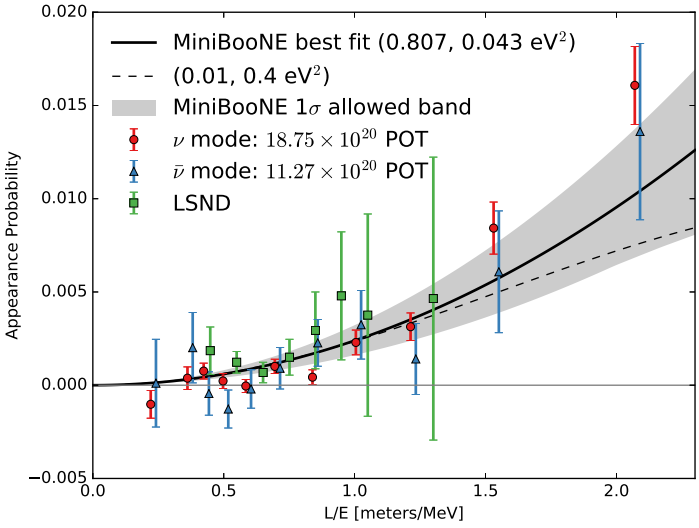


Figure 1.3: A comparison between results from LSND (green) and MiniBooNE electron neutrino (red) and antineutrino (blue) excess shown as appearance probabilities at different $L/E$. MiniBooNE's best fit point in $(\sin^2(2\theta), \Delta m^2)$ parameter space (assuming two neutrino flavour oscillation as in eq.1.24) is shown as a black line, together with $1\sigma$ allowed band. One other appearance probability is shown as a dashed line, corresponding to $(\sin^2(2\theta), \Delta m^2) = (0.01, 0.4\,\mathrm{eV}^2)$. Error bars show statistical uncertainties only. Fig. from [43].

neutrino experiments, what was nicknamed the "reactor antineutrino anomaly" [48]. One of the explanations included a presence of sterile neutrinos with $\Delta m^2_{new}$ in eV range. In 2016 Daya Bay looked at the shape of the spectra and found an *excess* of events around 5 MeV [49], raising concerns [50] about the uncertainties of the flux predictions, which lowers the significance of the anomaly [36]. Daya Bay also studied antineutrino fluxes from individual isotopes [51] indicating an incorrect prediction of neutrinos from $^{235}U$ (if oscillations into sterile neutrinos alone were causing this anomaly, there would be no dependence on the isotope studied) and combination with other experiments shows only a slight preference ($1.8\sigma$) for hybrid of sterile neutrino oscillations and incorrect flux prediction over no-sterile-oscillations hypothesis [52].

Other experiments capable of model-independent spectral measurements of nuclear neutrinos, DANSS and NEOS, found a small preference for sterile neutrinos over $3\nu$ hypothesis preferring ($\Delta m^2_{41} = 1.4\,\mathrm{eV}^2$, $\sin^2(2\theta_{14}) = 0.05$) by DANSS[53] and ($\Delta m^2_{41} = 1.73\,\mathrm{eV}^2$, $\sin^2(2\theta_{14}) = 0.05$) by NEOS[54] while also setting a strict limits on the rest of the parameter space. While results from individual experiments are insignificant to prove sterile neutrino oscillations, remarkable agreement between them makes their joint fit favour SBL $\overline{\nu}_e$ oscillations with statistical significance of $3.7\sigma$ [55] with preferred region showed at fig.1.5. However, experiment DANSS has recently updated [56] their analysis further reducing their significance for sterile neutrinos to a maximum of only $1.8\sigma$. These results have not been updated into a global fit yet and are not part of the fig.1.5.

Similar experiment Neutrino-4 claimed to observe oscillations with sterile neutrinos with significance $2.8\sigma$ with preferred parameters $\Delta m^2_{41} \approx 7.25 \pm 1.0\mathrm{eV}^2$ and

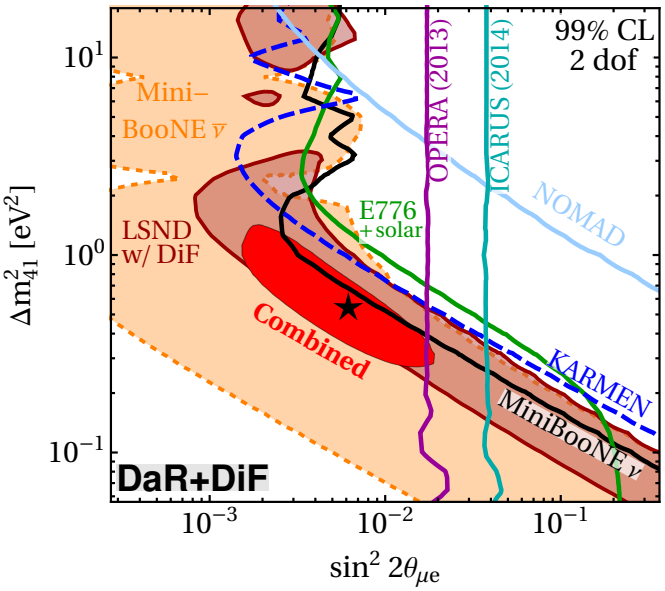


Figure 1.4: Overview and global fit of the up-to-date results of short baseline $\nu_\mu \to \nu_e/\overline{\nu}_\mu \to \overline{\nu}_e$ searches in context of one sterile neutrino in the (3+1) model. We show preferred oscillation parameter phase space for MiniBooNE and LSND experiments projected onto $\Delta m^2_{41}$ and $\sin^2(2\theta_{\mu e}) = 4\,|U_{e4}|^2\,|U_{\mu 4}|^2$ plane. For LSND we show both data from Decay at Rest (DaR) source and also added data from a Decay in Flight (DiF) source. We also show allowed regions (on left hand side of the unfilled lines) from other experiments, which leave unconstrained most of the preferred combined region and the combined best fit point. Figure is from [39].

$\sin^2(2\theta_{14}) \approx 0.26 \pm 0.09$ [57]. These results and stated significances have been however criticised [58] and we are not taking them into consideration.

### 1.3.3 $\nu_\mu$, $\overline{\nu}_\mu$ and NC disappearance searches

Atmospheric neutrino experiments make use of an enhancement of neutrino oscillation signature in presence of sterile neutrino due to additional matter effect, similar to the one in eq.1.9, caused by a disproportion of interactions in matter between active and sterile neutrinos [36]. Super-Kamiokande [59], IceCube [60] and IceCube's low-energy subarray DeepCore saw no significant evidence for oscillations with sterile neutrino and put strong limits on oscillation parameters $|U_{\mu 4}|^2$ and $|U_{\tau 4}|^2$ as can be seen on fig.1.6. Updated analysis from IceCube+DeepCore was recently published on arXiv [61] and shows a preference for the existence of sterile neutrino with the best fit point at $\Delta m^2 \sim 4.5\,\mathrm{eV}^2$ and $\sin^2(2\theta_{24}) \sim 0.9$ and a p-value of 8% against null hypothesis. This best fit point is however excluded at 99%CL by Super-Kamiokande, MiniBooNE and also MINOS/MINOS+.

Long baseline accelerator neutrino experiments MINOS/MINOS+ [62], T2K [63] and NOvA [64] are using two detectors, one near the source of $\nu_\mu$ beam and one far, to detect $\nu_\mu$ and NC (in case of sterile neutrinos) disappearance and $\nu_e$ appearance caused by oscillations. All of these experiments see results compatible with $3\nu$ scenario and in case of MINOS/MINOS+ set one of the strictest limits

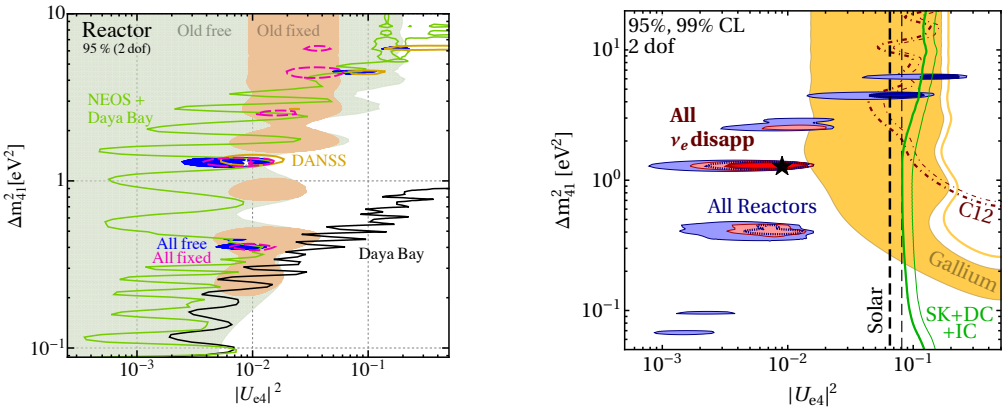


Figure 1.5: Electron antineutrino disappearance global fit best fit points and allowed regions. Left: Preferred and allowed regions of model-independent reactor neutrino experiments. Notice strong exclusion of $|U_{e4}|^2$ ($= \sin^2(\theta_{14})$ in our parametrization) for large range of $\Delta m^2_{41}$. These limits indicate small $\theta_{41}$ what we use in our sterile neutrino oscillation estimates at NOvA. Right: Comparison between joint fit of all $\overline{\nu}_e$ disappearance data (with best fit point indicated by the black star) and the gallium anomaly. Exclusion curves for solar neutrino experiments, atmospheric neutrino experiments (Super-Kamiokande+DeepCore+IceCube=SK+DC+IC) and $\nu_e$ $^{12}C$ scattering experiments are also shown (excluded region is on the right of these exclusion curves). It can be seen that none of these experiments excludes the best fit point of $\nu_e$ disappearance data. Both figures are from [39], published in 2018.

on sterile neutrino oscillation parameters, as can be seen on fig.1.6.

From fig.1.6 it is clear, that due to relations (1.26) between $\nu_e$ appearance and $\nu_{\mu,e}$ disappearance probabilities and their mutually exclusive results [39] there is a significant tension between these two channels. This tension can be quantified using a goodness-of-fit test a it can be shown [39] that removing result of any of the experiments does not significantly relax the tension and only removing results from LSND shows some improvement, indicating that the tension is strongly driven by LSND. From this it can be concluded that the sterile neutrino oscillation explanation of the electron neutrino appearance results from LSND and MiniBooNE is excluded at $4.7\sigma$ [39].

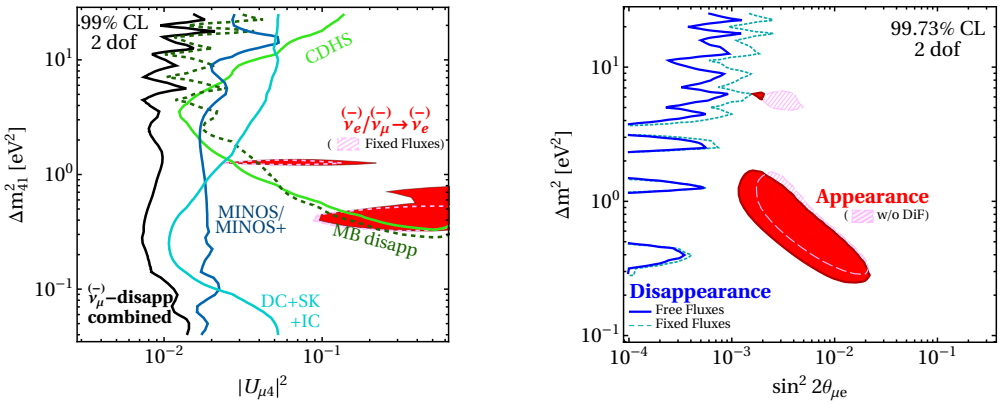


Figure 1.6: Tension between appearance and disappearance data shown as allowed regions in red and pink VS exclusion curves in the $\Delta m^2_{41}$ and $|U_{\mu 4}|^2$ (left) or $\sin^2(2\theta_{\mu e}) = 4|U_{e4}U_{\mu 4}|^2$ (right) parameter space. Left: $\nu_e$ appearance and disappearance allowed region (with(pink) and without(red) fixed reactor antineutrino flux) compared to exclusion curves of long baseline accelerator experiment MINOS/MINOS+, combination of atmospheric experiments DeepCore+SuperKamiokande+IceCube, short baseline accelerator experiment MiniBooNE and the CDHS experiment at 99%CL. It can be clearly seen that the allowed region is completely rejected by results of aforementioned experiments. Right: Comparison between appearance ($\nu_\mu \to \nu_e/\overline{\nu}_\mu \to \overline{\nu}_e$) and disappearance ($\nu_{\mu,e} \to \nu_{\mu,e}/\overline{\nu}_{\mu,e} \to \overline{\nu}_{\mu,e}$) and a clear showcase of the tension between them, since all of the preferred region from appearance experiment is excluded at 99.73%CL. Figure is from [39].

# 2. NOvA experiment

The NuMI Off-axis $\nu_e$ Appearance (NOvA) experiment is a two detector, long-baseline neutrino oscillation experiment designed for a precision measurement of $\nu_\mu \rightarrow \nu_e$, $\overline{\nu}_\mu \rightarrow \overline{\nu}_e$, $\nu_\mu \rightarrow \nu_\mu$ and $\overline{\nu}_\mu \rightarrow \overline{\nu}_\mu$ oscillations [65]. It is the second generation experiment on the NuMI beamline (Neutrinos from the Main Injector - see sec.2.1) after the MINOS experiment, having approximately three times more mass, twice as much beam power, better particle identification, eight times finer longitudinal sampling and the benefits of the off-axis siting over MINOS [66].

NOvA's primary scientific goals are to determine the neutrino mass hierarchy (normal or inverse ordering of the neutrino masses), determine whether $\theta_{23} > 45\,^\circ$ or $\theta_{23} < 45\,^\circ$ (whether the $\nu_3$ state has more $\nu_\mu$ or $\nu_\tau$ respectively) and get information on the amount of the CP violation in the neutrino sector (if there is any) [66]. NOvA's physics capability however includes also searching for light sterile neutrinos by studying disappearance of the neutral current (NC) events, measuring different neutrino cross-sections, observing supernova events, slow magnetic monopoles or light dark matter particles, investigating non-standard interactions and seasonal variations of cosmic-originated muons and more [67, 65].

The experiment is managed by Fermi National Accelerator Laboratory (commonly known as Fermilab) with most of NOvA's components located on Fermilabs premises in Batavia, Illinois, near Chicago, including the near detector (ND) located 1 km from the NuMI target hall and 105 m below ground. Only the Far Detector (FD) is located in Ash River, Minnesota, 810.5 km from Fermilab, partially below ground, covered with granite rock (see sec.2.2) [68, 69].

NOvA started collecting data in 2013, periodically switching between neutrino and antineutrino modes, with first results published in 2016 [70]. The current plan is to continue running until the launch of the DUNE experiment, NOvA's successor. NOvA's data taking history is visualized on fig.2.1.

NOvA experiment has currently more than 240 scientists and engineers from 51 institutions in six countries [69]. Institute of Particle and Nuclear Physics of Charles University, one of four Czech institutions in NOvA, has joined in in 2011 and the group currently consists of 4 people, including the author of this thesis.

## 2.1 Neutrino beam

NOvA's source of neutrinos is the upgraded version of the Neutrinos at the Main Injector (NuMI) [72] neutrino beam at Fermilab, also used by MINERvA and ArgoNeut experiments and in the past MINOS/MINOS+ experiment and the MiniBooNE experiment for a special, very off-axis analysis [73, 72]. NuMI produces the World's most powerful neutrino beam by steering a 120 GeV proton beam onto a graphite target producing hadrons, which decay into neutrinos [72]. This process is described in detail below and shown on fig.2.3.

Protons originate as $H^-$ ions, accelerated by the Linac to 400 MeV, converted to protons and further accelerated to 8 GeV in the Booster, to be passed to the Main Injector which finally accelerates them to 120 GeV . Protons are then extracted, bent down to point towards the MINOS/NOvA Far Detector, and

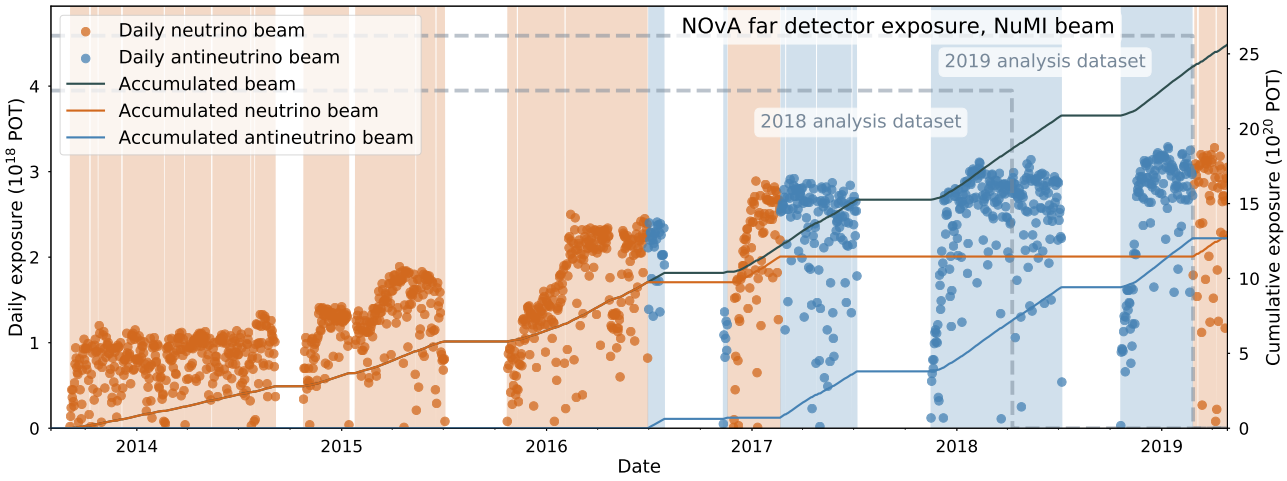


Figure 2.1: Daily NOvA far detector exposure shown as dots as well as cumulative NOvA far detector exposure shown as lines in POT (Protons On Target) units from the beginning of NOvA physics run. The graph shows exposures for both neutrinos and antineutrinos corresponding to FHC mode or RHC mode respectively, as well as the total exposure. Data from 2017 and 2018 datasets, both used in the published FHC+RHC analysis[71], are shown. Figure is from NOvA's internal database.

transported to the NuMI target [72]. The current beam power is $\sim 700\,\text{kW}$ with a plan [74] of reaching more than 1 MW beam power in the future upgrades.

Before hitting the target the proton beam passes through a collimating baffle, a 1.5 m graphite core with 11 mm hole for the beam ($\approx 5\,\sigma$ of typical beam spot size), designed to shield NuMI components further along the beam path from mis-steered protons. The NuMI target is a graphite fin, 7.4 mm wide, 63 mm tall and $\approx 120\,\text{cm}$ long (along the beam direction)[1] [75]. Protons interact in the target producing hadrons, predominantly pions and kaons [72].

Hadrons are focused and selected by two parabolic magnetic "horns", which act as hadron lenses. The horns are illustrated in fig.2.2. They consist of a 2-layered thin coaxial sheet conductor with volume between the layers filled with low-density gas. An electric current circulates in one direction in the inner layer and in the opposite direction in the outer layer generating a toroidal magnetic field that falls as $1/R$ further from the center of the horn and has zero value outside the horn [75]. Direction of the current can be changed to either focus positively charged particles in a so-called Forward Horn Current (FHC) mode ($\nu$ mode), or negatively charged particles in a Reverse Horn Current (RHC) mode ($\overline{\nu}$ mode) [72]. The parabolic shape makes the total distance travelled by a particle in the horn proportional to its transverse momentum $p_T$ [75].

Changing the relative distances between the target, Horn 1 and Horn 2, together with changing values of the horn current (HC) allows for the selection of the desired energy. The low energy (LE) configuration was used for the MINOS experiment with HC=185 kA[72]. The medium energy (ME) configuration, corre-

[1]Previous target proportion were 6.4 mm W, 15 mm H and 95.38 cm L used in low energy design (see lower) [72].

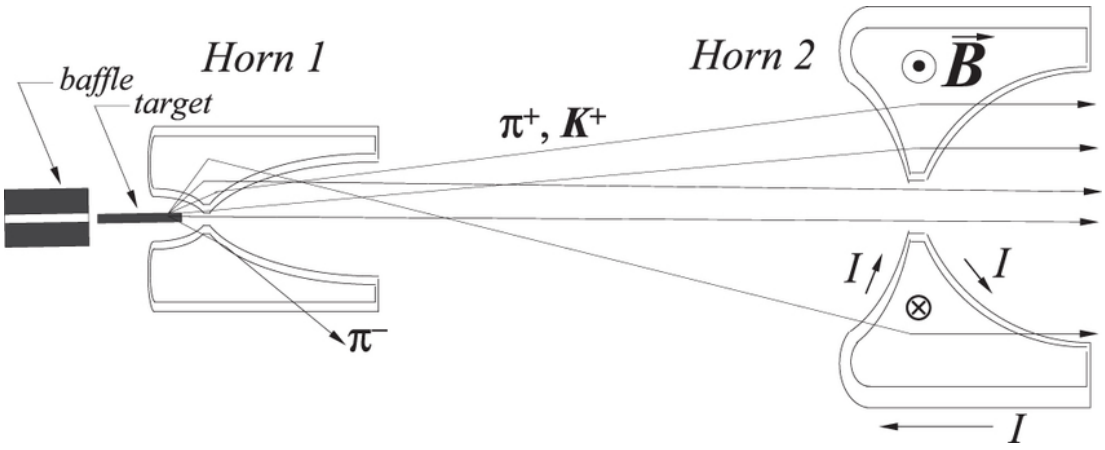


Figure 2.2: Schematic description of the NuMI baffle, target and magnetic horns. Protons coming from the LHS pass through the baffle, interact in the target producing hadrons, mostly pions and kaons. Two horns select and focus these hadrons by a magnetic field created by electric current flowing through the horns. Figure is from [76].

sponding to HC=200 kA, larger distance between the two horns and target pulled back from the Horn 1, was used by NOvA [75], but also MINOS+ experiment [77].

The focused and selected hadrons then pass through the decay pipe, a 675 m long cylinder with 2 m diameter, filled with helium [72, 75]. The main hadron decay modes resulting in a neutrino are shown in table 2.1. Almost all pions with energies $< 10$ GeV decay to $\nu_\mu$ in the decay pipe [75]. Muons can also be generated and decay, contributing to the neutrino flux.

| Decay channel | Branching ratio |
|---|---|
| $\pi^\pm \to \mu^\pm + \nu_\mu\,(\overline{\nu}_\mu)$ | 99.9877% |
| $K^\pm \to \mu^\pm + \nu_\mu\,(\overline{\nu}_\mu)$ | 63.56% |
| $K^\pm \to \pi^0 + e^\pm + \nu_e\,(\overline{\nu}_e)$ | 5.07% |
| $K^\pm \to \pi^0 + \mu^\pm + \nu_\mu\,(\overline{\nu}_\mu)$ | 3.352% |
| $K^0_S \to \pi^+ + \pi^-$ | 69.2% |
| $K^0_L \to \pi^\pm + e^\mp + \overline{\nu}_e\,(\nu_e)$ | 40.55% |
| $K^0_L \to \pi^\pm + \mu^\mp + \overline{\nu}_\mu\,(\nu_\mu)$ | 27.04% |
| $\mu^\pm \to e^\pm + \nu_e\,(\overline{\nu}_e) + \overline{\nu}_\mu\,(\nu_\mu)$ | $\approx 100\%$ |

Table 2.1: Main decay channels producing neutrinos for hadrons in the NuMI beamline [75, 19]

A hadron monitor is placed just before the 5 m thick absorber to record the profile of the residual hadrons. It is used to track the proton spot and the integrity of the NuMI target. The absorber is a massive structure made of aluminium, steel and concrete designed to stop most of the hadrons still in the beam [72]. Remaining muons are ranged out in a dolomite rock between the absorber and the near detector hall. There are three muon monitors in an excavated alcoves inside this rock providing a 2-dimensional profile of the muon beam to monitor the quality and relative intensity of the beam. The muon monitors are ionization

chambers with a detection thresholds due to muon range-out of 4 GeV, 10 GeV, and 20 GeV each [72].

## 2.2 Detectors

The two NOvA detectors are highly-segmented, highly-active functionally-identical tracking calorimeters. They consist of PVC cells (5.6 cm × 3.6 cm in cross-section), extending the full width or hight of the detector ($\approx$ 4 m for ND and $\approx$ 15 m for FD), containing liquid scintillator and a wavelength-shifting fibre connected to an avalanche photodiode (APD) [65, 68]. Cells are connected into planes which are layered perpendicular to the neutrino beam direction, alternating between horizontal and vertical orientations. There are 384 cells in one plane and 896 planes in the FD and in the ND there are 32 cells per module, 3×3 modules per plane and 192 planes in the active part. ND also contains the muon catcher, which has 3 modules per vertical plane, 2 modules per horizontal plane and 22 planes with interleaving steel plates. This makes the size of the FD 15.23 m × 15.14 m × 59.62 m and of the ND 3.83 m × 3.81 m × 15.87 m corresponding to *horizontal* × *vertical* × *longitudinal* orientation with respect to the neutrino beam direction respectively [65][2]. The size of the detectors and their layout can be seen in fig.2.4.

The liquid scintillator amounts for about 63% of the total detector mass (the rest being the PVC structure) [78] and consists primarily of mineral oil with 4.1% pseudocumene [1,2,4-Trimethybenzene] as the scintillant [68]. The radiation length in the detector (38 cm) is many times larger than the cell dimensions, which allows for a good reconstruction and separation of electromagnetic and hadronic showers, identification of muons and neutral pions [65].

Charged particles in the detector produce a scintillator light captured by the wavelength-shifting fibre directing it to one pixel on an APD mounted at the top of each cell. APD converts the light into electrical signal, which is then amplified, digitized and consolidated by the Data Concentrate Module into 5 ms time slices, buffered for a minimum of 20 s waiting for a spill trigger and finally written to a file for storage or shared memory for monitoring [79].

We are using the minimum ionizing part of cosmic-ray muon tracks that stop in the detectors to calibrate the absolute energy scale to within ±5% [71]. GEANT4 [80] simulation is used to calibrate the deposited energy of individual particles as well as the scintillation light, light transport and readout response [81].

Since most of the primary goals of NOvA depend on successfully observing $\nu_e$ charged-current interaction, the reconstruction chain was tailored for this task [82]. Different interactions as seen in a NOvA detector are shown on fig.2.5. Reconstruction begins by clustering hits into slices by time and space "density". Than a modified Hough transform identifies prominent features, which are used to determine the global 3D vertex for the slice. This vertex is used in the fuzzy k-means algorithm to produce prongs (a collection of cell hits with a start point and a direction) which are fed to a neural network to classify the degree to which the slice was like a $\nu_e$ CC (or other) interaction [82]. NOvA uses a convolutional

[2]All of the values for detector, planes and cells size and number were adjusted to the most precise detector specification from a private uncited document for NOvA users.

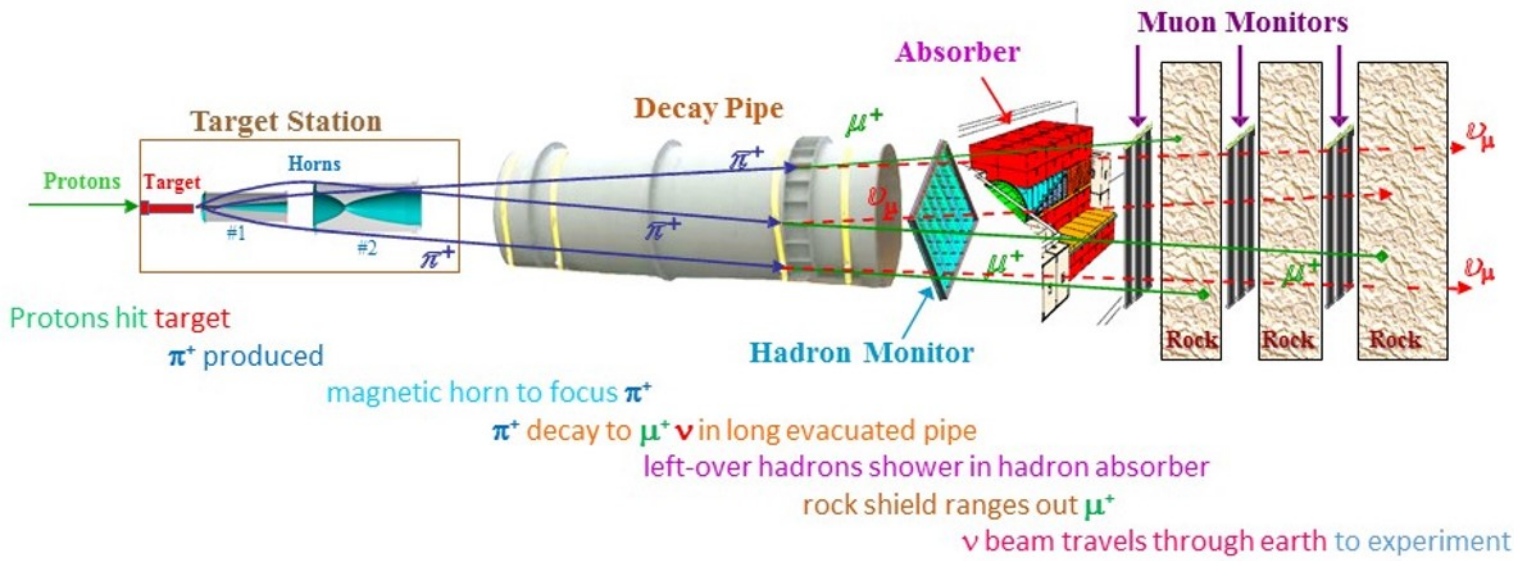


Figure 2.3: The schematic description of the Neutrinos at the Main Injector (NuMI) facility's beam line with a description of individual stages. The beam travels from left to right. Only the option where $\nu$ originated from $p \to \pi \to \mu + \nu_\mu$ interaction chain is shown, but there are other options, notably $p \to K \to \mu + \nu_\mu$ or $p \to \pi \to \mu \to e + \nu_e + \nu_\mu$. Figure is from NOvA's internal database.

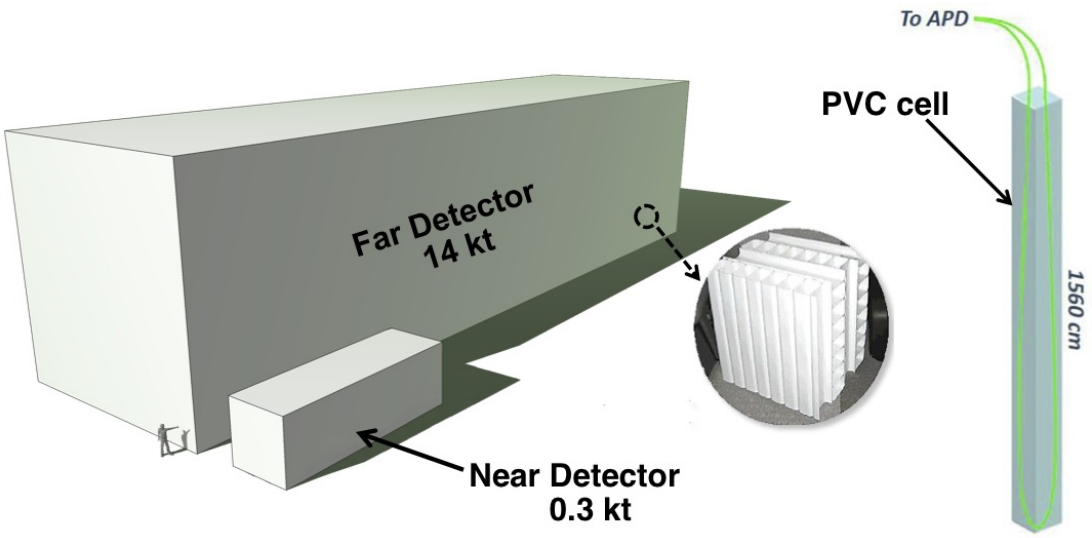


Figure 2.4: Schematic description of scale and composition of the NOvA detectors. Inset showing the orthogonal planes of PVC cells. One cell containing liquid scintillator and a loop of wavelength sifting fibre attached to an avalanche photodiode is also shown [78].

neural network called Convolution Visual Network (CVN) originally based on the GoogLeNet architecture. CVN identifies neutrino interactions based on their topology and therefore without the need for detailed reconstruction [83].

### 2.2.1 Off-axis concept

Both NOvA detectors are positioned 14.6 mrad ($\approx 0.8\,^\circ$) off the NuMI beam axis, giving NOvA a neutrino flux with narrow energy distribution and about 5 times more neutrinos at 2 GeV, than in a case of on-axis position, as shown on fig.2.6 [68].

This is caused by kinematics of hadron and lepton decays into neutrinos. In the rest frame, the decay is isotropic and the neutrinos are mono energetic. Boosting hadrons into laboratory frame gives neutrinos an angle-dependent energy [68, 73]:

$$E_\nu \approx \frac{\left(1 - \frac{m_\mu^2}{m_{\pi/K}^2}\right) E_{\pi/K}}{1 + \gamma^2 \tan^2 \theta} \tag{2.1}$$

where $\theta$ is the angle between the hadron (pion/kaon) direction and the neutrino direction, $E_{\pi/K}$ and $m_{\pi/K}$ are energy and mass of the respective parent hadron and $\gamma = \frac{E_{\pi/K}}{m_{\pi/K}}$.

This relationship between energy of neutrino and it's parent hadron is shown on fig.2.7. Off-axis neutrinos originating from pions have almost constant energies independent on the energy of the parent particle. The narrowness of the off-axis spectra enhances background rejection for a $\nu_e$ appearance analysis [68].

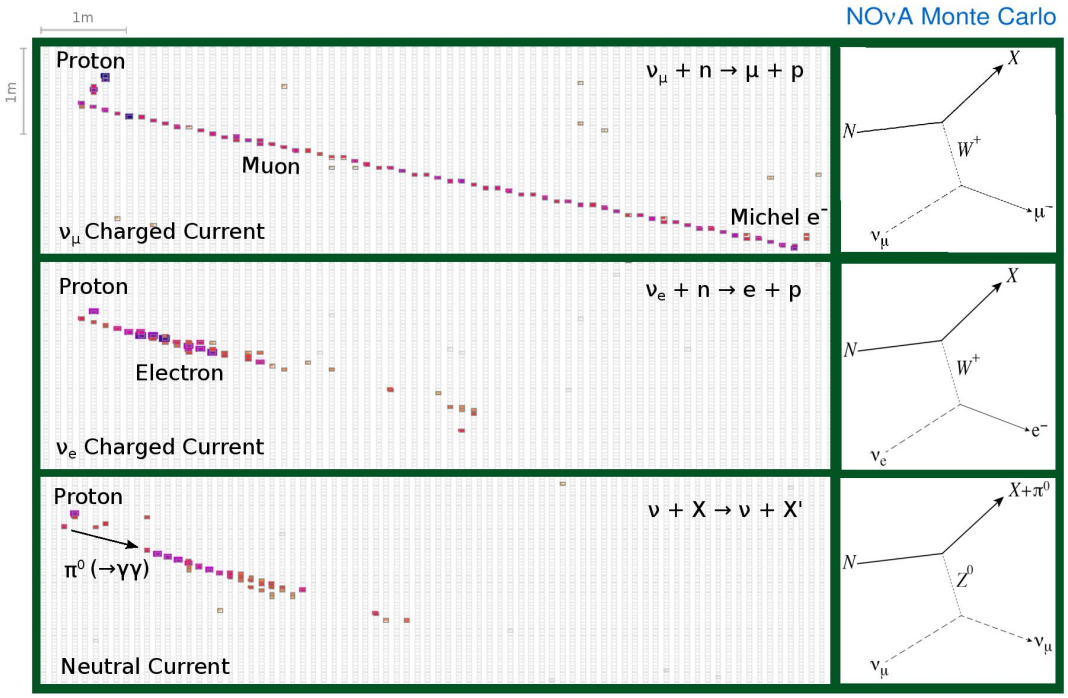


Figure 2.5: Different event topologies as seen in NOvAs detectors with corresponding feynman diagrams. Figure is from [84].

## 2.3 Simulation

NOvA uses GEANT4-based [80] Monte Carlo (MC) simulation called g4numi [75] to calculate the production and transportation of the neutrino flux through the beamline components and ends when a neutrino is created. From there GENIE event generator [85] simulates neutrino interactions in the detector [71] and another GEANT4 simulates the detector response [81].

The simulation starts with a 120 GeV kinetic energy primary proton beam entering the NuMI target [86]. There are often multiple interactions within the target and in the materials downstream of it and since the hadron production process is governed by non-perturbative QCD and occurs in the nucleus, highly accurate theoretical predictions are not possible [86, 75]. NOvA therefore tunes and corrects possible mismodeling of the model using external data in a package developed for MINERvA experiment called Package to Predict the Flux (PPFX) [75]. NOvA also tunes the cross-section model of the GENIE simulation to the ND data to reduce uncertainties in the extrapolation of measurements on the ND to the FD [71].

### 2.3.1 PPFX

PPFX is used to correct each interaction of neutrino's ancestry chain by weighting it with a factor computed from external experimental measurements of yields or invariant differential cross-sections: [75]

$$c_i = \frac{N_i^{data}}{N_i^{MC}}, \tag{2.2}$$

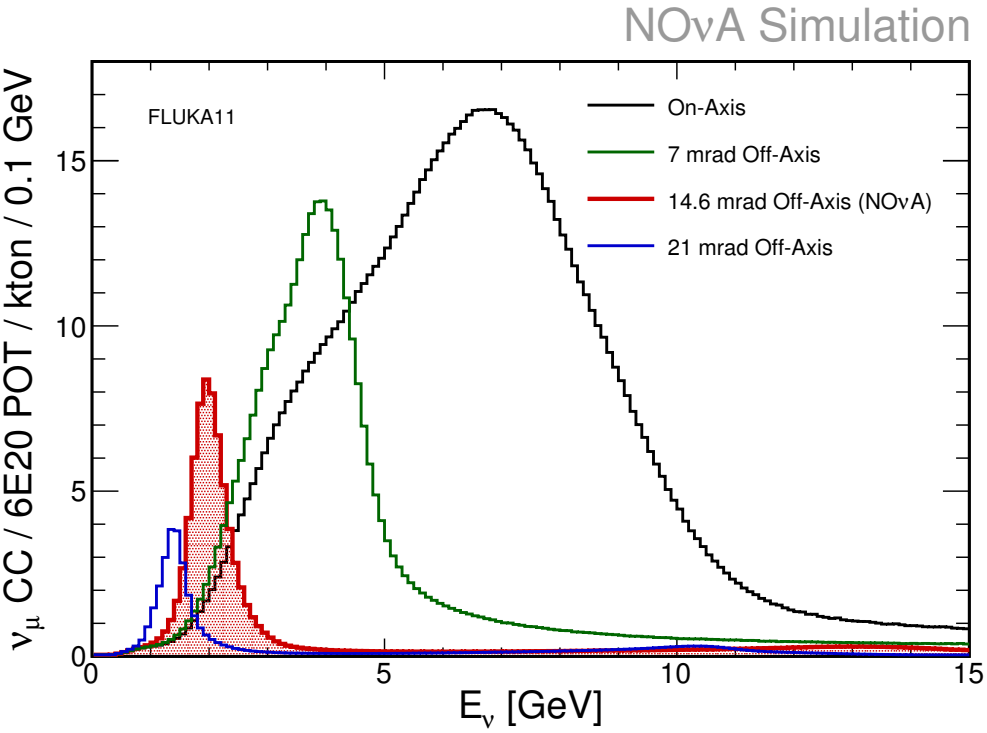


Figure 2.6: Dependence of the neutrino intensity on its energy for four different angles off the main axis. The case for NOvA (shown here in red) shows a narrow peak around 2 GeV, ideal for studying "atmospheric" oscillations driven by $\Delta^2_{31}$ at the NOvA far detector, with still enough intensity. Figure is from NOvA's internal database.

where $i$ denotes either initial or final state.

This weighting factor depends on the identity of prejectile, target, hadrons and also on the initial and final state kinematics [75]. The kinematical distributions of the most dominant hadrons, pions and kaons, after leaving the target, are shown on fig.2.9.

The kinematical values of the initial particles (like the initial 120 GeV proton interacting on carbon in NuMI) are not always the same between the measured interaction and the required values. To solve this we use the *Feynman-x* ($x_F$) scaling variable, which is defined as:

$$x_F \equiv \frac{p^*_\parallel}{p^*_\parallel\,(max)} \simeq \frac{2p^*_\parallel}{\sqrt{s}}, \tag{2.3}$$

where $p^*_\parallel$ is the longitudinal momentum in the center of mass (CMS) frame and it's maximum value $p^*_\parallel\,(max) \simeq \sqrt{s}/2$ ($\sqrt{s}$ is the energy of the CMS). Feynman speculated [87] that expressing the cross-sections of inclusive high energy hadronic collisions in terms of $x_F$ would make the cross-section scaling energy independent [75].

PPFX makes two corrections:

- Attenutation correction,
- Particle production correction.

Attenuation correction is for the probability that a particle interacts (or not) within a material while crossing a distance $r$, while the particle production correction is for the instances when an interaction does happen. This corrections depend on the agreement between the predicted and measured cross-section [75].

There are two main experiments whose results are used in the PPFX. NA49 [88], which used 158 GeV protons interacting on carbon thin target, and MIPP [89] which used protons from the Main Injector and both thin carbon target and the low energy NuMI target (thick target) [90]. Energy scaling of the external data to calculate the PPFX weight is performed by FLUKA and for example for the NA49 data looks like [86]

$$c\left(x_F, p_T, p\right) = \frac{f_{Data}\left(x_F, p_T, p_0 = 158\,\mathrm{GeV/c}\right)}{f_{MC}\left(x_F, p_T, p_0 = 158\,\mathrm{GeV/c}\right)} \times scale\left(x_F, p_T, p\right), \tag{2.4}$$

where

$$scale\left(x_F, p_T, p\right) = \frac{\sigma_{FLUKA}\left(x_F, p_T, p\right)}{\sigma_{FLUKA}\left(x_F, p_T, p_0 = 158\,\mathrm{GeV/c}\right)}. \tag{2.5}$$

For kaons with $x_F < 0.2$ PPFX uses weights based on NA49 measurements[91] and for kaons with $0.2 < x_F < 0.5$ PPFX uses the $K/\pi$ yield ratio from the MIPP thin target measurements[89] multiplied by NA49 thin target yields. $p_T - p_z$ distribution of the PPFX weights for pions and kaons are shown on fig.2.11.

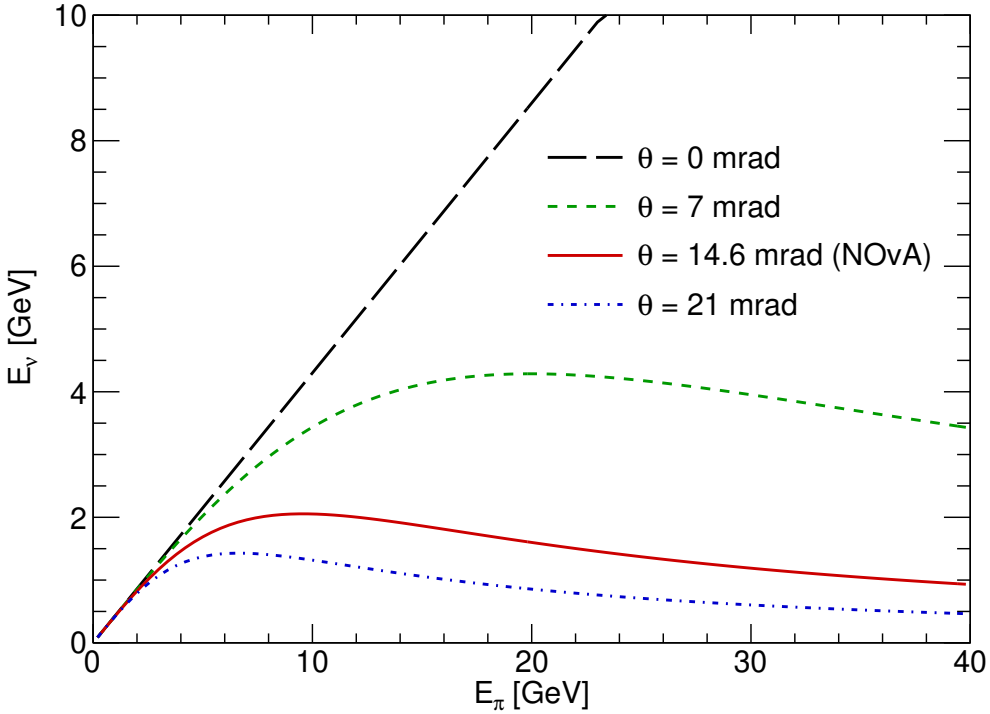


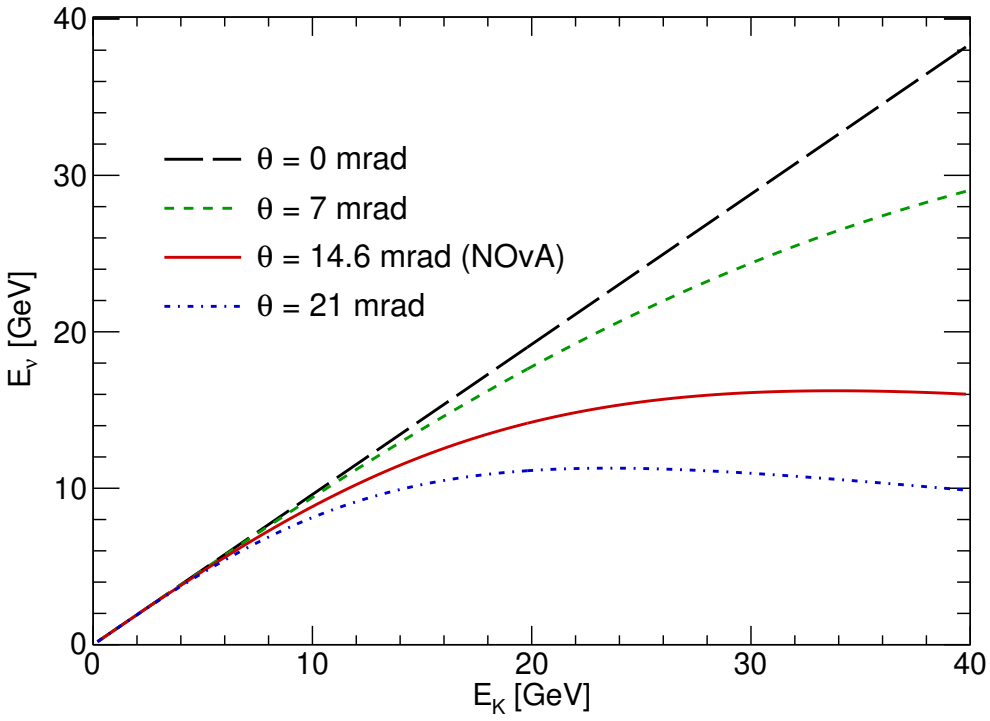


Figure 2.7: Top: Energy dependencies of neutrino on its parent pion for 4 different angles from the main axis. The angle coloured red is the one used in the NOvA experiment where the energy of neutrinos coming from pions flattens to almost a constant close to 2 GeV giving NOvA the desired narrow energy peak.
Bottom: The same plot for kaon neutrino parent. Comparing these plots we can see that neutrinos originating from kaons can have energies $> 2$ GeV comprising the high energy tail of the neutrino spectrum in the NOvA detectors. The plot was constructed using eq.2.1.

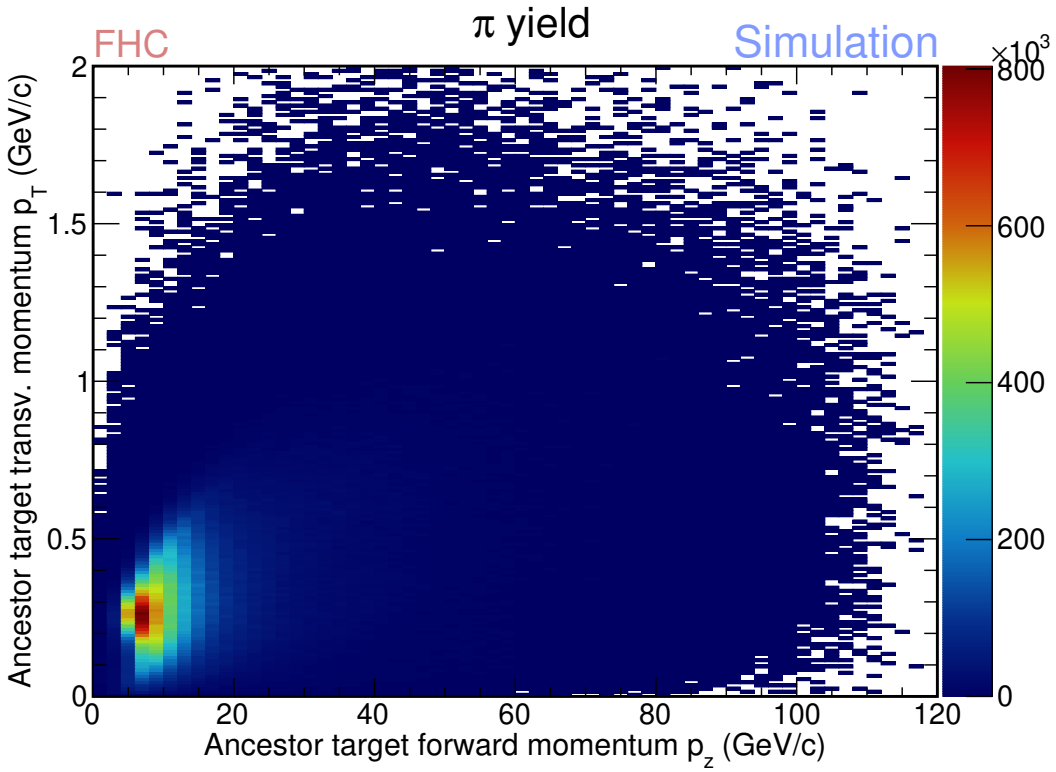


Figure 2.8: Yield of pion ancestors of neutrinos in NOvA detectors in the transverse and forward momentum phase space. This plot depicts pions right after exiting the graphite target. Yield is shown for $14.2 \times 10^{20}$ protons on target.

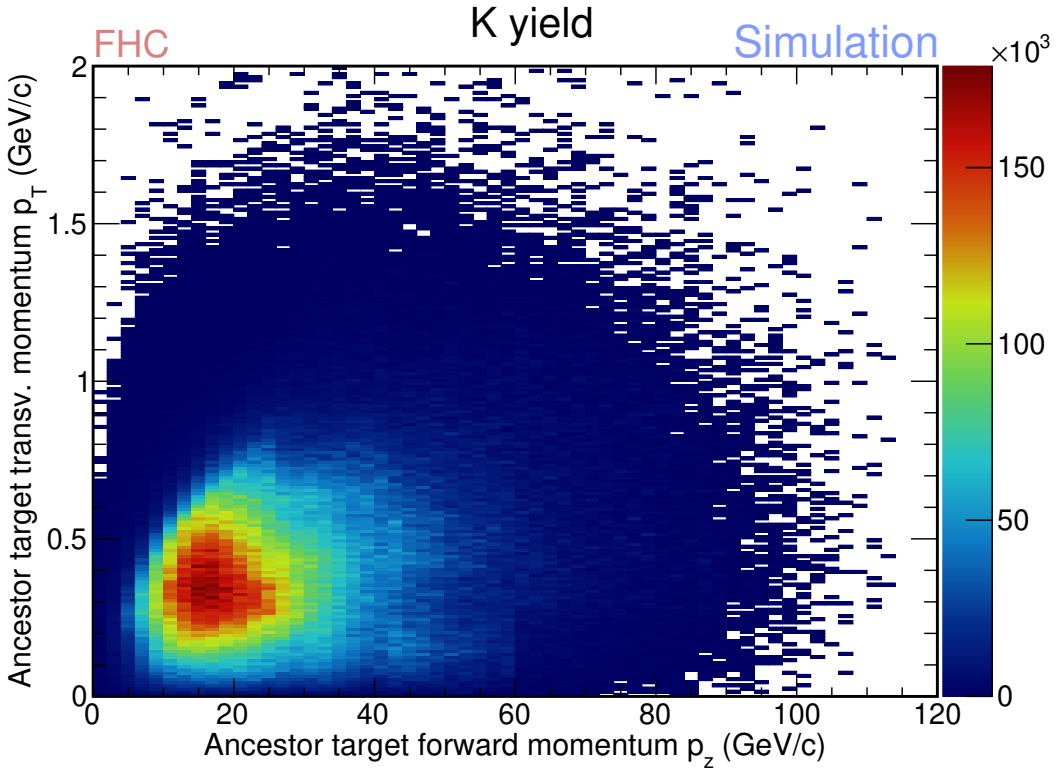


Figure 2.9: Yield of kaon ancestors of neutrinos in NOvA detectors in the transverse and forward momentum phase space. This plot depicts kaons right after exiting the graphite target showing relatively high kaon momentums resulting in neutrinos with higher energies in comparison to neutrinos originating from pions. Yield is shown for $14.2 \times 10^{20}$ protons on target.

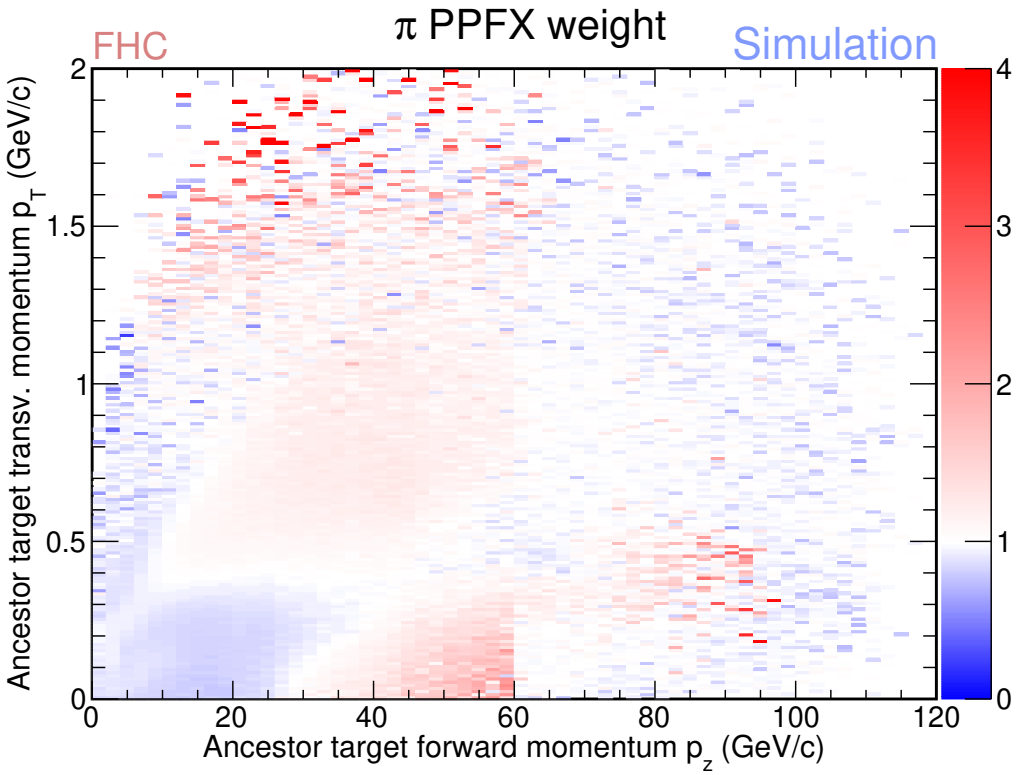


Figure 2.10: PPFX weights of pion ancestors of neutrinos in NOvA detectors in the transverse and forward momentum phase space. There are larger weights than 3.

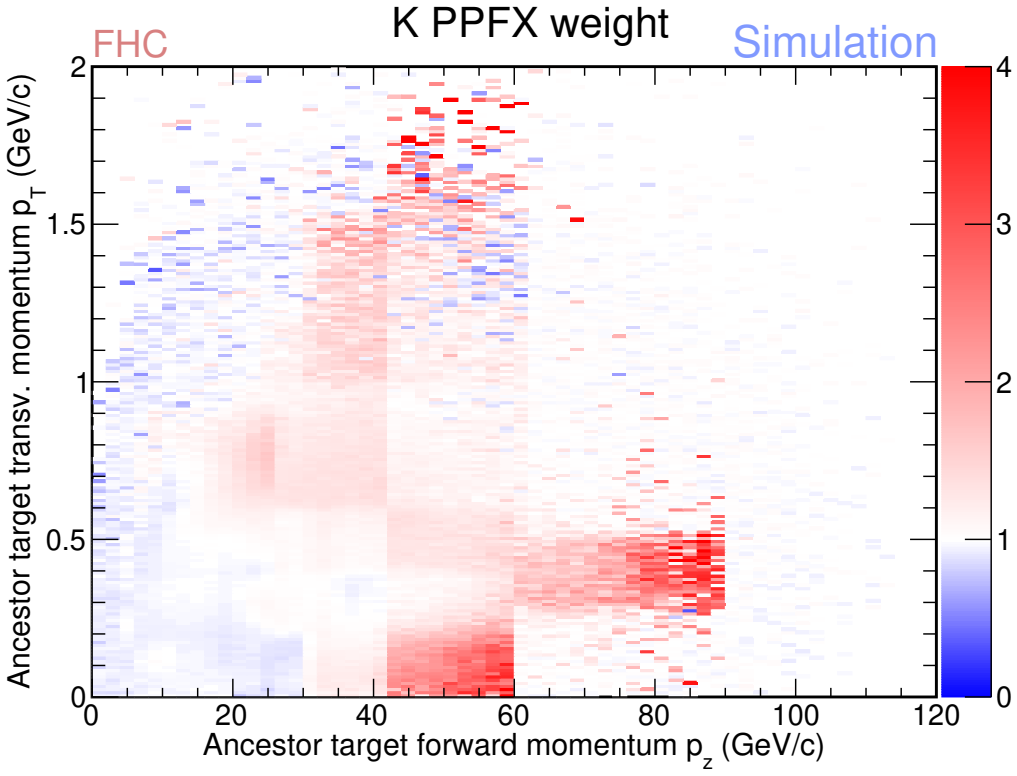


Figure 2.11: PPFX weights of kaon ancestors of neutrinos in NOvA detectors in the transverse and forward momentum phase space.

# 3. Search for the sterile neutrino in NOvA

### 3.0.1 Previous NOvA sterile neutrino searches

Past NOvA searches for oscillations into sterile neutrinos were performed by looking at rate-only depletion (no spectral shape information) of neutral current events between ND and FD, which would be left unchanged if only three active neutrinos participated in oscillations [64]. Previous analysis were restricted to a $\nu_s$ mass range that would not induce oscillations within the ND baseline, since the ND was used as a reference to better constraint the simulation. This can be seen on fig.3.1, where for $\Delta m^2_{41} < 0.5\,\text{eV}$ there are no oscillations in the ND. Using ND to better predict the spectra at the FD helps reduce some systematic uncertainties correlated between the two detectors.

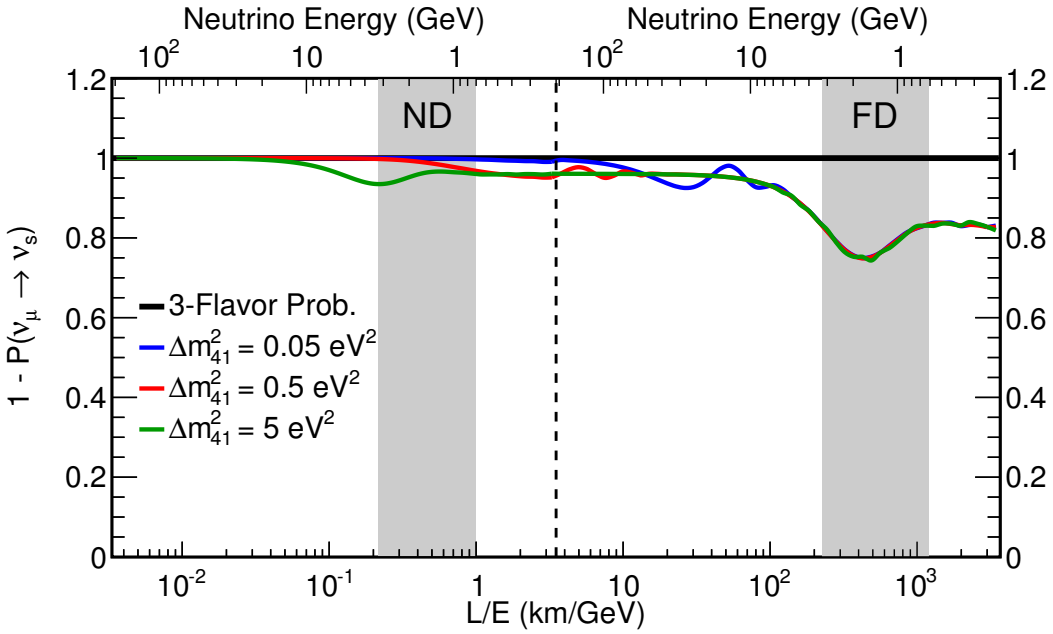


Figure 3.1: Probability of $\nu_\mu$ oscillation into any of the 3 active flavours (i.e. not into sterile neutrino) for NOvA and the effect of changing the sterile neutrino oscillation parameter $\Delta m^2_{41}$ on the probability. The $L/E$ values corresponding to the NOvA near and far detectors are shown. We can see that the oscillations into sterile neutrinos can occur already in the ND if the $\Delta m^2_{41}$ is large enough and that oscillation in the FD don't have sensitivity to $\Delta m^2_{41}$ due to too rapid oscillations. In this plot $\theta_{14} = 0°,\ \theta_{24} = 10°,\ \theta_{34} = 35°$.

The first sterile neutrino analysis looked at neutrinos with energies between 0.5 GeV and 4 GeV in the FHC mode (neutrino mode). The main systematics included difference between ND data and simulation (MC), energy calibration, normalization from data-MC discrepancy from cosmogenic data and reconstruction, uncertainties of cross-sections and neutrino beam. It was published in 2017 [64] and its results are shown on fig.3.2. This result is consistent with 3-flavour mixing within $1.03\,\sigma$.

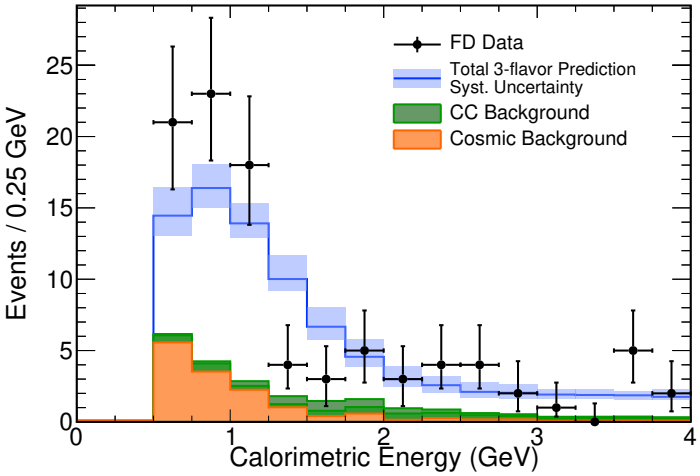


Figure 3.2: Results of the 2017 sterile neutrino search in NOvA using NC disappearance analysis with the FHC flux. This analysis was rate-only and the depicted results are consisted with $3\nu$ flavours [64].

Update in 2018 showed results [92] with more data and better cosmic rejection and NC/CC separation, while looking at data with up to 10 GeV. This result also didn't show any sign of NC disappearance.

In 2019 the first results on sterile neutrino oscillations in the RHC mode (antineutrino mode) [93] were shown (fig.3.3). Experimental uncertainties were similarly large as the neutrino analysis and the results have been consistent with sterile neutrino oscillations. This RHC analysis looked at neutrinos with energies up to 20 GeV

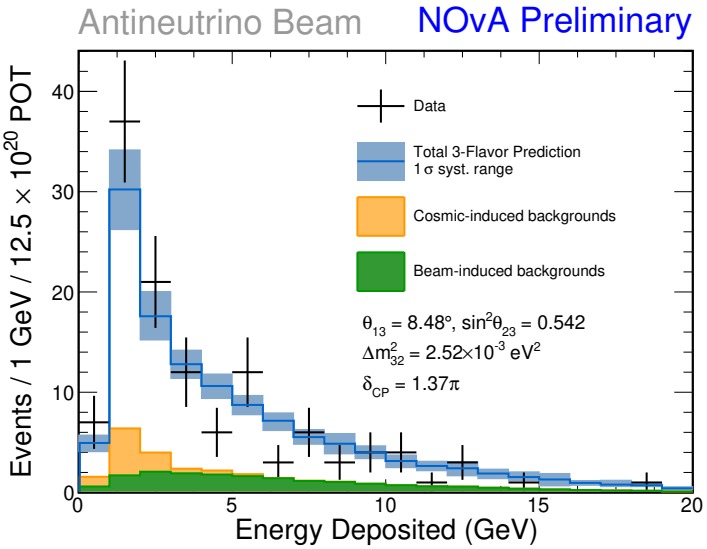


Figure 3.3: Results of the 2019 sterile neutrino search in NOvA using NC disappearance analysis with the RHC flux. These results are consistent with $3\nu$ flavours [93].

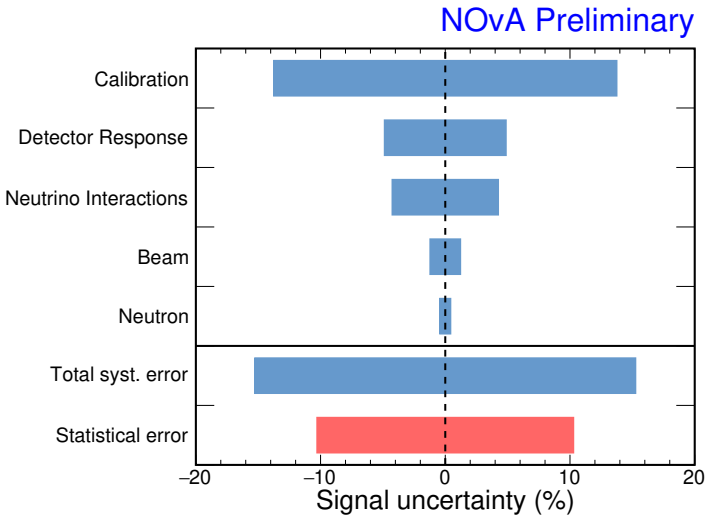


Figure 3.4: Uncertainties of the NC disappearance analysis with the RHC NOvA flux [93].

### 3.0.2 Current NOvA sterile neutrino searches

This thesis shows work done for the currently ongoing analysis, where we want to look at higher values of $\Delta m^2_{41}$, similar to the ones seen in the LSND, MiniBooNE, Reactor Neutrino Anomaly, Gallium Anomaly, or SBL Reactor experiments (see chapter1). In order to do that we need to consider oscillations in both ND and FD. To maintain the cancellation of the correlated uncertainties between the two detectors we use a novel method with a covariance matrix. It combines Poisson likelihood treatment of statistical uncertainties with a Gaussian multivariate treatment of systematic uncertainties [94]. This is similar to the technique recently used by MINOS/MINOS+ [62].

In a standard (3-flavour) analysis we extrapolate ND data-corrected MC to the FD MC. We examine the effect of systematic uncertainties by replacing ND data with systematically shifted ND prediction and follow the same extrapolation procedure to get "corrected" FD prediction. We then compare this FD prediction with directly shifted FD prediction and the remaining disagreement is the relevant systematic uncertainty [95]. This way the correlated systematic uncertainties, like the uncertainty from misprediction of the neutrino flux, almost completely cancels out, which is the huge benefit of a two detector experiment.

However, in our ongoing two-detector NC disappearance analysis, we cannot use the standard extrapolation procedure and some of the systematic uncertainties, that would have only negligible effect on the 3-flavour analysis, make a major contribution for sterile neutrino search. One of these systematics is the beam flux uncertainty, which consists of hadron production uncertainties and beam focusing uncertainties.

Hadron production uncertainties are calculated using PPFX, which was described in the previous chapter. Since the PPFX was build for and is used by multiple experiments, including MINOS, we use the results of the Horn-Off (no focusing of hadron ancestors of neutrinos) study by MINOS, showed on fig.3.5, which was made as a cross-check of the PPFX weights and uncertainties on the unfocused neutrino beam. As can be seen, the PPFX for neutrinos with high en-

ergies at MINOS actually miscorrects the horn-off neutrino flux prediction compared to horn-off data. Since the high-energy neutrino region is dominated by neutrinos with kaon ancestors, we assign an additional conservative 30% uncertainty, which is approximately the disagreement caused by PPFX miscorrection at MINOS, for all neutrinos that have kaon ancestors.

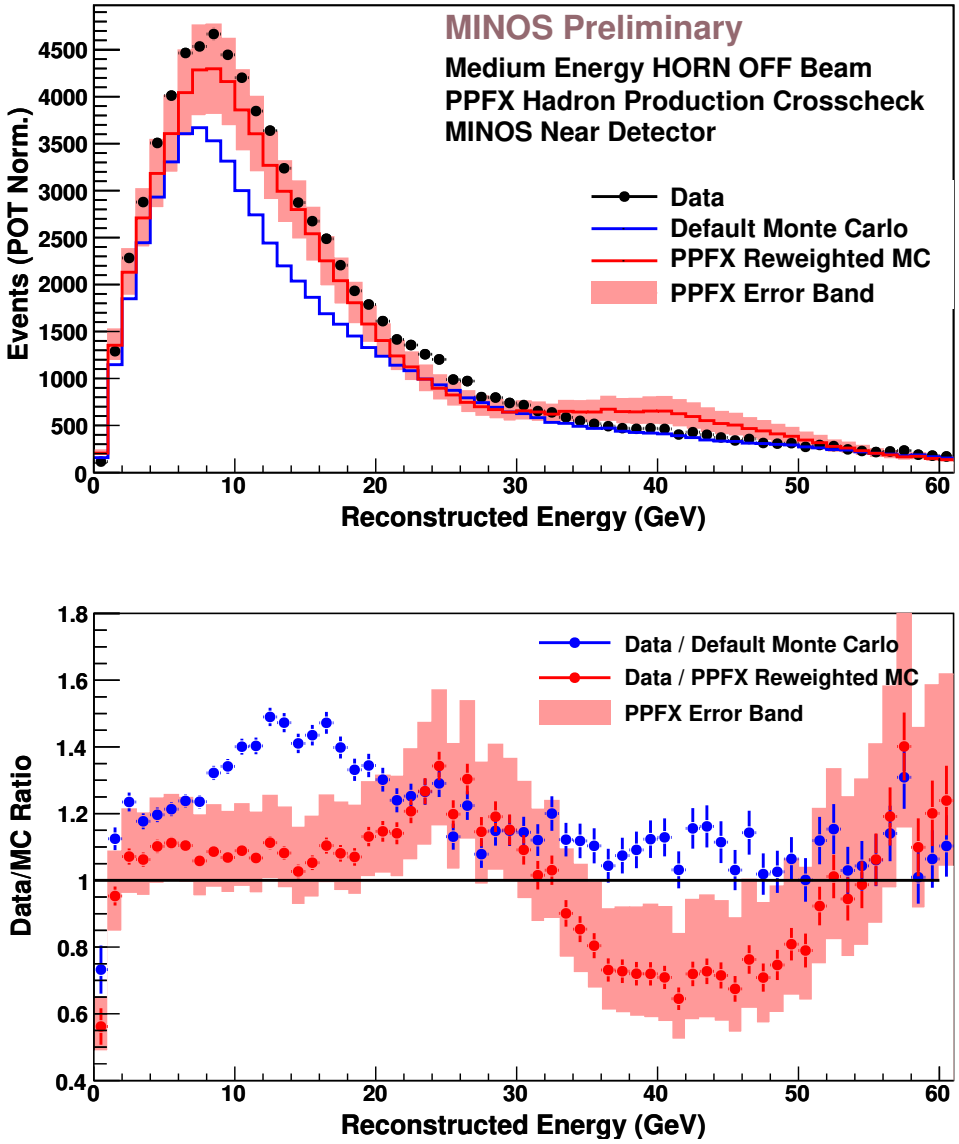


Figure 3.5: MINOS horn-off crosscheck of hadron production correction of PPFX. We can see a miscorrection of PPFX at higher energies, which are dominated by neutrinos with kaon ancestors. This is most likely caused by the lack of good hadron production data for that kaon phase space [96, 97].

We can get a better handle on the sterile neutrino oscillation parameters, if we consider neutrinos in a bigger energy range. We look at neutrinos with energies up to 20 GeV in the current NC disappearance analysis. In plots 3.6 and 3.7 we can see, that higher energies are dominated by neutrinos with kaon ancestors. In our analysis we have up to 10 times bigger relative contribution compared to

the $\nu_\mu$CC and $\nu_e$CC analyses ($\nu_\mu$CC and $\nu_e$CC analyses contain about $3-4\%$ neutrinos from kaons, NC disappearance analysis contains about $20-40\%$). This makes the 30% uncertainty for all neutrinos from kaons a serious contribution to the overall uncertainty.

PPFX hadron production uncertainties, hadron focusing uncertainties and the 30% *kaon* uncertainty make together what we call the neutrino beam uncertainty, which is the largest overall uncertainty and highest uncertainty for neutrinos with energies $> 2\,\text{GeV}$ for our two-detector NC disappearance analysis with covariance matrix. This thesis looks at different ways of reducing the kaon uncertainty.

### 3.0.3 Reducing neutrino beam uncertainty

#### Horn Off for NOvA

Since a major portion of the neutrino beam uncertainty comes from the conservative 30% uncertainty on neutrinos from kaon, which is deduced form MINOS horn-off study, the first idea for reducing it is to reproduce the Horn-Off analysis for NOvA and to see whether the 30% value is justified. However, since we consider oscillations already in the ND, a simple horn-off ND data/MC comparison wouldn't suffice to decide the correct value of the shift for neutrinos from kaons and a more complex analysis is necessary. This is discussed in greater detail in the following section 3.1.

#### ND data fit

There already is a technique utilized by NOvA for estimating the portion and reducing the effect of kaon-originated neutrinos. It is called Beam Electron Neutrino Decomposition (BENDecomp) [98, 99] and it is used in the $\nu_e$CC analysis for better estimation of the beam $\nu_e$ component ($\nu_e$s that are created in the NuMI and not oscillated from $\nu_\mu$s), which is a significant background of the $\nu_e$CC appearance search. This is done by looking at a special kaon-enhanced ND events selection of uncontained $\nu_\mu$CC events ($\nu_\mu$CC events for which the outgoing muon doesn't stop in the detector - i.e. the muon is not contained in the detector). These events tend to have higher energies and therefore bigger contribution of neutrinos with kaon ancestors. These kaon ancestors are the same for the uncontained $\nu_\mu$CC events and for the beam $\nu_e$ events, therefore scaling ND MC to fit uncontained $\nu_\mu$CC data gives us a good estimate of the correct scaling needed to correct the beam $\nu_e$ portion of the neutrino flux.

Using ND data to constraint the neutrino flux would not be so straight forward for the two-detector NC disappearance analysis. The main problem is the possibility of oscillations in the ND, which would require any kind of ND fit to be incorporated into the covariance matrix fit method. Also, the recent MINOS/MINOS+ sterile neutrino search[62] used both NC and $\nu_\mu$CC disappearance, which makes any use of $\nu_\mu$CC data in both detectors for a MC fit undesirable, since we don't want to use the same data for MC fit and analysis. This is an open possibility for the future for NOvA sterile neutrino search.

There is however the possibility of using the horn-off MC and data comparisons, possibly in a horn-on (standard FHC or RHC flux) / horn-off ratio, since

we will not look at horn-off data in any analysis. This is also partially discussed in the following section 3.1.

**Upgrading the PPFX**

We are currently using only thin target external measurements from NA49 and MIPP experiments for the hadron production correction. This measurements do not cover sufficiently the whole parameter space of the NOvA hadron production, especially for kaons, and their uncertainties are relatively high. Thin target measurements are also insufficient for correct thick target prediction and only with the experiment replica target it is possible to achieve flux uncertainties below 5% [100].

There are however new hadron production and other hadron interactions measurements from the NA61/SHINE experiment [101]. NA61 is a CERN spectrometer with one of its goals to measure hadron production for neutrino experiments at J-PARC (T2K experiment) and Fermilab (NOvA experiment). First measurement of $\pi^{\pm}$ and $K^{\pm}$ spectra from proton carbon interaction at 31 GeV/c on a thin target were published in 2011/2012 and latest update, also including $K^0_S, \Lambda$ and $p$ production (also from $p + C$ interaction at 31 GeV/c) was published in 2015 [101]. There are other published results interesting for NOvA and neutrino beam prediction and there are also yet unpublished analyses of $p + C$ hadron production cross-sections at 120 GeV/c (NuMI energy) and even of NuMI replica target. None of these results have been included in the PPFX yet, but given their higher statistics and phase space coverage (compared to data we currently use in PPFX), it is likely that adding them would result in an improvement of hadron production simulation for NOvA, especially for kaons (and therefore for higher energetic neutrino regions) [102].

We can use the horn-off data and MC to cross-check whether adding different new hadron production / interaction cross-sections into PPFX actually helps with correcting the neutrino flux, to decide what kind of data (thin VS thick / MIPP vs NA61 / ... ) we want to add.

## 3.1 Horn-off studies

If we turn off horn focusing of hadron ancestors and parents of neutrinos, we can see the effect of hadron production models and predictions on the spectra. This is the main benefit of the horn-off (0HC) analysis. However, without focusing, the phase space of hadron neutrino ancestors is notably different from focused hadrons. This can be seen on fig.3.8 and 3.10 where the $p_T - p_z$ distribution is shifted towards higher momenta and therefore energies. This is expected, since the lower energy hadrons are not focused as much.

Comparing the phase space plots 3.8 and 3.10 to the off-axis effect on pions and kaons (fig.2.7) it can be seen, that neutrinos with the same energies come from hadrons with different momenta for horn-on and horn-off. Since the PPFX applies weights depending on the hadron energy, this can mean that looking at the effect of PPFX for higher-energetic neutrinos in horn-off does not directly reflect the PPFX effect for horn-on. However, looking at the current PPFX weights in the $p_T - p_z$ phase space for pions (fig.3.9) and kaons (fig.3.11) it can

be seen that the weights for respective phase space in FHC and 0HC are similar in value, but most importantly, in direction (PPFX weights $< 1$). This means that weights for neutrinos from hadrons with higher energies would not cancel out the weights for neutrinos from hadrons with lower energies. Also, since the external data (NA49, MIPP) in PPFX have worse statistics and phase space coverage for higher energies, it can be expected that looking at bigger portion of more energetic hadrons would only results in a worse disagreement of PPFX weighted / unweighted spectra comparison (if there is any disagreement).

There was previously a horn-off analysis in NOvA made by Dr. Anna Holin [96], but it was abandoned in late 2019 due to strange behaviour of the horn-off MC after shifting the analysis to a different production. We uncovered the source of the problem and remade the horn-off MC from scratch to allow us to use it properly.

There was a special NOvA run with horn-off in June 2015 and then again in October 2015. However, the latter one had too low POT (too low statistics) so we decided to not include it in our analysis. We based our horn-off simulation on the real conditions during the horn-off data taking (real horn current, real positions of beam instruments,...), while in previous NOvA horn-off analysis, the MC was based on ideal conditions, which was most likely the main cause of the problems. We also included a proper treatment of rock events, i.e. a special sample of horn-off neutrinos that interact in the rock surrounding the ND and particles resulting from this interaction might be mistaken for particles from interactions inside the detector. In the previous analyses the rock events simulation was either not made at all, or made with an FHC setting. We will use rock events below in the energy containment analysis.

### 3.1.1 Events selections for Horn-Off analysis

Since the results of the horn-off analysis should not qualitatively depend on the event selection used, we have looked at several different selection. Since we are most interested in the NC disappearance analysis application of the results, we will show the results for the standard NC events selection used in the ongoing analysis and for our new special NC selection for horn-off, which has looser fiducial cuts (energy and events containment in the detector) and looser PID (CVN) cut, since there are only low statistics for horn-off and we want to keep in as many events as is reasonable. Also, since the horn-off data and prediction only exists (and makes sense) for the ND, we focus only on the ND selections.

We could also look at $\nu_\mu$CC and $\nu_e$CC selections, for example the BENDecomp selection that has an enhanced contribution of kaon originated neutrinos, but the $\nu_\mu$CC and $\nu_e$CC energy estimator are created solely for contained events in FHC or RHC mode and are not directly applicable to our analysis. It would be possible, however, to create a special energy estimator for horn-off spectra, which is the plan for future improvements of the horn-off analysis. For the NC events, we use the FHC NC energy estimator created for the ongoing analysis, since it has been shown that it works very well for both horn-on FHC and for horn-off events.

**Standard NC selection**

The standard ND NC events selection of the current analysis requires events to have vertices inside a loose fiducial volume (volume inside the ND, without the detector edges and the muon catcher), to pass a loose PID cut and to not pass the standard $\nu_\mu$CC and $\nu_e$CC selection. This is to reject the most apparent background events and to ensure mutual exclusion of the different analyses. This part of the selection is called the NC ND preselection.

Events that pass the preselection are further required to have at least one reconstructed vertex and at least one reconstructed prong that spans at least two continuous planes. This is called the NC quality cut and further rejects easily recognizable background events.

To include only events that have energy well contained within the detector and to reject rock events, we apply the fiducial cuts, which can be viewed as specifying a volume inside the ND for vertices and all parts of prongs, which correspond to events that satisfy our conditions.

On top of the previous cuts, we apply the NC PID cut using a CVN variable. Since we are performing a two detector fit, we choose the correct value of the cut jointly for ND and FD. This results in a very strict cut for ND (and therefore very pure selection of ND NC events), which is not a problem for the standard analysis, which has got a substantial number of data available at the ND.

The standard NC selections was developed by other NOvA collaborators and is not part of this thesis results.

**Special higher statistics NC selection for Horn-Off**

Requirements put on the NC events in the standard selection significantly reduce number of events available in the ND. While for the standard (FHC or RHC) analysis this is not too big of a problem, the horn-off data have only very limited set of events and any unnecessarily conservative cut reduces the significance of the obtained results. We have therefore made a new NC selection, that has kept the preselection and quality cuts of the standard selection, but has looser fiducial and PID cut.

We have looked at the distribution of vertices for true NC events and true NC rock events on fig.3.13, 3.14 and 3.15. We want to find the best place to cut to achieve a sample with low rock events content (red plots) and high true NC content (blue plots). The dotted lines on the plots are the vertex part of the fiducial cuts for the standard NC selection. The greyed area marks the new cuts we place to achieve more statistics without significantly reducing sample quality.

We have also selected a new CVN cut, shown on fig.3.16. We looked at the $signal/\sqrt{signal + background}$ figure of merit, shown as a purple line on the plot, and the CVN variable value at which it reached its maximum is the new CVN cut. In our case this value is 0.35.

### 3.1.2 Data/MC ratio results

We want to reproduce the PPFX crosscheck result from MINOS (fig.3.5) and see whether the PPFX weights miscorrect our MC prediction the same way as was seen on MINOS.

Besides the PPFX weights, in the standard 3-flavour analysis we also apply cross-section (XSec) weights, which are a theory and experimental data based corrections of the neutrino interaction simulation, similarly to how the PPFX weights are the neutrino beam prediction corrections. Result spectra can depend both on PPFX weights and on XSec weights and a possible miscorrection in the horn-off sample can be due to either of those not working properly. That is why we are showing results for both XSec weighted and unweighted spectra, to be able to disentangle the possible effect.

We are showing three different energy binnings of the spectra histograms. One is the standard NC disappearance binning, which is inspired by the statistics and the bins are getting progressively larger with energy. Second is another statistics inspired binning, where the energy region is divided into four regions with different bin sizes. This is the binning that was used in the previous Horn-Off analysis by Dr. Anna Holin. Third binning is an equidistant (simple) binning, where each bin corresponds to 1 GeV, but high energy bins have high statistical uncertainties.

In the plots 3.17, 3.18, 3.19 and 3.20 we show data/MC comparisons for different binnings and selections described above, including XSec weights. In plots 3.21, 3.22, 3.23 and 3.24 we show the same ratios, but without applying XSec weights. On these plots we can see that there is no visible significant disagreement between horn-off data and MC and most of the disagreement lies within the range of PPFX uncertainties shown as peach areas. We also don't see the PPFX miscorrection that was seen on MINOS and that is the source of the 30% kaon uncertainty. Plots without applied XSec weights do not differ significantly from the plots with applied XSec weights, so the discrepancies would be mostly caused by other factors than the XSec weights.

What we do for sterile neutrino analysis in NOvA is to take into account both PPFX systematic uncertainties and an additional 30% kaon systematic uncertainty. We are showing these two uncertainties on the ratio plots 3.25 and 3.26 (with XSec weights) and 3.27 and 3.28 (without XSec weights). We are showing results only for the standard NC binning, but for both NC selections. From these plots we can see that the two uncertainties are largely similar and using both of them is to a large extent double-counting of the same uncertainty.

Without including ND oscillations into these plots, we can't yet confidently say what should be the correct value of the kaon uncertainty, or whether it should be discarded completely and only the PPFX should be kept. A possible solution to this and a way to qualitatively decide on the correct value of the kaon normalization would be to do a horn-on / horn-off data / MC double ratio and fit it with a kaon normalization as one of the parameters. We can also look at the horn-on / horn-off oscillated / unoscillated double ratio and see how much does it change with different oscillation values. If it doesn't change much, the oscillations would not influence the horn-on / horn-off ratios and we could use the horn-off results even without considering ND oscillations.

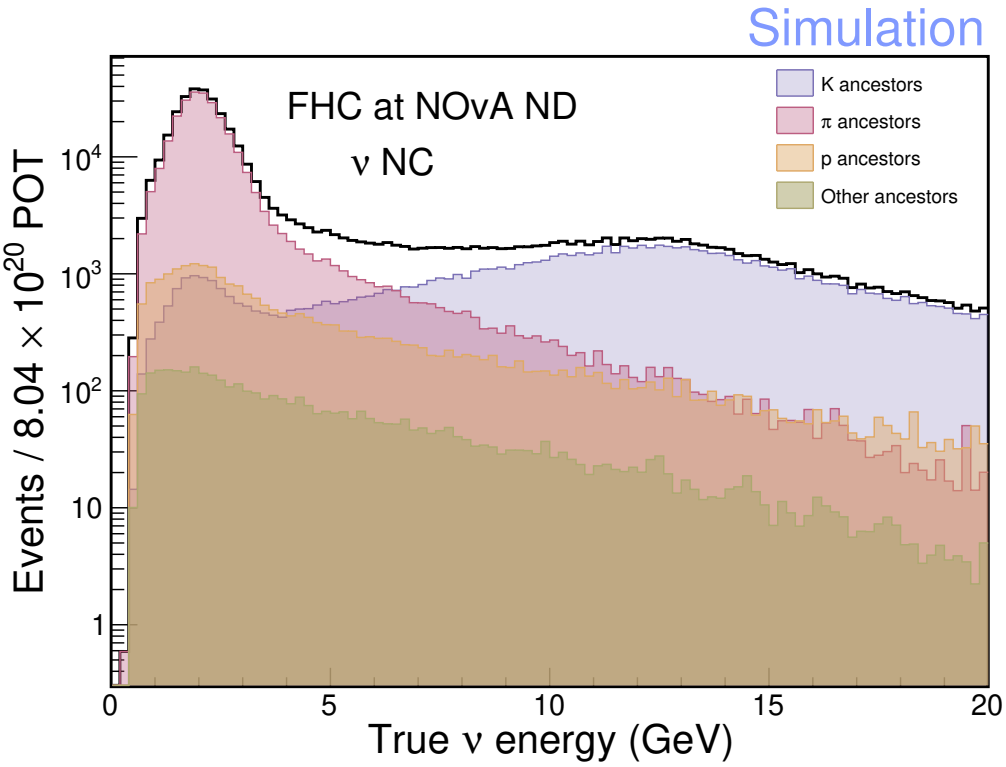


Figure 3.6: NOvA ND spectrum for FHC with different neutrino ancestors (off-target hadrons that later on produce the neutrino). This spectrum corresponds to the selection of NC events showing high contribution of neutrinos originating from kaons. Scaled to the official ND neutrino flux for the 2018 analysis.

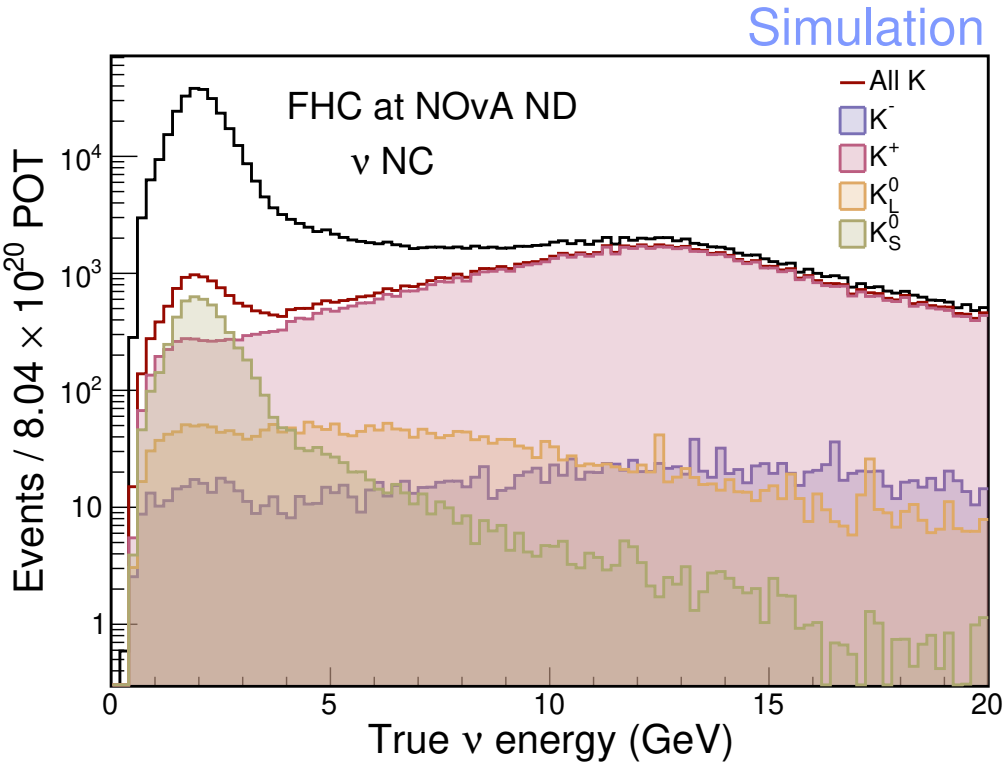


Figure 3.7: Decomposition of the kaon part of the previous spectra into different kaon types.

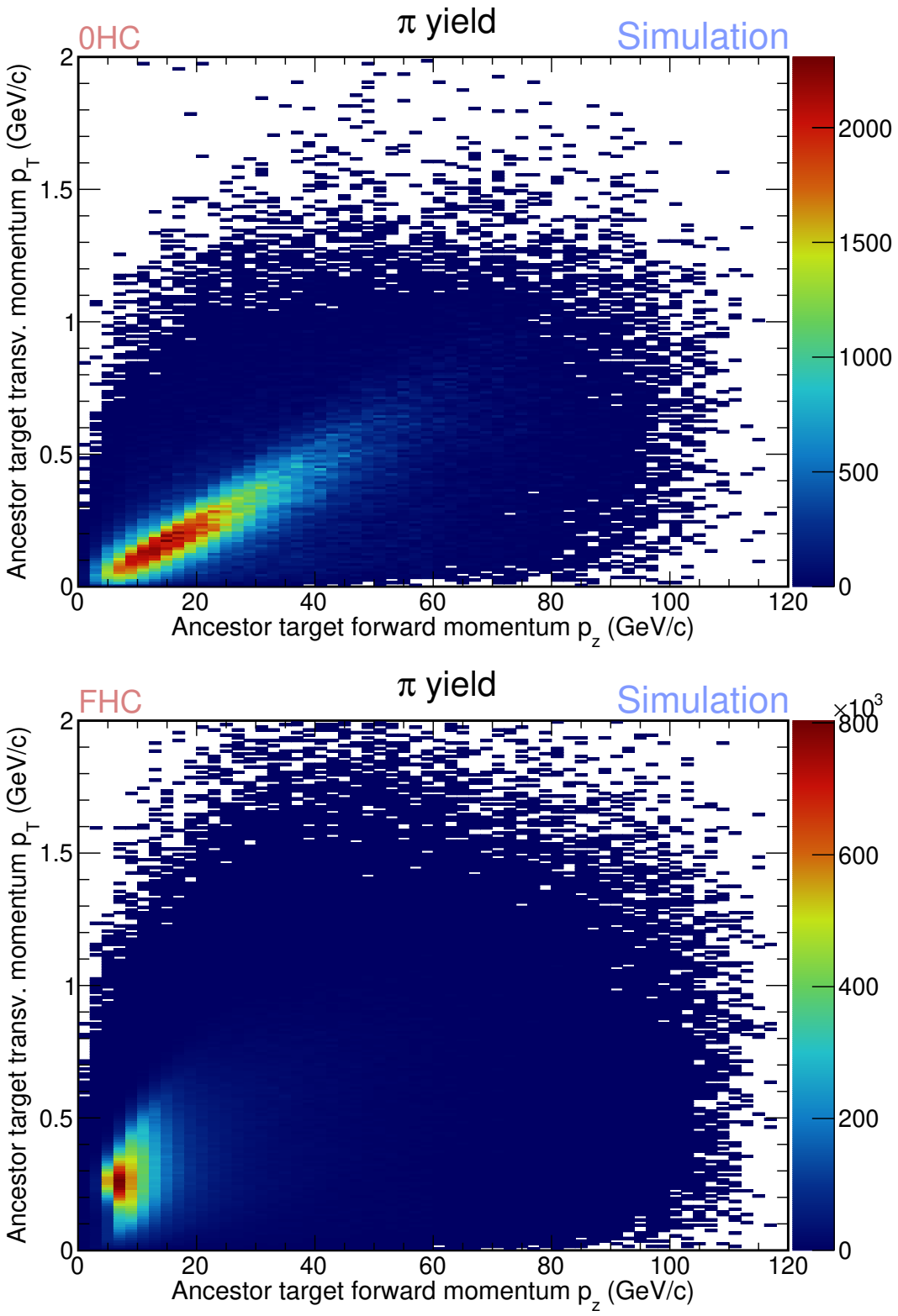


Figure 3.8: Comparison between horn-off and horn-on pion ancestor off-target momentum distribution.

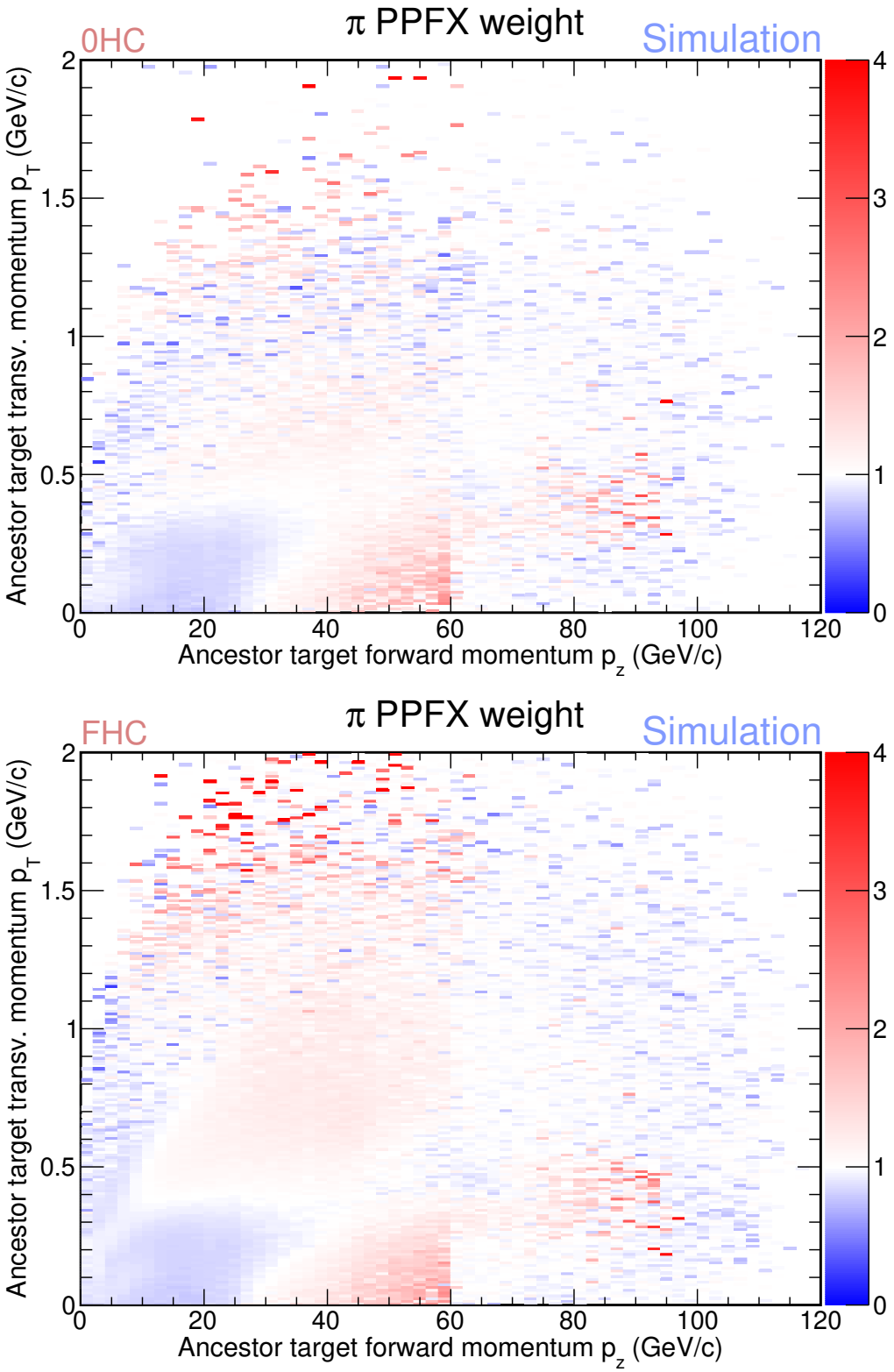


Figure 3.9: Comparison between horn-off and horn-on pion ancestor off-target momentum distribution. White spaces mean either no events or no PPFX weights.

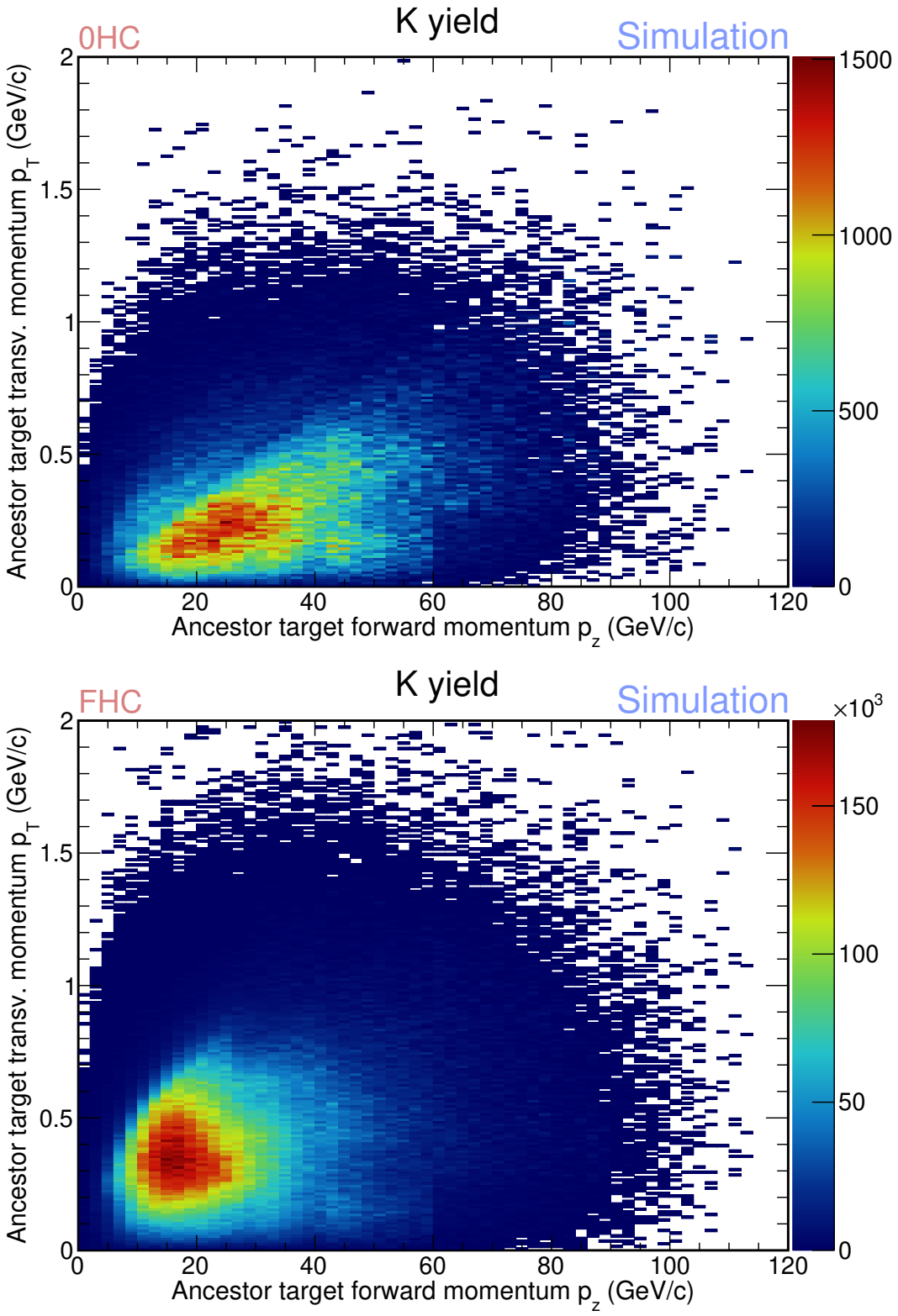


Figure 3.10: Comparison between horn-off and horn-on kaon ancestor off-target momentum distribution

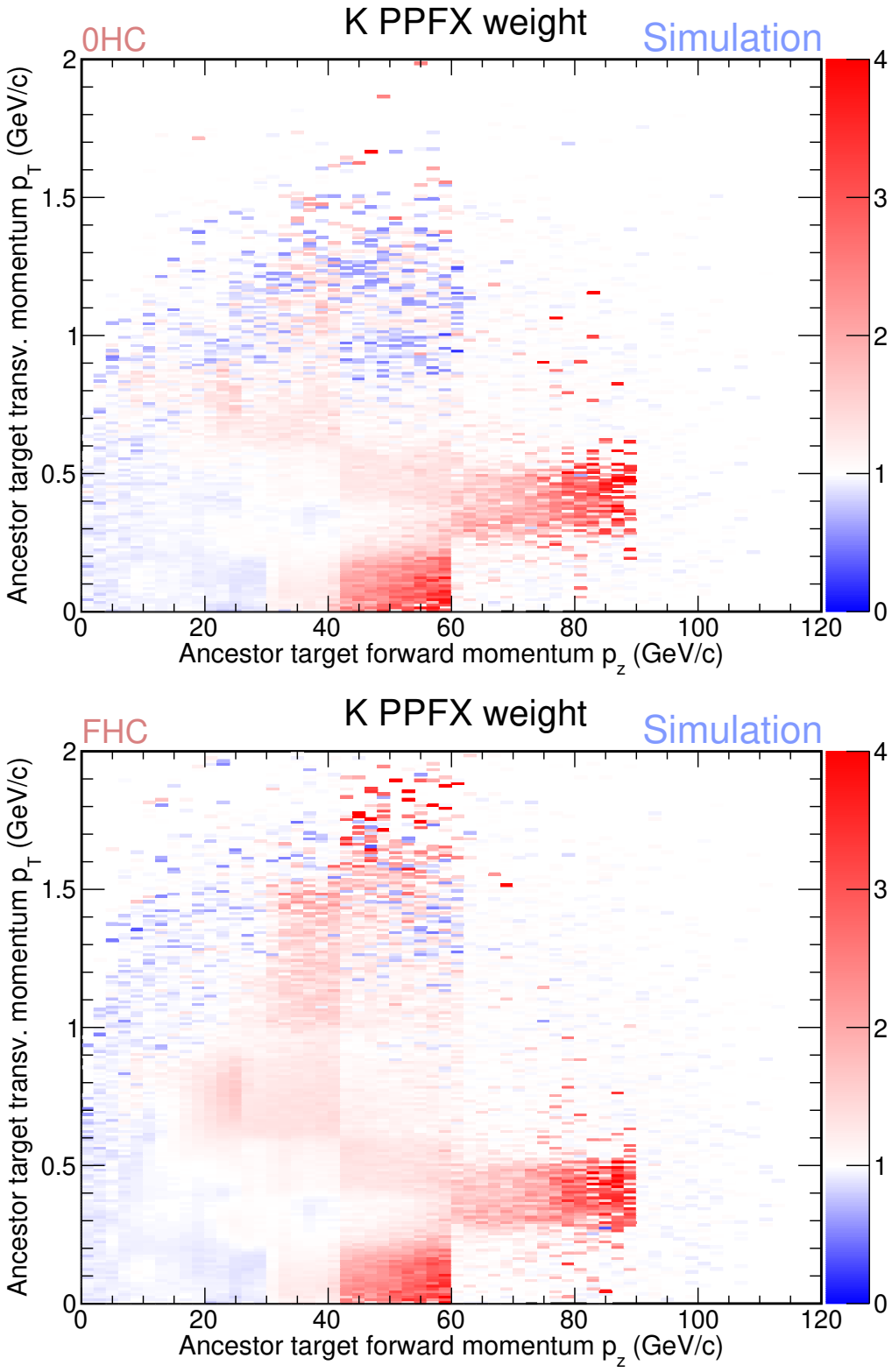


Figure 3.11: Comparison between horn-off and horn-on kaon ancestor PPFX weights. White spaces mean either no events or no PPFX weights.

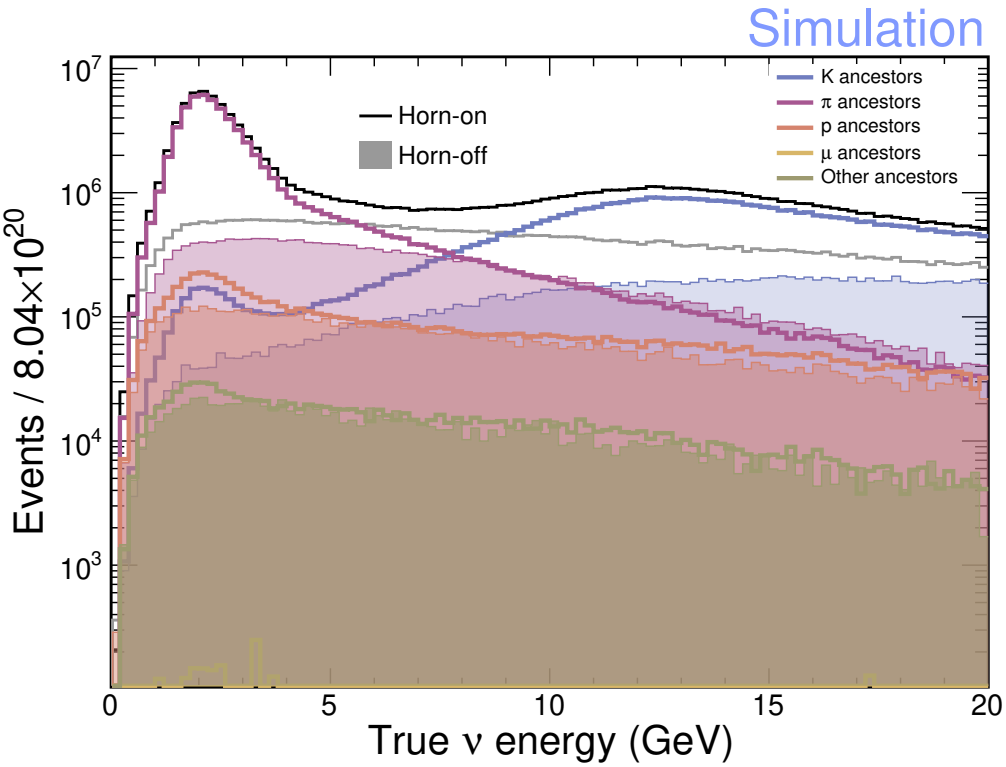


Figure 3.12: Ancestor composition and comparison between FHC horn-on and horn-off samples. The relative composition of different neutrino ancestors remains more or less the same for horn-off, as is for horn-on. There is a tendency for $\pi$ and $K$ ancestors to have lower relative composition for horn-off and for proton ancestors to increase their contribution to the 0HC neutrino spectra.

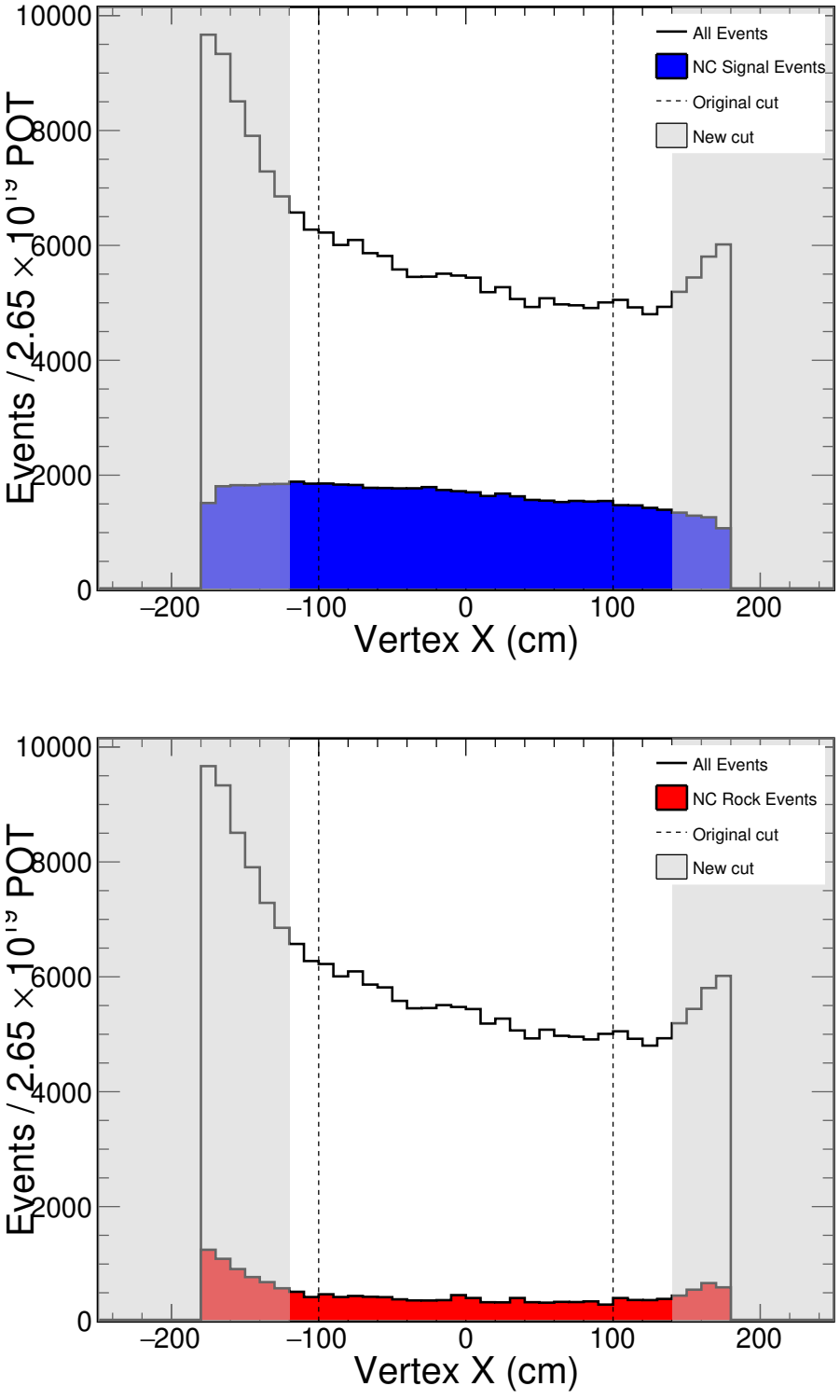


Figure 3.13: Distribution of vertex X position for TrueNC events (top) and True NC rock events (bottom). Rock events are events that interacted outside the detector. The NC preselection and quality cuts are already applied. Dotted lines are the cuts for the standard NC analysis and the greyed area is for the new horn-off NC selection. We are placing the new cuts such that we maintain low rock events content and high NC content.

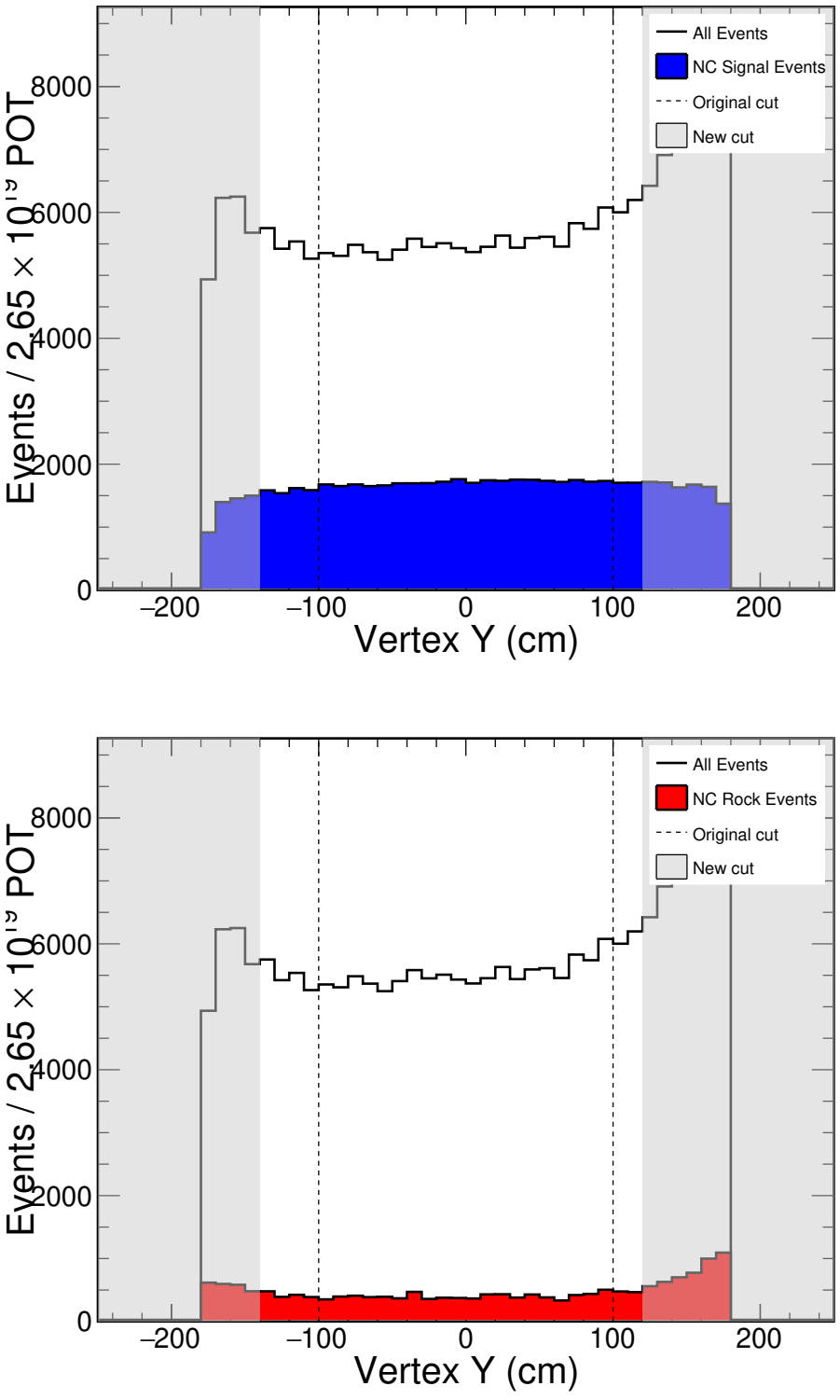


Figure 3.14: Distribution of vertex Y position for TrueNC events (top) and True NC rock events (bottom). Rock events are events that interacted outside the detector. The NC preselection and quality cuts are already applied. Dotted lines are the cuts for the standard NC analysis and the greyed area is for the new horn-off NC selection. We are placing the new cuts such that we maintain low rock events content and high NC content.

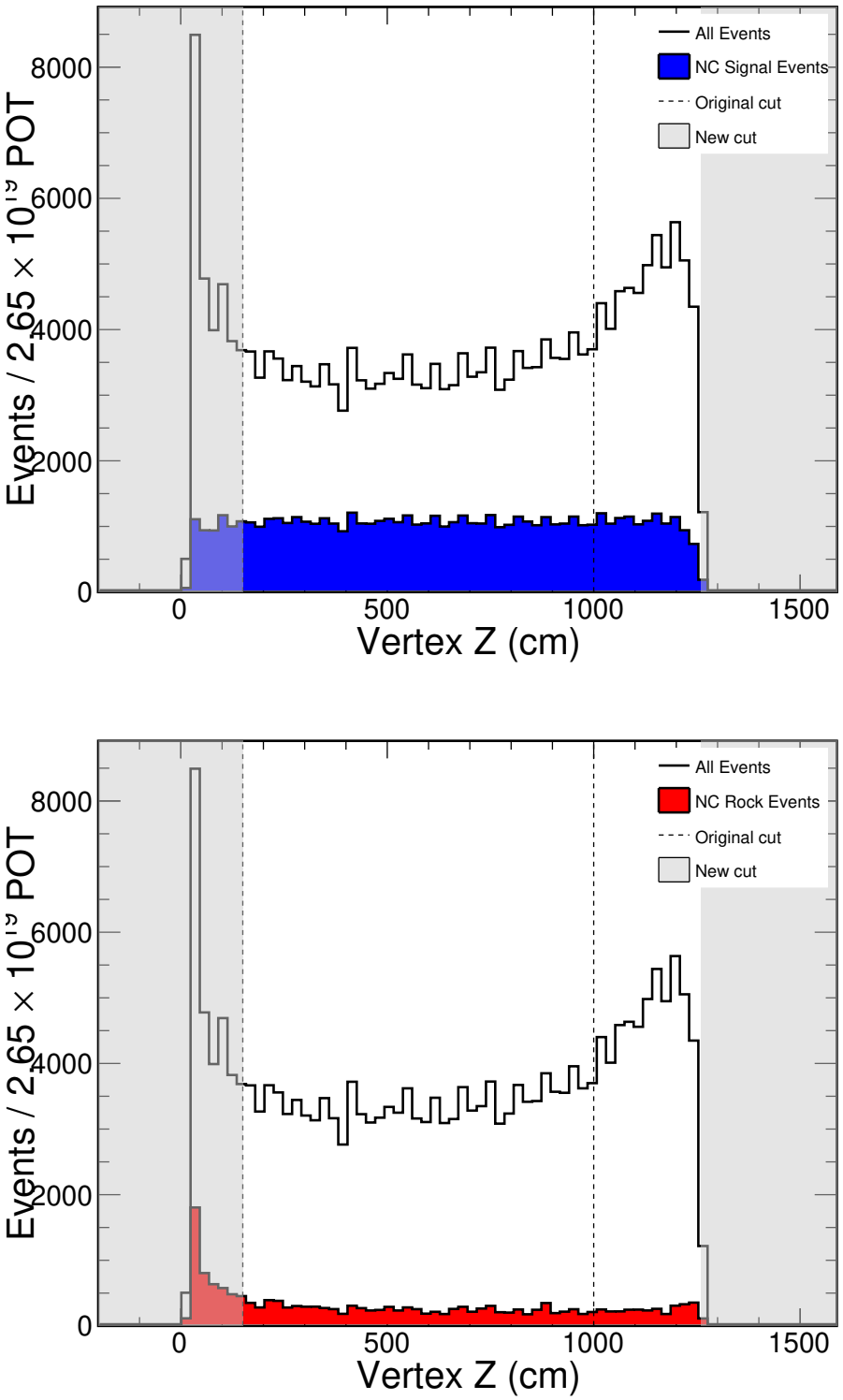


Figure 3.15: Distribution of vertex Z position for TrueNC events (top) and True NC rock events (bottom). Rock events are events that interacted outside the detector. The NC preselection and quality cuts are already applied. Dotted lines are the cuts for the standard NC analysis and the greyed area is for the new horn-off NC selection. We are placing the new cuts such that we maintain low rock events content and high NC content.

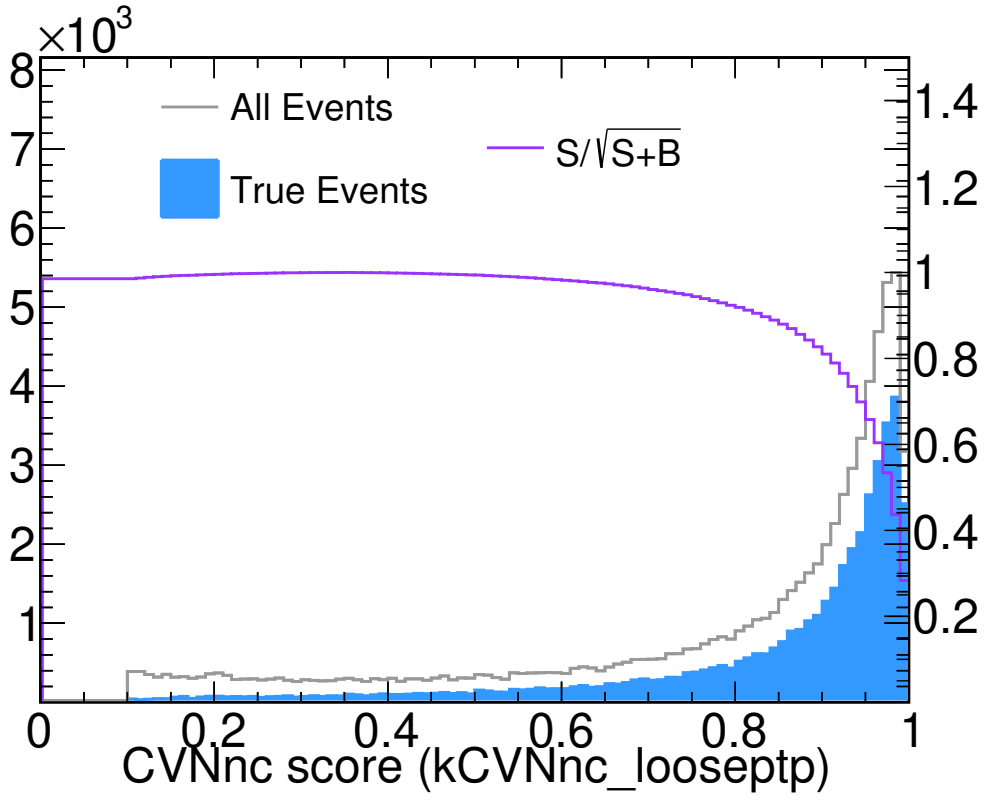


Figure 3.16: CVN selection for the new horn-off NC ND selection. We are showing a histogram for all events and for true NC events (signal). Background is the difference between all events and true NC events. The cut value is determined based on the maximum value of the figure of merit $signal/\sqrt{signal + background}$. In our case the CVN value is 0.35.

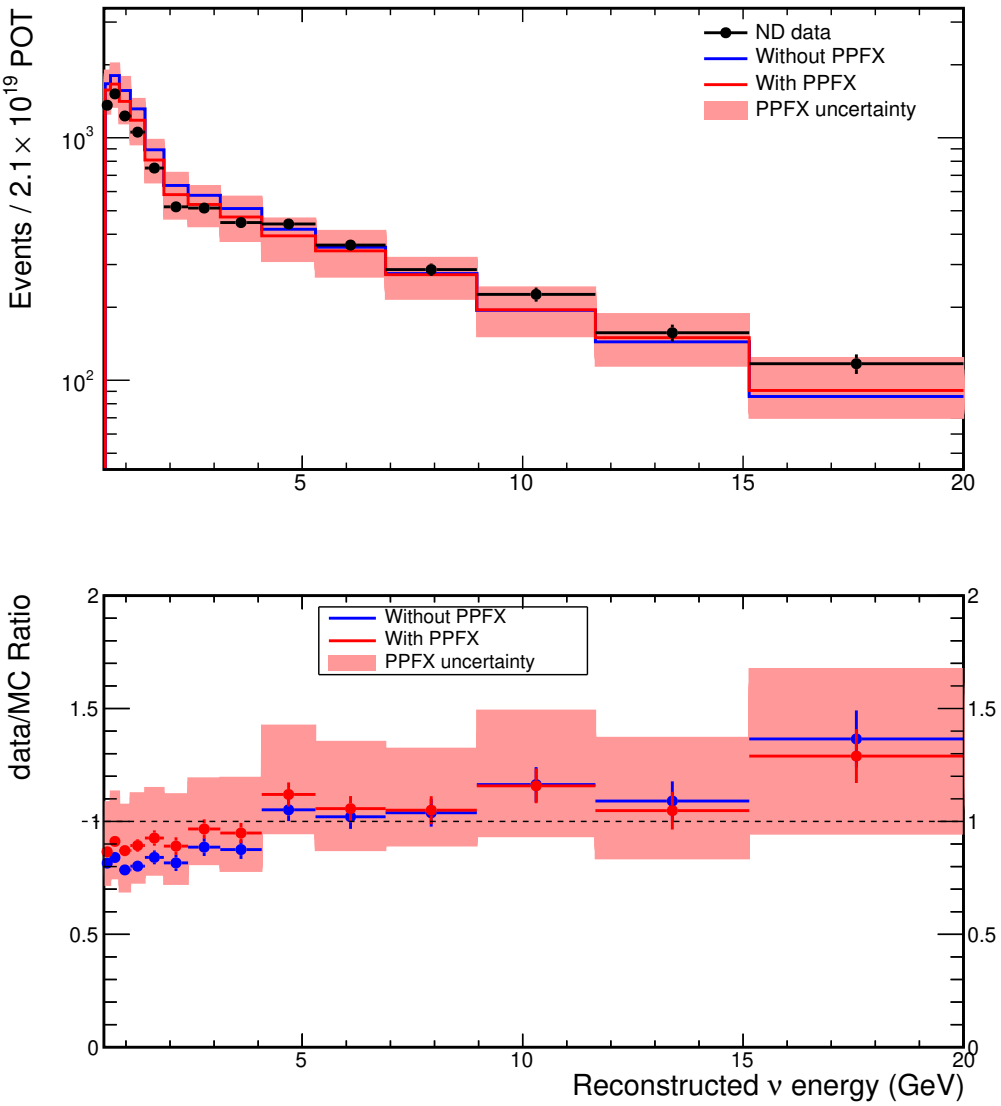


Figure 3.17: Horn-Off results of data/MC ratio for special Horn-Off NC selection and standard NC binning with applied cross-section weights.

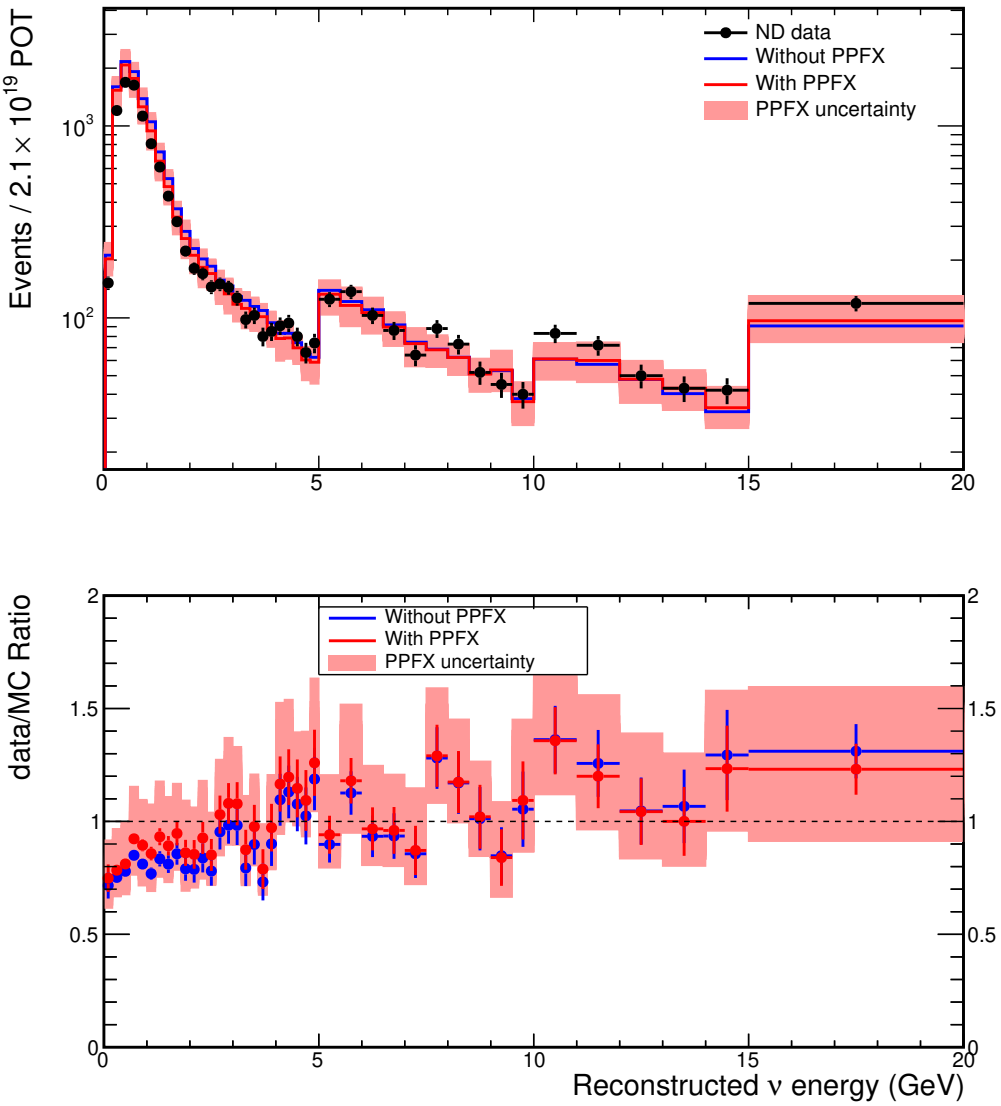


Figure 3.18: Horn-Off results of data/MC ratio for special Horn-Off NC selection and special horn-off NC binning with applied cross-section weights.

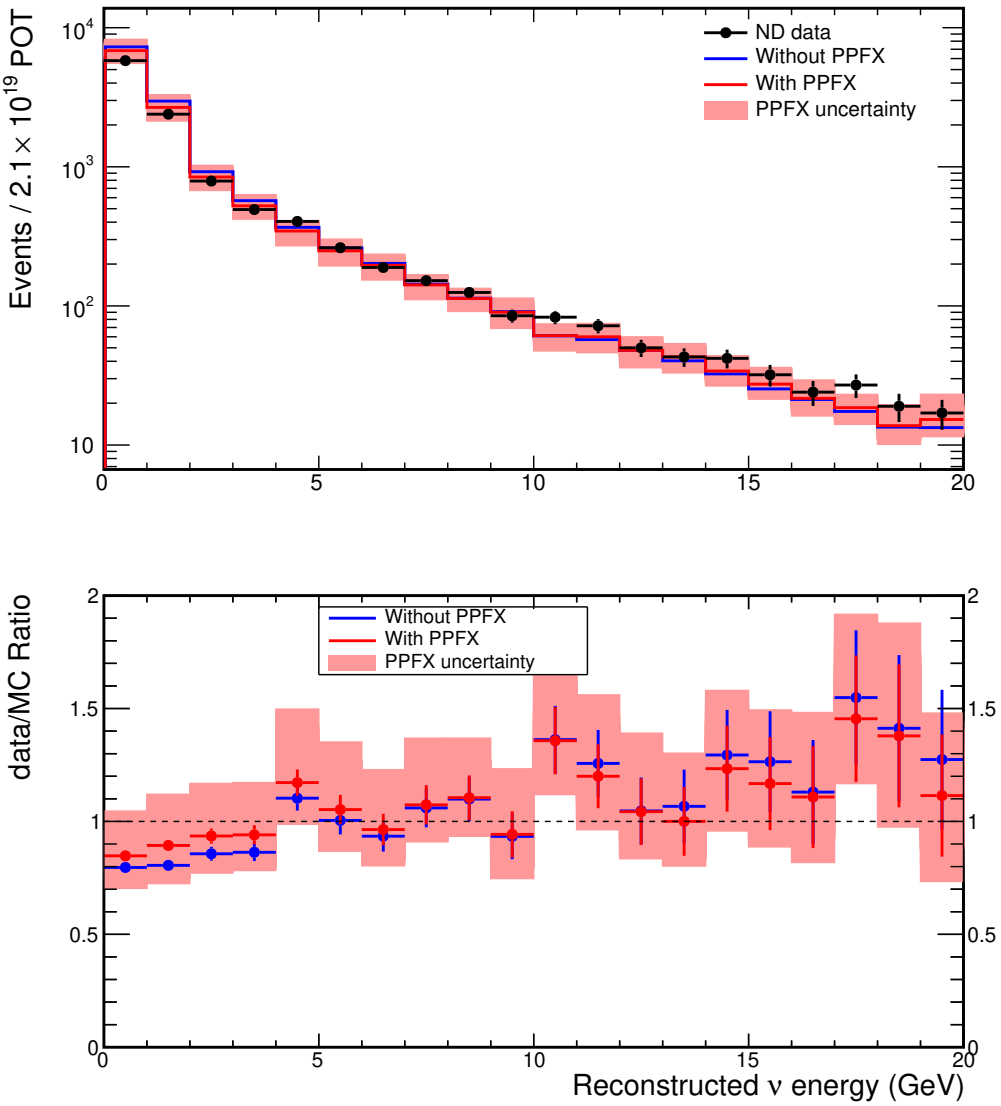


Figure 3.19: Horn-Off results of data/MC ratio for special Horn-Off NC selection and simple binning with applied cross-section weights.

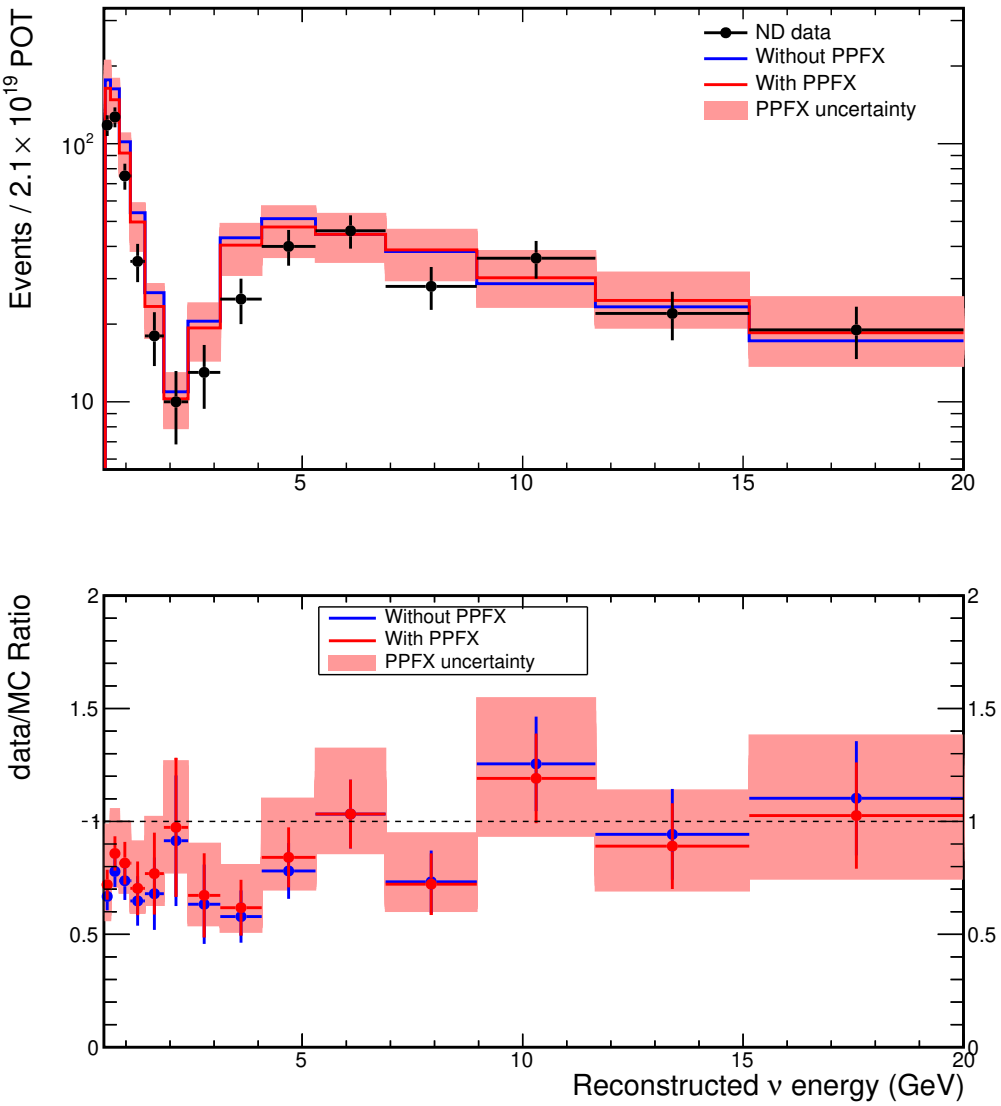


Figure 3.20: Horn-Off results of data/MC ratio for standard NC selection and standard NC binning with applied cross-section weights.

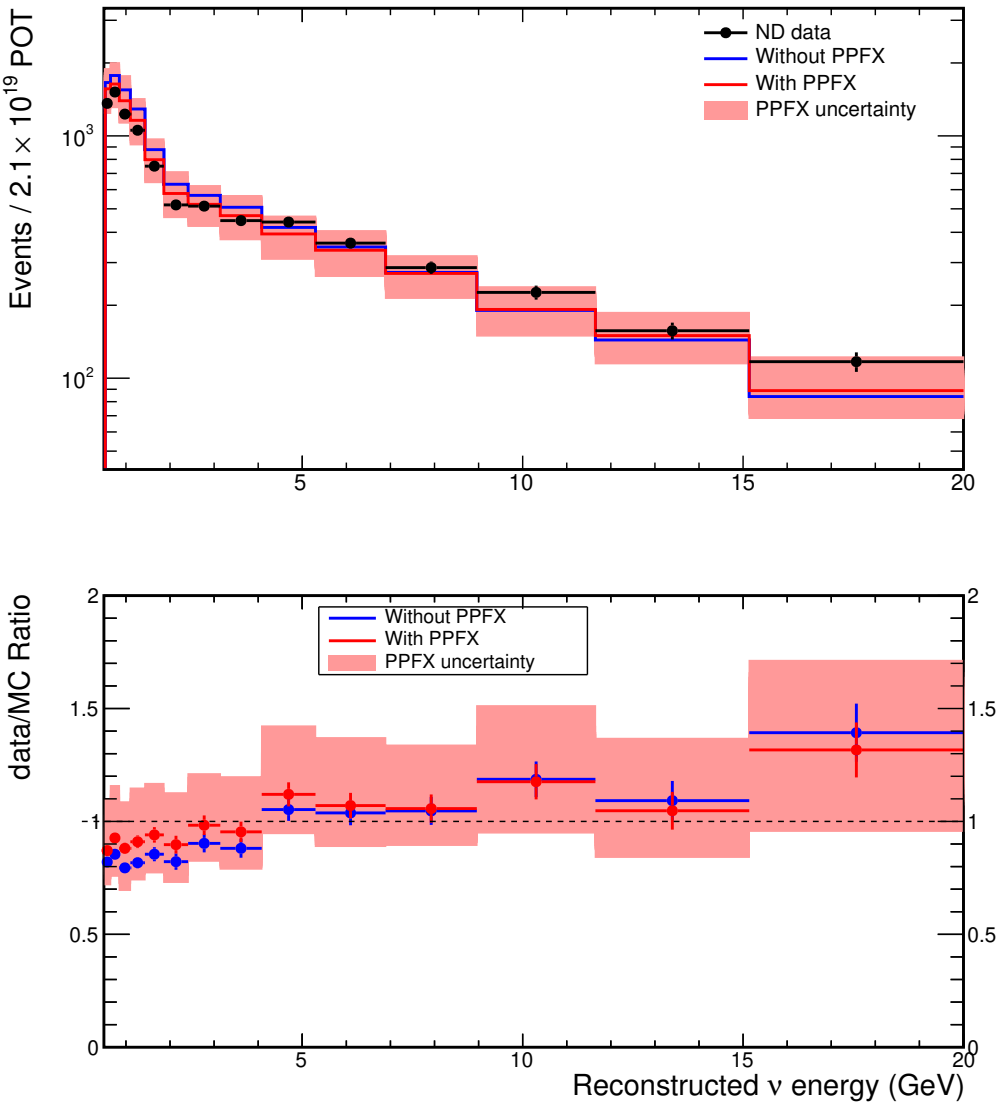


Figure 3.21: Horn-Off results of data/MC ratio for special Horn-Off NC selection and standard NC binning without applying cross-section weights.

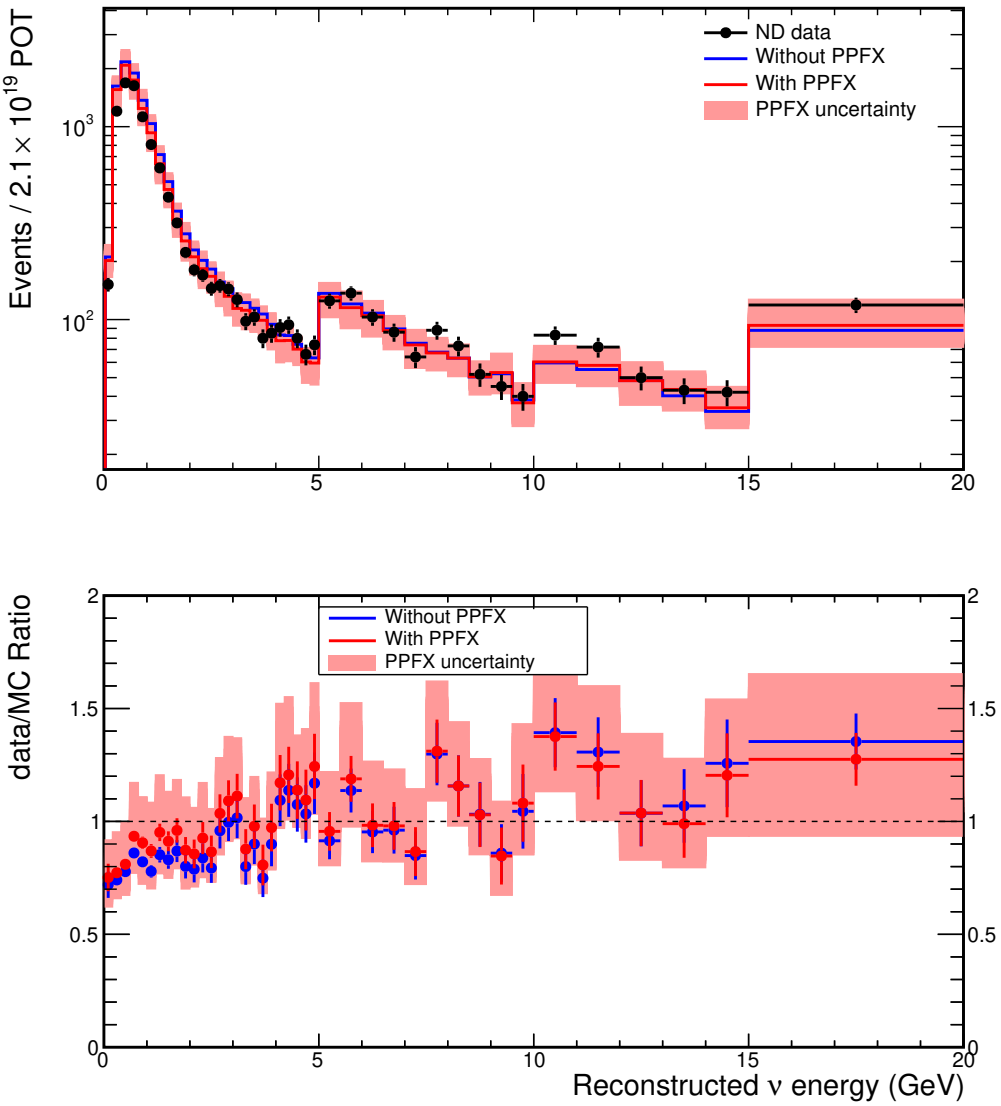


Figure 3.22: Horn-Off results of data/MC ratio for special Horn-Off NC selection and special horn-off NC binning without applying cross-section weights.

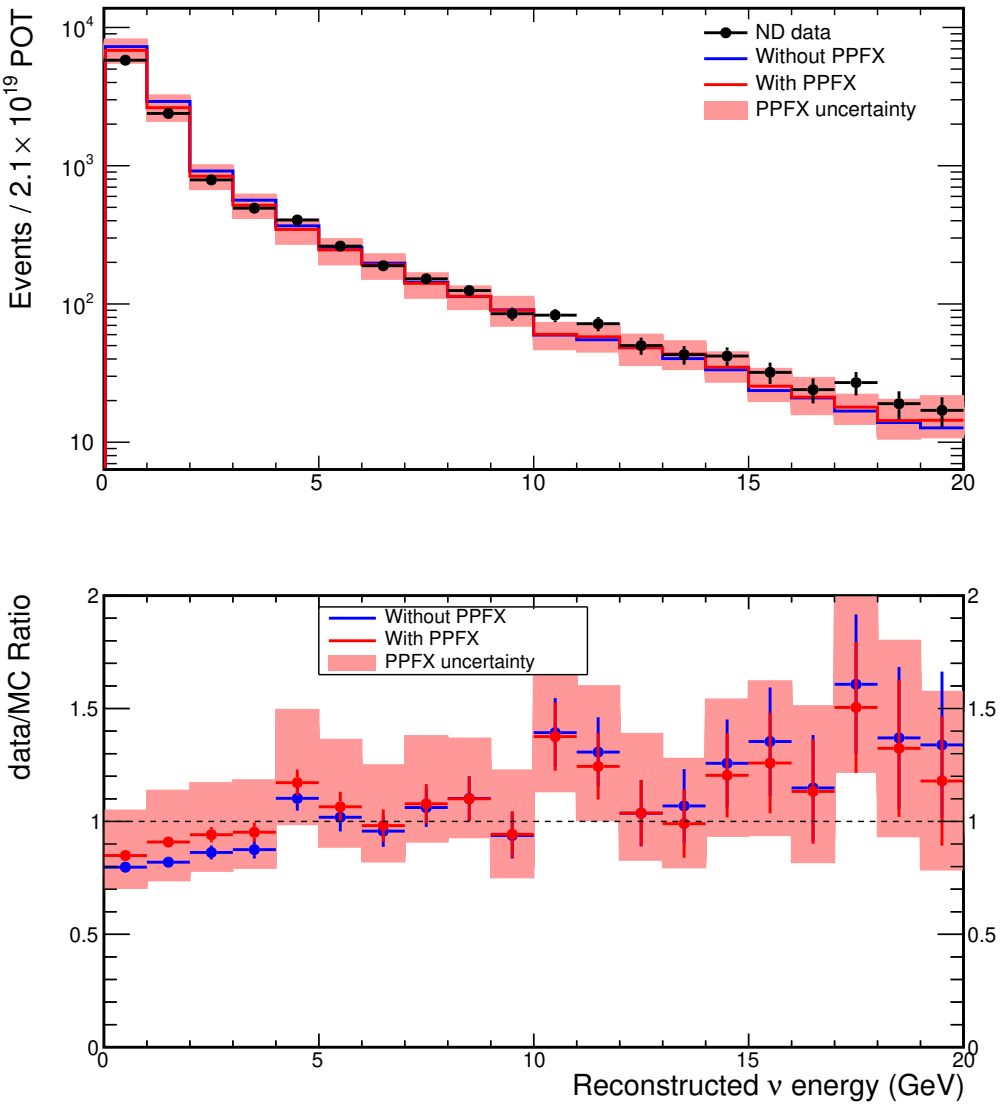


Figure 3.23: Horn-Off results of data/MC ratio for special Horn-Off NC selection and simple binning without applying cross-section weights.

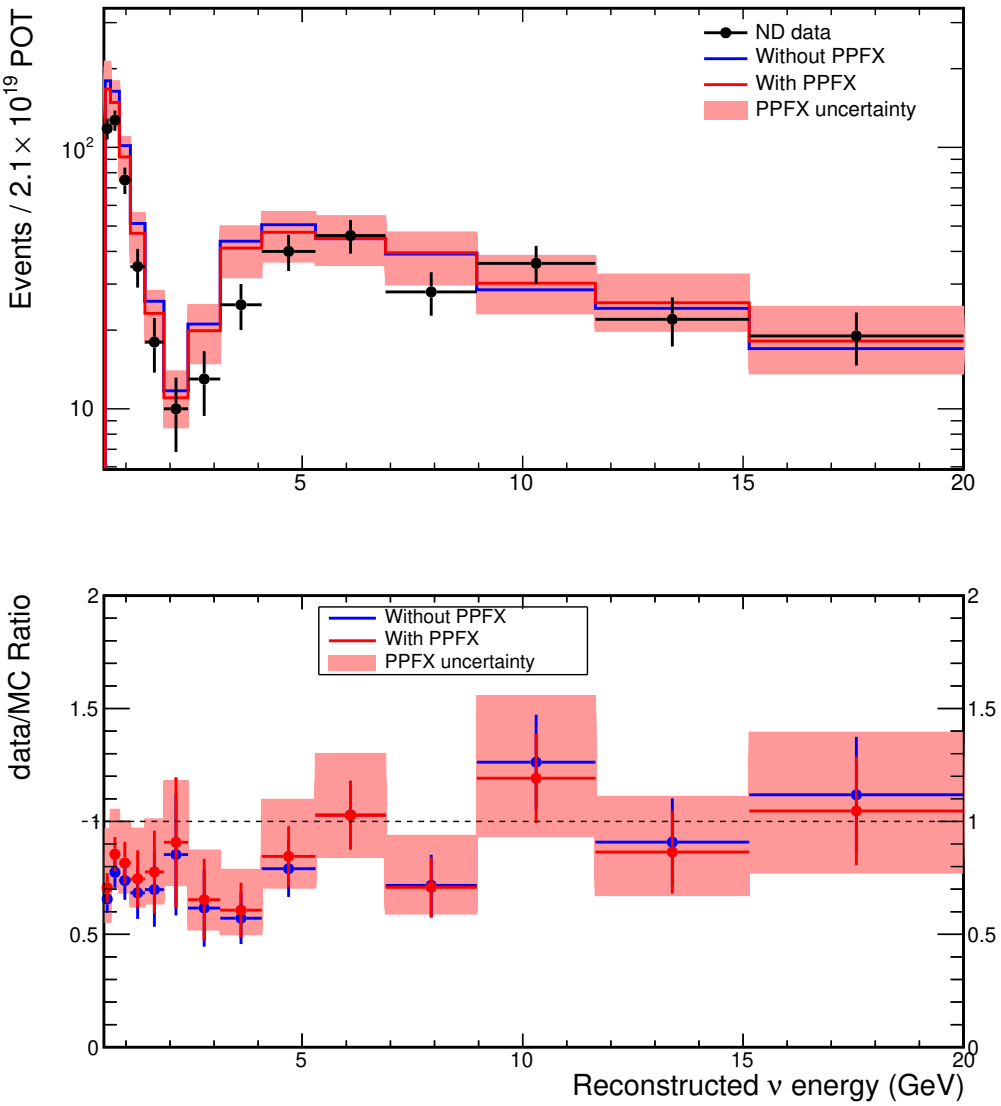


Figure 3.24: Horn-Off results of data/MC ratio for standard NC selection and standard NC binning without applying cross-section weights.

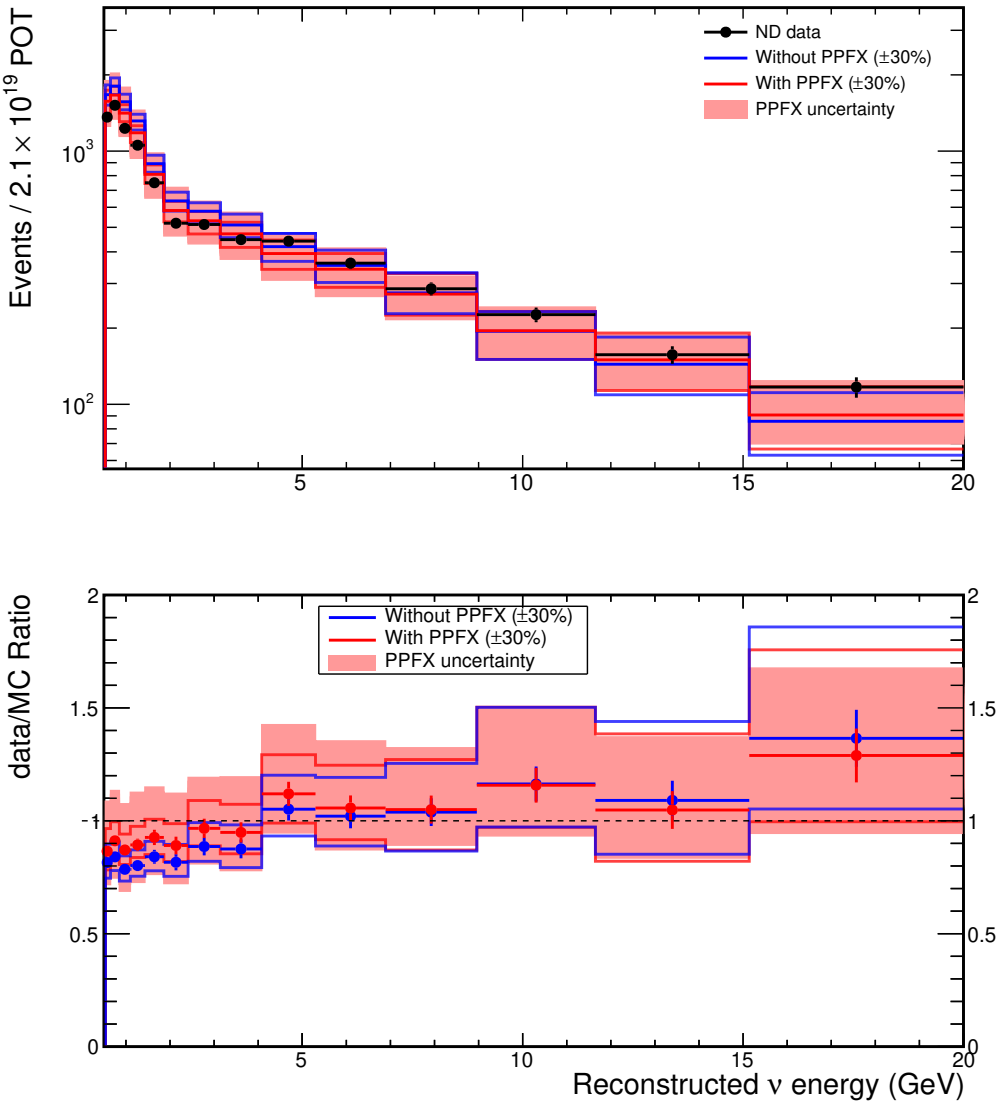


Figure 3.25: Special horn-off NC selection and standard NC binning results of data/MC ratio with kaon uncertainty with applying XSec weights. These plots intend to show the effect of additional 30% uncertainty on the data/MC comparison. This is actually what is currently done in the NC disappearance studies. We take the flux with its PPFX uncertainty (shown in peach) and atop of that we add 30% uncertainty for all neutrinos originating from kaons. This shows that a lot (most) of this kaon uncertainty is actually double counting for the already accounted for PPFX uncertainty.

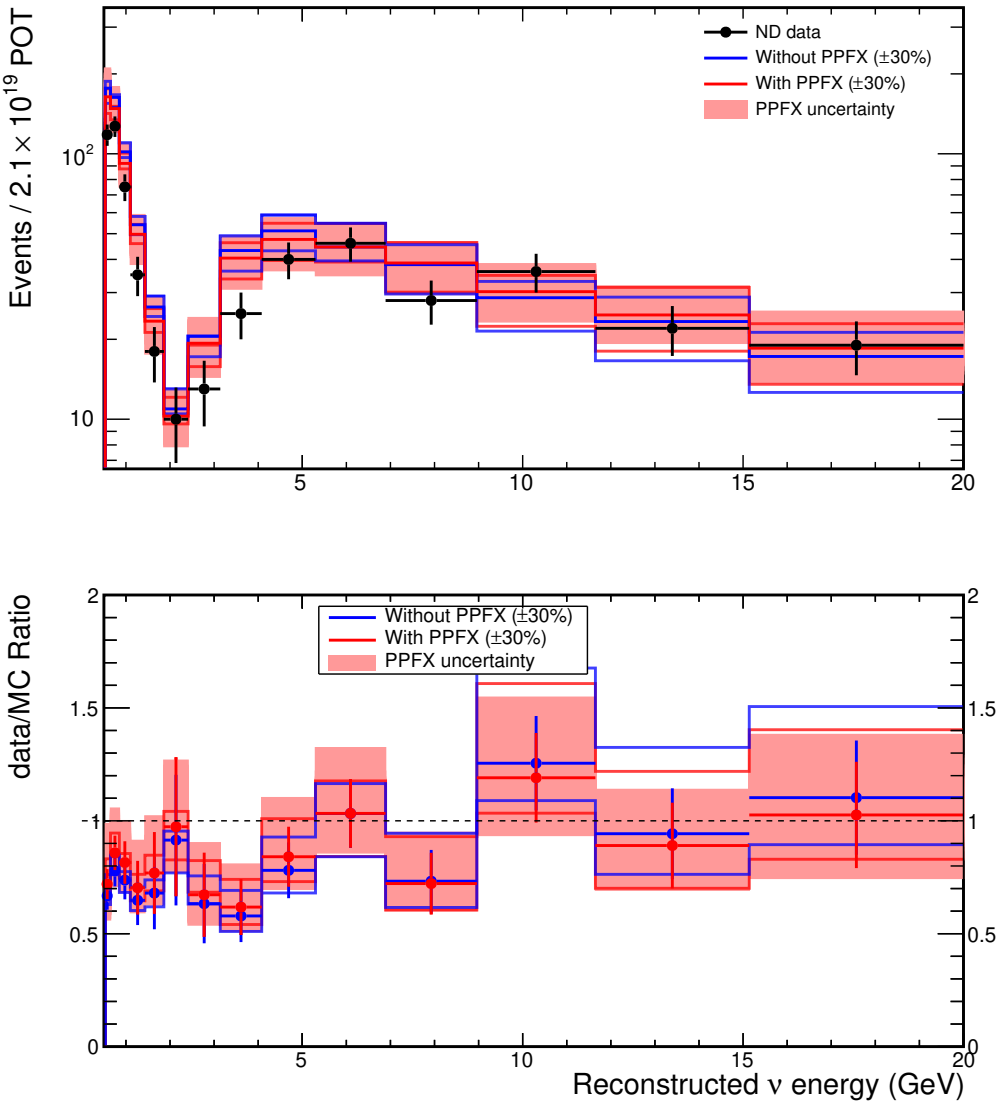


Figure 3.26: Standard NC selection and standard NC binning results of data/MC ratio with kaon uncertainty with applying XSec weights. These plots intend to show the effect of additional 30% uncertainty on the data/MC comparison. This is actually what is currently done in the NC disappearance studies. We take the flux with its PPFX uncertainty (shown in peach) and atop of that we add 30% uncertainty for all neutrinos originating from kaons. This shows that a lot (most) of this kaon uncertainty is actually double counting for the already accounted for PPFX uncertainty.

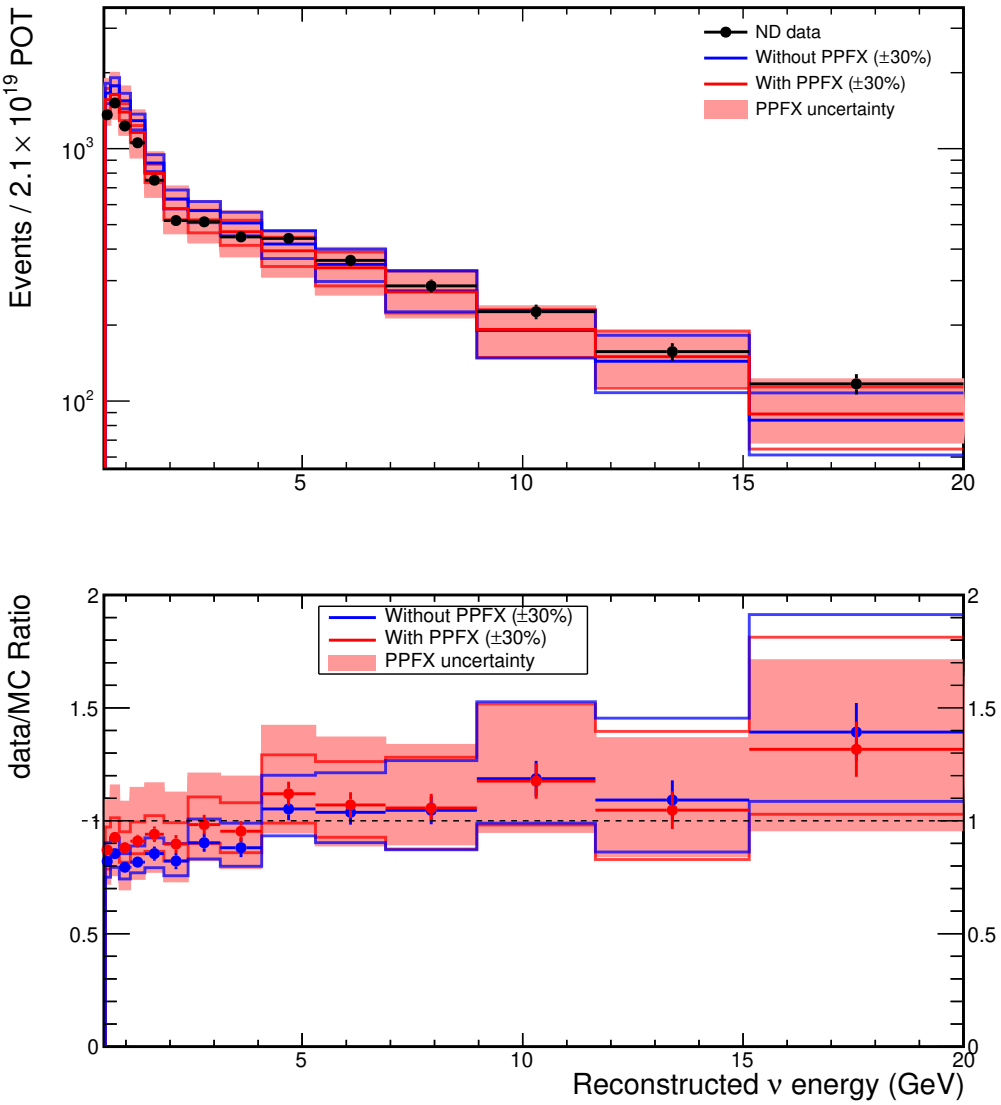


Figure 3.27: Special horn-off NC selection and standard NC binning results of data/MC ratio with kaon uncertainty without applying XSec weights. These plots intend to show the effect of additional 30% uncertainty on the data/MC comparison. This is actually what is currently done in the NC disappearance studies. We take the flux with its PPFX uncertainty (shown in peach) and atop of that we add 30% uncertainty for all neutrinos originating from kaons. This shows that a lot (most) of this kaon uncertainty is actually double counting for the already accounted for PPFX uncertainty.

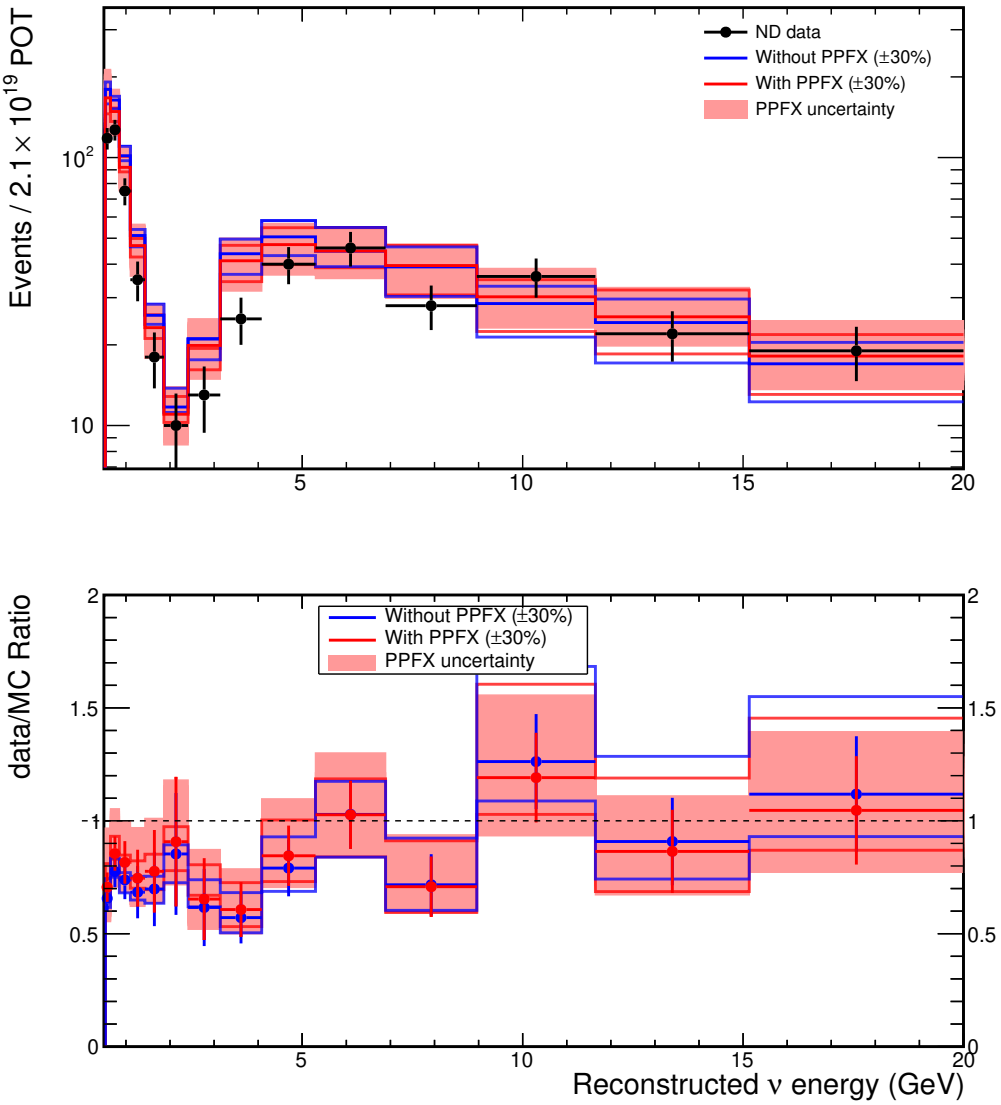


Figure 3.28: Standard NC selection and standard NC binning results of data/MC ratio with kaon uncertainty without applying XSec weights. These plots intend to show the effect of additional 30% uncertainty on the data/MC comparison. This is actually what is currently done in the NC disappearance studies. We take the flux with its PPFX uncertainty (shown in peach) and atop of that we add 30% uncertainty for all neutrinos originating from kaons. This shows that a lot (most) of this kaon uncertainty is actually double counting for the already accounted for PPFX uncertainty.

# Conclusion

In this thesis we focused on reducing the systematic uncertainty of the ongoing sterile neutrino search at NOvA experiment. Current analysis differs from the previous analyses by including both NOvA detectors and considering neutrino oscillations already in the NOvA near detector to extend our sterile oscillations parameters coverage. This shift of analysis method however caused that the ongoing analysis has a bigger contribution of neutrino flux systematic uncertainty.

We devised several ways of reducing the flux systematic and pointed out the Horn-Off analysis as the first step in achieving a reduction in the sterile analysis uncertainty. We remade the Horn-Off Monte Carlo simulation basing it on real Horn-Off data, which is the first time a proper and correct Horn-Off spectra analysis has been performed in NOvA, since the previous Horn-Off analyses suffered from a wrong Monte Carlo simulation.

We analysed the Horn-Off spectra in comparison to the previous MINOS analysis to use it as a crosscheck of the hadron production correction package PPFX and to see its effect. Our results show a good agreement between horn-off data and simulation and we did not confirm the disagreement caused by PPFX weights seen in the MINOS Horn-Off results. The MINOS results are, however, for neutrinos from hadrons with different parameter phase space to NOvA and we did not expect to see the same effect. Also, in our results, we do not consider neutrino oscillations in the near detector and we therefore cannot use our results to make an informed decision on the kaon normalization. These results can still be reassuring and might indicate that the neutrino beam simulation might not be as incorrect as we are conservatively taking into account and serve as a good motivation for the future attempts at reducing the neutrino flux uncertainty.

We have also compared the PPFX uncertainties of the Horn-Off data / simulation ratio and showed that using both PPFX uncertainties and a 30% kaon uncertainty is to a large extent a double counting of the same uncertainty.

In the future, the newly made horn-off simulation can be a base to several different ways of reducing the neutrino flux uncertainty, such as using the horn-on / horn-off ratios for a fit of the kaon normalization, or using the horn-off data / MC ratio as a crosscheck for the addition of different new hadron production data to the PPFX.

# Bibliography


[1] L. M. Brown. The idea of the neutrino. *Physics Today*, 31(9):23–28, September 1978. doi: 10.1063/1.2995181. (Including translation of W. Pauli, Aufsdtze und Vortrdge u'ber Physik und Erkenntnistheorie, Braunschweig (1961)).

[2] Erasmo Recami. Majorana, the neutron, and the neutrino: Some elementary historical remarks. *Hadronic J.*, 40:149–185, 09 2017.

[3] Fred L. Wilson. Fermi's theory of beta decay. *American Journal of Physics*, 36(12):1150–1160, 1968. doi: 10.1119/1.1974382. (A complete English translation of E.Fermi, Zeitschrift fur Physik 88, 161 (1934)).

[4] F. Reines and C.L. Cowan. Neutrino physics. *Physics Today*, 10(8):12–18, 1957. doi: 10.1063/1.3060455.

[5] H. Bethe and R. Peierls. The "neutrino". *Nature*, 133:532, April 1934. doi: 10.1038/133532a0.

[6] H. Bethe and R. Peierls. The neutrino. *Nature*, (133):689–690, May 1934. doi: 10.1038/133689b0.

[7] H. R. Crane and J. Halpern. New experimental evidence for the existence of a neutrino. *Phys. Rev.*, 53:789–794, May 1938. doi: 10.1103/PhysRev.53.789. URL `https://link.aps.org/doi/10.1103/PhysRev.53.789`.

[8] E. Amaldi. From the discovery of the neutron to the discovery of nuclear fission. *Physics Reports*, 111(1-4):1–331, 1984. doi: 10.1016/0370-1573(84)90214-X.

[9] F. Reines and C. L. Cowan. Detection of the free neutrino. *Phys. Rev.*, 92:830–831, Nov 1953. doi: 10.1103/PhysRev.92.830. URL `https://link.aps.org/doi/10.1103/PhysRev.92.830`.

[10] Harrison F.B. Kruse H.W. McGuire A.D. Cowan Jr. C.L., Reines F. Detection of the free neutrino: A confirmation. *Science*, 124(3212):103–104, July 1956. doi: 10.1126/science.124.3212.103.

[11] The official web site of the nobel prize. URL `https://www.nobelprize.org/`. Cited 05.2020.

[12] B Pontecorvo. Mesonium and antimesonium. *Sov. Phys. JETP*, 33:549–551, 8 1957.

[13] B. Pontecorvo. Inverse beta processes and nonconservation of lepton charge. *Sov. Phys. JETP*, 7:172–173, 1958.

[14] M. C. Goodman. Resource letter anp-1: Advances in neutrino physics. *American Journal of Physics*, 84:309–319, 2016. doi: 10.1119/1.4962228.

[15] M. Schwartz. Feasibility of using high-energy neutrinos to study the weak interactions. *Phys. Rev. Lett.*, 4:306–307, Mar 1960. doi: 10.1103/PhysRevLett.4.306. URL https://link.aps.org/doi/10.1103/PhysRevLett.4.306.

[16] G. Danby, J-M. Gaillard, K. Goulianos, L. M. Lederman, N. Mistry, M. Schwartz, and J. Steinberger. Observation of high-energy neutrino reactions and the existence of two kinds of neutrinos. *Phys. Rev. Lett.*, 9:36–44, Jul 1962. doi: 10.1103/PhysRevLett.9.36. URL https://link.aps.org/doi/10.1103/PhysRevLett.9.36.

[17] Ziro Maki, Masami Nakagawa, and Shoichi Sakata. Remarks on the unified model of elementary particles. *Prog. Theor. Phys.*, 28:870–880, 1962. doi: 10.1143/PTP.28.870.

[18] M.C. Gonzalez-Garcia and Yosef Nir. Neutrino Masses and Mixing: Evidence and Implications. *Rev. Mod. Phys.*, 75:345–402, 2003. doi: 10.1103/RevModPhys.75.345.

[19] M. Tanabashi et al. Review of Particle Physics. *Phys. Rev. D*, 98(3):030001, 2018. doi: 10.1103/PhysRevD.98.030001. 2019 update.

[20] Bruce T. Cleveland, Timothy Daily, Jr. Raymond Davis, James R. Distel, Kenneth Lande, C. K. Lee, Paul S. Wildenhain, and Jack Ullman. Measurement of the solar electron neutrino flux with the homestake chlorine detector. *The Astrophysical Journal*, 496(1):505–526, mar 1998. doi: 10.1086/305343. URL https://doi.org/10.1086%2F305343.

[21] Jr. Davis, Raymond, Don S. Harmer, and Kenneth C. Hoffman. Search for neutrinos from the sun. *Phys. Rev. Lett.*, 20:1205–1209, 1968. doi: 10.1103/PhysRevLett.20.1205.

[22] Y. Fukuda et al. Solar neutrino data covering solar cycle 22. *Phys. Rev. Lett.*, 77:1683–1686, Aug 1996. doi: 10.1103/PhysRevLett.77.1683. URL https://link.aps.org/doi/10.1103/PhysRevLett.77.1683.

[23] L. Wolfenstein. Neutrino oscillations in matter. *Phys. Rev. D*, 17:2369–2374, May 1978. doi: 10.1103/PhysRevD.17.2369. URL https://link.aps.org/doi/10.1103/PhysRevD.17.2369.

[24] S.P. Mikheyev and A.Yu. Smirnov. Resonance Amplification of Oscillations in Matter and Spectroscopy of Solar Neutrinos. *Sov. J. Nucl. Phys.*, 42:913–917, 1985.

[25] *1st CERN - CLAF School of High-energy Physics*, Geneva, 2003. CERN, CERN. doi: 10.5170/CERN-2003-003. URL http://cds.cern.ch/record/485010.

[26] M. Aglietta et al. Experimental study of atmospheric neutrino flux in the NUSEX experiment. *Europhysics Letters (EPL)*, 8(7):611–614, apr 1989. doi: 10.1209/0295-5075/8/7/005. URL https://doi.org/10.1209%2F0295-5075%2F8%2F7%2F005.

[27] K. Daum et al. Determination of the atmospheric neutrino spectra with the fréjus detector. *Zeitschrift für Physik C Particles and Fields*, 66(3):417–428, 1995. ISSN 1431-5858. URL https://doi.org/10.1007/BF01556368.

[28] R. Becker-Szendy et al. Electron- and muon-neutrino content of the atmospheric flux. *Phys. Rev. D*, 46:3720–3724, Nov 1992. doi: 10.1103/PhysRevD.46.3720. URL https://link.aps.org/doi/10.1103/PhysRevD.46.3720.

[29] Y. Fukuda et al. Atmospheric $\nu_\mu/\nu_e$ ratio in the multi-GeV energy range. *Phys. Lett. B*, 335(GIFU-PH-94-01. ICRR-321. INS-Rep-1035. KEK-Preprint-94-50. KOBE-AP-94-01. NGTHEP-94-1. OULNS-94-01. TIT-HPE-94-04. TKU-PAP-94-2. UPR-0226-E):237–245. 25 p, Jun 1994. URL https://cds.cern.ch/record/266736.

[30] Y. Fukuda et al. Evidence for oscillation of atmospheric neutrinos. *Phys. Rev. Lett.*, 81:1562–1567, 1998. doi: 10.1103/PhysRevLett.81.1562.

[31] Q.R. Ahmad et al. Direct evidence for neutrino flavor transformation from neutral current interactions in the Sudbury Neutrino Observatory. *Phys. Rev. Lett.*, 89:011301, 2002. doi: 10.1103/PhysRevLett.89.011301.

[32] B. Adeva et al. Measurement of $Z^0$ decays to hadrons and a precise determination of the number of neutrino species. *Phys. Lett. B*, 237:136–146, 1990. doi: 10.1016/0370-2693(90)90476-M.

[33] S. Schael et al. Precision electroweak measurements on the $Z$ resonance. *Phys. Rept.*, 427:257–454, 2006. doi: 10.1016/j.physrep.2005.12.006.

[34] K. Kodama et al. Observation of tau neutrino interactions. *Phys. Lett. B*, 504:218–224, 2001. doi: 10.1016/S0370-2693(01)00307-0.

[35] Olga Mena and Stephen J. Parke. Unified graphical summary of neutrino mixing parameters. *Phys. Rev. D*, 69:117301, 2004. doi: 10.1103/PhysRevD.69.117301.

[36] Sebastian Böser, Christian Buck, Carlo Giunti, Julien Lesgourgues, Livia Ludhova, Susanne Mertens, Anne Schukraft, and Michael Wurm. Status of Light Sterile Neutrino Searches. *Prog. Part. Nucl. Phys.*, 111:103736, 2020. doi: 10.1016/j.ppnp.2019.103736.

[37] Carlo Giunti and T. Lasserre. eV-scale Sterile Neutrinos. *Ann. Rev. Nucl. Part. Sci.*, 69:163–190, 2019. doi: 10.1146/annurev-nucl-101918-023755.

[38] M Maltoni, T Schwetz, and J.W.F Valle. Cornering (3+1) sterile neutrino schemes. *Physics Letters B*, 518(3):252 – 260, 2001. ISSN 0370-2693. doi: https://doi.org/10.1016/S0370-2693(01)01068-1. URL http://www.sciencedirect.com/science/article/pii/S0370269301010681.

[39] Mona Dentler, Álvaro Hernández-Cabezudo, Joachim Kopp, Pedro A.N. Machado, Michele Maltoni, Ivan Martinez-Soler, and Thomas Schwetz. Updated Global Analysis of Neutrino Oscillations in the Presence of eV-Scale Sterile Neutrinos. *JHEP*, 08:010, 2018. doi: 10.1007/JHEP08(2018)010.

[40] Joachim Kopp, Pedro A. N. Machado, Michele Maltoni, and Thomas Schwetz. Sterile Neutrino Oscillations: The Global Picture. *JHEP*, 05: 050, 2013. doi: 10.1007/JHEP05(2013)050.

[41] A. Aguilar et al. Evidence for neutrino oscillations from the observation of $\overline{\nu}_e$ appearance in a $\overline{\nu}_\mu$ beam. *Phys. Rev. D*, 64:112007, Nov 2001. doi: 10.1103/PhysRevD.64.112007. URL `https://link.aps.org/doi/10.1103/PhysRevD.64.112007`.

[42] A.A. Aguilar-Arevalo et al. Significant Excess of ElectronLike Events in the MiniBooNE Short-Baseline Neutrino Experiment. *Phys. Rev. Lett.*, 121(22):221801, 2018. doi: 10.1103/PhysRevLett.121.221801.

[43] A.A. Aguilar-Arevalo et al. Updated miniboone neutrino oscillation results with increased data and new background studies. 6 2020.

[44] F. Kaether, W. Hampel, G. Heusser, J. Kiko, and T. Kirsten. Reanalysis of the GALLEX solar neutrino flux and source experiments. *Phys. Lett. B*, 685:47–54, 2010. doi: 10.1016/j.physletb.2010.01.030.

[45] J.N. Abdurashitov et al. Measurement of the solar neutrino capture rate with gallium metal. III: Results for the 2002–2007 data-taking period. *Phys. Rev. C*, 80:015807, 2009. doi: 10.1103/PhysRevC.80.015807.

[46] Joel Kostensalo, Jouni Suhonen, Carlo Giunti, and Praveen C. Srivastava. The gallium anomaly revisited. *Phys. Lett. B*, 795:542–547, 2019. doi: 10.1016/j.physletb.2019.06.057.

[47] Th.A. Mueller et al. Improved Predictions of Reactor Antineutrino Spectra. *Phys. Rev. C*, 83:054615, 2011. doi: 10.1103/PhysRevC.83.054615.

[48] G. Mention, M. Fechner, Th. Lasserre, Th.A. Mueller, D. Lhuillier, M. Cribier, and A. Letourneau. The Reactor Antineutrino Anomaly. *Phys. Rev. D*, 83:073006, 2011. doi: 10.1103/PhysRevD.83.073006.

[49] Feng Peng An et al. Measurement of the Reactor Antineutrino Flux and Spectrum at Daya Bay. *Phys. Rev. Lett.*, 116(6):061801, 2016. doi: 10.1103/PhysRevLett.116.061801. [Erratum: Phys.Rev.Lett. 118, 099902 (2017)].

[50] Patrick Huber. Reactor antineutrino fluxes – Status and challenges. *Nucl. Phys. B*, 908:268–278, 2016. doi: 10.1016/j.nuclphysb.2016.04.012.

[51] F.P. An et al. Evolution of the Reactor Antineutrino Flux and Spectrum at Daya Bay. *Phys. Rev. Lett.*, 118(25):251801, 2017. doi: 10.1103/PhysRevLett.118.251801.

[52] C. Giunti, Y.F. Li, B.R. Littlejohn, and P.T. Surukuchi. Diagnosing the Reactor Antineutrino Anomaly with Global Antineutrino Flux Data. *Phys. Rev. D*, 99(7):073005, 2019. doi: 10.1103/PhysRevD.99.073005.

[53] I Alekseev et al. Search for sterile neutrinos at the DANSS experiment. *Phys. Lett. B*, 787:56–63, 2018. doi: 10.1016/j.physletb.2018.10.038.

[54] Y.J. Ko et al. Sterile Neutrino Search at the NEOS Experiment. *Phys. Rev. Lett.*, 118(12):121802, 2017. doi: 10.1103/PhysRevLett.118.121802.

[55] S. Gariazzo, C. Giunti, M. Laveder, and Y.F. Li. Model-independent $\overline{\nu}_e$ short-baseline oscillations from reactor spectral ratios. *Physics Letters B*, 782:13 – 21, 2018. ISSN 0370-2693. doi: https://doi.org/10.1016/j.physletb.2018.04.057. URL `http://www.sciencedirect.com/science/article/pii/S0370269318303514`.

[56] Mikhail Danilov. Recent results of the DANSS experiment. In *2019 European Physical Society Conference on High Energy Physics*, 11 2019.

[57] A.P. Serebrov et al. Preparation of the Neutrino-4 experiment on search for sterile neutrino and the obtained results of measurements. 5 2020.

[58] M. Andriamirado et al. Note on arXiv:2005.05301, 'Preparation of the Neutrino-4 experiment on search for sterile neutrino and the obtained results of measurements'. 6 2020.

[59] K. Abe et al. Limits on sterile neutrino mixing using atmospheric neutrinos in Super-Kamiokande. *Phys. Rev. D*, 91:052019, 2015. doi: 10.1103/PhysRevD.91.052019.

[60] M.G. Aartsen et al. Search for sterile neutrino mixing using three years of IceCube DeepCore data. *Phys. Rev. D*, 95(11):112002, 2017. doi: 10.1103/PhysRevD.95.112002.

[61] M.G. Aartsen et al. An eV-scale sterile neutrino search using eight years of atmospheric muon neutrino data from the IceCube Neutrino Observatory. 5 2020.

[62] P. Adamson et al. Search for sterile neutrinos in MINOS and MINOS+ using a two-detector fit. *Phys. Rev. Lett.*, 122(9):091803, 2019. doi: 10.1103/PhysRevLett.122.091803.

[63] K. Abe et al. Search for light sterile neutrinos with the T2K far detector Super-Kamiokande at a baseline of 295 km. *Phys. Rev. D*, 99(7):071103, 2019. doi: 10.1103/PhysRevD.99.071103.

[64] P. Adamson et al. Search for active-sterile neutrino mixing using neutral-current interactions in NOvA. *Phys. Rev. D*, 96(7):072006, 2017. doi: 10.1103/PhysRevD.96.072006.

[65] R.B. Patterson. The NOvA Experiment: Status and Outlook. *Nucl. Phys. B Proc. Suppl.*, 235-236:151–157, 2013. doi: 10.1016/j.nuclphysbps.2013.04.005.

[66] Gary Feldman for the NOvA Collaboration. Physics of the nova experiment. White paper, 2012. URL `https://nova-docdb.fnal.gov/cgi-bin/ShowDocument?docid=7733`. Public NOvA document: NOVA-doc-7733-v1, cited on 05.2020.

[67] Athanasios Hatzikoutelis. Prospective exotic searches with the nova detectors. 2012. URL `https://nova-docdb.fnal.gov/cgi-bin/ShowDocument?docid=7686`. Public NOvA document: NOVA-doc-7686-v2, cited on 05.2020.

[68] D. S. Ayres et al. The nova technical design report. *NOvA Collaboration*, 2007. doi: 10.2172/935497.

[69] Nova experiments official homepage. URL `https://novaexperiment.fnal.gov`. Cited 05.2020.

[70] P. Adamson et al. First measurement of muon-neutrino disappearance in NOvA. *Phys. Rev. D*, 93(5):051104, 2016. doi: 10.1103/PhysRevD.93.051104.

[71] M.A. Acero et al. First Measurement of Neutrino Oscillation Parameters using Neutrinos and Antineutrinos by NOvA. *Phys. Rev. Lett.*, 123(15): 151803, 2019. doi: 10.1103/PhysRevLett.123.151803.

[72] P. Adamson et al. The NuMI Neutrino Beam. *Nucl. Instrum. Meth. A*, 806:279–306, 2016. doi: 10.1016/j.nima.2015.08.063.

[73] P. Adamson et al. First Measurement of $\nu_\mu$ and $\nu_e$ Events in an Off-Axis Horn-Focused Neutrino Beam. *Phys. Rev. Lett.*, 102:211801, 2009. doi: 10.1103/PhysRevLett.102.211801.

[74] The PIP-II Reference Design Report. 6 2015. doi: 10.2172/1365571.

[75] Leonidas Aliaga Soplin. *Neutrino Flux Prediction for the NuMI Beamline*. PhD thesis, William-Mary Coll., 2016.

[76] P. Adamson et al. A Study of Muon Neutrino Disappearance Using the Fermilab Main Injector Neutrino Beam. *Phys. Rev. D*, 77:072002, 2008. doi: 10.1103/PhysRevD.77.072002.

[77] G. Tzanankos et al. MINOS+: a Proposal to FNAL to run MINOS with the medium energy NuMI beam. 5 2011. doi: 10.2172/1028838.

[78] Yury Kudenko. Neutrino detectors for oscillation experiments. *JINST*, 12 (06):C06003, 2017. doi: 10.1088/1748-0221/12/06/C06003.

[79] Xinchun Tian. NOvA Data Acquisition Software System. In *Meeting of the APS Division of Particles and Fields*, 9 2011.

[80] S. Agostinelli et al. GEANT4–a simulation toolkit. *Nucl. Instrum. Meth. A*, 506:250–303, 2003. doi: 10.1016/S0168-9002(03)01368-8.

[81] A. Aurisano, C. Backhouse, R. Hatcher, N. Mayer, J. Musser, R. Patterson, R. Schroeter, and A. Sousa. The NOvA simulation chain. *J. Phys. Conf. Ser.*, 664(7):072002, 2015. doi: 10.1088/1742-6596/664/7/072002.

[82] M. Baird, J. Bian, M. Messier, E. Niner, D. Rocco, and K. Sachdev. Event Reconstruction Techniques in NOvA. *J. Phys. Conf. Ser.*, 664(7):072035, 2015. doi: 10.1088/1742-6596/664/7/072035.

[83] A. Aurisano, A. Radovic, D. Rocco, A. Himmel, M.D. Messier, E. Niner, G. Pawloski, F. Psihas, A. Sousa, and P. Vahle. A Convolutional Neural Network Neutrino Event Classifier. *JINST*, 11(09):P09001, 2016. doi: 10.1088/1748-0221/11/09/P09001.

[84] Kanika Sachdev. A Data-Driven Method of Background Prediction at NOvA. In *Meeting of the APS Division of Particles and Fields*, 9 2013.

[85] C. Andreopoulos et al. The GENIE Neutrino Monte Carlo Generator. *Nucl. Instrum. Meth. A*, 614:87–104, 2010. doi: 10.1016/j.nima.2009.12.009.

[86] L. Aliaga et al. Neutrino Flux Predictions for the NuMI Beam. *Phys. Rev. D*, 94(9):092005, 2016. doi: 10.1103/PhysRevD.94.092005. [Addendum: Phys.Rev.D 95, 039903 (2017)].

[87] Richard P. Feynman. Very high-energy collisions of hadrons. *Phys. Rev. Lett.*, 23:1415–1417, 1969. doi: 10.1103/PhysRevLett.23.1415.

[88] C. Alt et al. Inclusive production of charged pions in p+C collisions at 158-GeV/c beam momentum. *Eur. Phys. J. C*, 49:897–917, 2007. doi: 10.1140/epjc/s10052-006-0165-7.

[89] Andrey V. Lebedev. *Ratio of Pion Kaon Production in Proton Carbon Interactions*. PhD thesis, 2007.

[90] Leonidas Aliaga Soplin. Ppfx tech-note for the 2017 analysis. NOvA private document: NOVA-doc-23441-v4 (cited on 07.2020), 2017.

[91] Gemma Maria Tinti. *Sterile neutrino oscillations in MINOS and hadron production in pC collisions*. PhD thesis, 2010.

[92] Tomas Nosek. Latest results from searches for neutral current disappearance in nova. In *APS April Meeting*, volume 63, 2018. URL `http://meetings.aps.org/link/BAPS.2018.APR.H08.1`. Public NOvA document NOVA-doc-28295-v3, cited on 07.2020.

[93] Michael Wallbank. Sterile neutrino search via neutral-current disappearance with antineutrinos in nova (dpf 2019) – new rhc nc results. In *APS April Meeting 2019*, 2019. URL `http://meetings.aps.org/Meeting/APR19/Session/Z14.6`. Public NOvA document: NOVA-doc-37020-v2, cited on 05.2020.

[94] Jeremy Hewes. Poisson likelihood covariance technique for 3+1 sterile neutrino searches in nova. In *XXIX International Conference on Neutrino Physics*, 2020. URL `https://nusoft.fnal.gov/nova/nu2020postersession/pdf/posterPDF-431.pdf`.

[95] Jeremy Wolcott. Impact of cross section modelingon nova oscillation analyses. In *NuInt*, 2018. URL `https://nova-docdb.fnal.gov/cgi-bin/private/ShowDocument?docid=33384`. Public NOvA document: NOVA-doc-33384-v2 (cited on 07.2020).

[96] Anna Holin. Nova beam studies and lessons from minos+. Private NOvA document NOVA-doc-35802-v3.

[97] Anna Holin. Numi beam lessons and work in progress minos/mino+. In *CENF-ND General Meeting*, November 2017. URL `https://indi.to/vJNB8`.

[98] Zelimir Djurcic Shiqi Yu. Bendecomp technical notes for $nu_e$ appearance 2018 analysis. Private NOvA document: NOVA-doc-27833-v6 (cited on 07.2020).

[99] Kuldeep Kaur Maan. *EMPIRICAL DETERMINATION OF THE NEUTRINO FLUX AT THE NOvA EXPERIMENT*. PhD thesis, Punjab U., 2018.

[100] Matej Pavin. Hadron production measurements for neutrino experiments. In *Neutrino 2020*, 2020. URL `https://indico.fnal.gov/event/43209/contributions/187869/attachments/130502/159028/HadronProduction_neutrino2020.pdf`. (cited on 07.2020).

[101] N. Abgrall et al. Measurements of $\pi^{\pm}$ , $K^{\pm}$ , $K^0_S$ , $\Lambda$ and proton production in proton–carbon interactions at 31 GeV/c with the NA61/SHINE spectrometer at the CERN SPS. *Eur. Phys. J. C*, 76(2):84, 2016. doi: 10.1140/epjc/s10052-016-3898-y.

[102] Yoshikazu Nagai. Na61/shine experiment - results from the neutrino program and future prospects. In *Fermilab Neutrino Seminar*, 2020. URL `https://if-docdb.fnal.gov/cgi-bin//ShowDocument?docid=528`. Public NOvA document: IF-doc-528-v1 (cited on 07.2020).

# List of Figures

# List of Tables

# List of Abbreviations

| | |
|---|---|
| PMNS | Pontecorvo-Maki-Nakagawa-Sakata (matrix) |
| SNU | Solar Neutrino Unit |
| CC | Charged Current (interaction) |
| NC | Neutral Current |
| MSW | Mikheyev-Smirnov-Wolfenstein (effect) |
| SK | Super-Kamiokande (experiment) |
| NO | Normal Ordering (of masses) |
| IO | Inverted Ordering (of masses) |
| SBL | Short Baseline |
| LBL | Long Baseline |
| LSND | Liquid Scintillator Neutrino Detector |
| MiniBooNE | Mini Booster Neutrino Experiment |
| SBN | Short Baseline Neutrino (program) |
| NOvA | NuMI Off-axis $\nu_e$ Appearance (experiment) |
| NuMI | Neutrinos from the Main Injector |
| ND | Near Detector |
| FD | Far Detector |
| FHC | Forward Horn Current (neutrino mode) |
| RHC | Reverse Horn Current (antineutrino mode) |
| HC | Horn Current |
| LE | Low Energy (mode of NuMI) |
| ME | Medium Energy (mode of NuMI) |
| APD | Avalanche Photodiode |
| CVN | Convolutional Neural Network |
| MC | Monte Carlo |
| PPFX | Package to Predict the Flux |
| CMS | Center of Mass (frame) |
| BENDecomp | Beam Electron Neutrino Decomposition |